Partially Coherent Detection of PSK Signals in Rician Channels

by

Yaşar Tunca, B.A.Sc.

A thesis submitted to the
School of Graduate Studies and Research
in partial fulfilment of the requirements
for the degree

Master of Applied Science

Ottawa-Carleton Institute for Electrical Engineering
Department of Electrical Engineering
Faculty of Engineering
University of Ottawa

National Library
of Canada

Acquisitions and
Bibliographic Services Branch

395 Wellington Street
Ottawa, Ontario
K1A 0N4

Bibliothèque nationale
du Canada

Direction des acquisitions et
des services bibliographiques

395, rue Wellington
Ottawa (Ontario)
K1A 0N4

Your file Votre référence

Our file Notre référence

ISBN 0-315-85799-4

Canada

UNIVERSITÉ D'OTTAWA
UNIVERSITY OF OTTAWA

Abstract

Coherent detection which has the best performance in ideal channels suffers in environments where there is significant phase noise (e.g. fading channels). In this thesis, we developed channel models for noisy phase reference and Rician fading channels and assuming that partially coherent detection could be an alternative, we derived metric expressions for partially coherent detection of signals in general and applied it to PSK signals. Simulation programs were run using the developed channel models and the results were compared to other detection schemes under same conditions.

I hereby declare that I am the sole author of this thesis.

I authorize The University of Ottawa to lend this thesis to other institutions or individuals for the purpose of scholarly research.

Yaşar Tunca

I further authorize The University of Ottawa to reproduce this thesis by photocopying or by other means, in total or in part, at the request of other institutions or individuals for the purpose of scholarly research.

Yaşar Tunca

Acknowledgement

I would like to thank Dimitrios Makrakis for our lengthy discussions and scientific interactions that lead to a successful choice of thesis topic and helped to carry on a valuable and enjoyable research work. I would like to thank my supervisor Dr.Abbas Yongacoglu for providing financial support for some duration of my studies. I am grateful to my family, the School of Graduate Studies, especially to Ms. Colette Mangin, for their financial aid and Dr. W. Steenaart for having me as a research assistant which made my survival, thus my graduation possible. I would also like to thank the professors and friends for their encouragement and Dr. Jean-Yves Chouinard and Dr. Jim Wight for reading the thesis and for their valuable suggestions.

Contents

List of Figures

Acronyms

AWGN	Additive White Gaussian Noise
BER	Bit Error Rate
BPSK	Binary Phase Shift Keying
CBPSK	Coherent BPSK
CPM	Continuous Phase Modulation
CQPSK	Coherent QPSK
DBPSK	Differentially Detected BPSK
DECBPSK	Differentially Encoded Coherent BPSK
DECQPSK	Differentially Encoded Coherent QPSK
DMSK	Differentially Detected Minimum Shift Keying
DOQPSK	Differentially Detected Offset QPSK
DQPSK	Differentially Detected QPSK
FDMA	Frequency Division Multiple Access
FEC	Forward Error Correction
FSK	Frequency Shift Keying
GMSK	Gaussian Minimum Shift Keying
LOS	Line-of-Sight
MDPSK	M-ary Differential Phase Shift Keying
OKQPSK	Offset Keyed QPSK
pdf	Probability Density Function
PLL	Phase-Locked Loop
PSK	Phase Shift Keying
QAM	Quadrature Amplitude Modulation
QPSK	Quarternary Phase Shift Keying
SNR	Signal to Noise Ratio
TDMA	Time Division Multiple Access
VCO	Voltage Controlled Oscillator

Nomenclature

a	Constant fading amplitude
$a(t)$	Fading amplitude of the received signal
B	Fading bandwidth or 3dB bandwidth of a loop filter
$\bar{B}$	Binary information sequence
$\bar{C}(\bar{A})$	Sequence of symbols after signal mapping and differential encoding
c_k	Samples of possible signals that could be sent by the transmitter
D	Signal power of the diffuse component
d	Average power of either components of filtered complex Gaussian process
$\frac{E_b}{N_0}$	Signal energy per bit to noise spectral density ratio
E_{b_f}	Signal energy per bit in the presence of fading
$E_{b_{nf}}$	Bit energy in the absence of fading
$h_c(t)$	Channel response
$h_{c,B}(\bar{C}(\bar{A}),t)$	Baseband equivalent of channel response
$h_E(t)$	Overall baseband impulse response of the transmitter and the channel
$INT(\cdot)$	Function defined as $INT(x_B(\bar{C}(\bar{A}),t)) = \frac{1}{2}\int_{t_L}^{t_U} \lvert x_B(\bar{C}(\bar{A}),\tau)\rvert^2 d\tau$
$IRE(\cdot)$	Function defined as $IRE(x_r(t), x_B(\bar{C}(\bar{A}),t)) = \int_{t_L}^{t_U} x_r(t) e^{-j(\omega_c t+\hat{\psi})} x_B^*(\bar{C}(\bar{A}),t)dt$
I_k	k^{th} order modified Bessel function of the first kind
K	K-factor (Rice factor): Direct component power to diffuse component power ratio
n_k^I, n_k^Q	Samples of inphase and quadrature components of a Gaussian process
$\underline{n}_k$, $\underline{n}_k'$, $\underline{n}_k''$	Samples of complex Gaussian process
$p(\cdot)$	Probability density function
P	Signal power
P_b	Probability of bit error
P_s	Probability of symbol error
$Q(\cdot)$	Q function

$Q(\cdot,\cdot)$	Generalized Q function (Marcum Q function)
$\underline{r_k}$	Samples of complex baseband signal at the output of the channel
S	Signal power of direct component
$s(t)$	Demodulated signal at the receiver
$s'(t)$	Demodulated signal after the filtering of multiple frequencies of the carrier
T	Symbol duration
T_b	Bit duration
$x_B(\bar{C}(\bar{A}),t)$	Baseband equivalent of the channel response to the transmitted signal
$\underline{X_k}$	Samples of complex baseband equivalent of symbols entering the channel
$x_r(t)$	Signal at the input of a partially coherent receiver
$x_{tr}(\bar{C}(\bar{A}),t)$	Transmitter output
$x_{tr,B}(\bar{C}(\bar{A}),t)$	Complex baseband representation of transmitter output
y_k	Samples of received signal
ω_c	Angular carrier frequency
ϕ	Phase error
ψ	Initial phase of the modulator
$\hat{\psi}$	Estimate of the initial phase of the modulator
$\rho(\phi)$	Correlation loss due to phase error ϕ
σ^2	Variance of inphase and quadrature components of a complex Gaussian process
θ	Arbitrary phase of the carrier
$\Delta\theta_m$	Differential information phases
$\hat{\theta}$	Estimate of carrier phase
ξ	(Effective) signal to noise ratio at the output of the carrier recovery circuit
ξ_0	Nominal loop signal to noise ratio
θ_m	Information phases
Γ	Total gain of the phase-locked loop
Γ_1	The gain of the voltage controlled oscillator
$\sqrt{A}$	The gain of the phase detector
$<\cdot,\cdot>$	Inner product of two vectors
$(\cdot)_I$	Inphase component of $\cdot$
$(\cdot)_Q$	Quadrature component $\cdot$
$\otimes$	Convolution operator

Chapter 1

INTRODUCTION

1.1 Problem Statement

Coherent and noncoherent detection are the two major detection techniques which are widely employed in digital communication systems. Coherent detection assumes that the carrier phase can be estimated precisely at the receiver and is based on the demodulation of the received bandpass signal by locally generating a synchronous replica of the carrier. If the phase coherence requirement is relaxed, one can use differential detection, where rather than an absolute phase reference, an incremental phase difference between two successive symbols is sufficient. Differential detection is often classified as noncoherent detection. In the strict sense in noncoherent detection (e.g., envelope detection), it is assumed that no estimate of the phase of the carrier is available at the receiver and no attempt is made to estimate it.

Coherent detection has the best probability of error performance in Additive White Gaussian Noise (AWGN) channels under the assumption of perfect carrier estimation (i.e. frequency and phase). In environments where significant phase noise is introduced into the system or in mobile communication channels which is characterized by fading and Doppler shifts, the performance of this detection technique not only can degrade severely but also can sit on some high error floors. Furthermore, in burst communication systems (e.g. Time Division Multiple Access (TDMA)) where fast acquisition is required, this technique can become unsuitable due to increased

overhead needed for carrier recovery.

In digital communication systems, irrespective of the modulation scheme, noncoherent detection is always inferior to the coherent detection in AWGN channels if perfect carrier recovery is assumed. This is expected since in coherent detection systems, there is a deterministic knowledge of the carrier signal which is not available in noncoherent detection systems (cf. [1, p.485]). The most important factor that makes noncoherent detection attractive is its simplicity whether it is discriminator, envelope or differential detection. Furthermore, since in an increasing number of important applications the AWGN channel provides an entirely inappropriate model of the propagation environment [2], in some cases noncoherent detection can perform better than coherent detection, e.g. in fading channels [3]. Finally, having a short acquisition time makes noncoherent detection techniques more advantageous over coherent detection for burst communication systems.

Considerable research has been going on to improve both detection techniques to minimize the effects that are considered to be drawbacks. Very briefly, they range from utilizing special signal constellation sets to employing adaptive techniques [4]-[6]. They will be reviewed in more detail in the following section.

Our objective in this work was to design a new receiver structure that would be a kind of combination of both techniques. The main idea here was that although the estimate of the carrier phase in coherent detection in many environments may not be accurate, it may still provide some knowledge which can be made use of in the detection process. Instead of considering the worst case (as is done in noncoherent detection where it is assumed that the carrier phase is randomly changing and has a uniform probability density function), we took into consideration the phase error density function of the carrier recovery circuit (in our case, we assume use of PLL's for the carrier recovery due to their popularity) and came up with some metric expressions. In time dispersive channels, using the metric expressions in detection process gave encouraging results [7]. Applying the metric expressions to Phase Shift Keying (PSK) signals resulted in an expression that is made up of a combination of differen-

tial terms and a coherent term which will be presented and interpreted in Chapter 4. But the application of the whole expression would increase the complexity and the processing time of the receiver considerably. So we decided to truncate the metric expression and apply it to slow fading Rician Channels employing Viterbi Decoding. The resulting receiver structure is more complex than a receiver which employs only a coherent detector or a differential detector. However, the proposed receiver is much simpler than an optimal receiver. The performance of the receiver is evaluated using Monte Carlo simulations. The simulation results for uncoded BPSK and QPSK for different values of signal to noise ratio at the output of the PLL and for different values of direct-to-multipath signal power ratio (Rice factor) will also be presented in Chapter 4.

1.2 Literature Review

It is well known that in many applications, the channel can be reasonably accurately modeled as a Rician fading channel. In [8], Bello identifies five propagation channels and characterizes the links as 1) air-air, 2) air-ground 3) air-space 4) ground-space and 5) ground-air. He states that the channel of major importance in satellite-based air traffic control systems is the surface scatter channel ("the collection of radio paths between a transmitter and receiver, which exists solely due to the intervention of the earth's surface, plus a distortion-free "direct path" between transmitter and receiver") and shows that it can be modeled as a Rician fading channel. In [9], Davarian explains that the presence of a strong and stable path in a fading link will change the envelope statistics of the received waveform from Rayleigh to a more favorable Rician distribution in satellite-to-ground mobile channels. In a number of papers, various autocorrelation functions for the fading processes have been assumed and the spectrum of the processes have been derived. A summary of these autocorrelation functions is given in [10] by Mason. A statistical model for a land mobile satellite link in a rural environment is derived and described in [11] and statistical parameters for

a mobile radio channel is measured and presented in [12]. It is also shown in [10]-[12] that Rician fading channel is a reasonably accurate model for these channels.

For modulation and detection techniques in fading environments, Davarian in [3] examines and discusses different modulation and detection techniques for an aeronautical mobile satellite channel. He considers PSK, GMSK, and QAM as candidates and gives the power vs. standard deviation of carrier phase jitter for these signals. He, as well, discusses coding and interleaving for these channels.

The combination of trellis coding and MPSK signaling is discussed for mobile satellite channels in [4] where only the effect of fading on the amplitude of the signal is considered. It is shown that an asymmetric signal constellation, when used with trellis coded systems, improves the performance. They also give the performance of this new signal constellation when interleaving is used and channel state information is available at the receiver. The same authors in [13] compare the coherent and differential detection of MPSK under the same conditions and for the same channel, except that this time they consider the effect of fading on the phase of the signals, derive some upper bounds from pairwise error probabilities and provide also their curves together with some simulation results. Wilson *et al.*, in [14] deal with DPSK performance on L-band aeronautical satellite channels and give test and simulation results and then investigate error burst characteristics of the channel. Also, the performance of diffuse convolutional codes are evaluated by simulation.

In [15], error rate performances of MDPSK systems are obtained analytically for L-band satellite/aircraft channel for low baud rates considering time selectivity caused by the Doppler Rayleigh interference and the diffuse/specular composite interference. Also, symbol error rate expressions are derived for three kinds of space diversity reception. The performance of coherent and differential PSK systems are compared.

In [2], the performance of short constraint length convolutional codes used with BPSK modulation is given for slow-fading and time-varying Rician channels as well as for uncoded systems. Also, upper bound expressions for error performances are derived.

Lodge *et al.* [16] compare DMSK, DOQPSK and coherently detected BPSK with tone-in-band processing for land mobile satellite channels by running computer simulation programs. Miyagaki *et al.* [17], this time derives double symbol error rates for M-ary DPSK in a satellite-aircraft multipath channel. In [18], analytical performance bounds are derived for trellis coded PSK signals for Rayleigh, Rician and shadowed Rician channels and compared with simulation results. Korn [19] derives error probability expressions for M-ary DPSK and M-ary FSK with limiter discriminator detection in Rician, Rayleigh and Gaussian channels for various values of fading bandwidth symbol duration products. Loo, based on his model of shadowed Rician channel [11], derives analytical expressions for bit error probabilities of noncoherent FSK, CPSK and calculates irreducible probability of bit error for CPSK due to phase variations and fading [20].

The phase error probability density function (pdf) which we employ in the derivation of our metric expressions is originally obtained for Phase Locked Loops (PLL's) by observing that the pdf of the phase error is satisfying the Fokker-Planck differential equation [21]. From the literature it was interesting to see that PLL's still find many applications in modern digital transmission systems. Our main interest here is their application in coherent detection systems. Phase comparator is an important component in PLL's. Because of their easy implementation in analog circuitry, sinusoidal phase detectors are preferred. But efforts to improve acquisition performance of PLL and other applications of PLL, e.g. clock recovery, led to the use of sawtooth phase comparators. Öberst [22] investigates a generalized phase comparator which he calls a "phase-and-frequency comparator", gives several circuit implementations and shows that pull-in range is greatly increased without altering the performance of the loop in filtering mode. The complexity of this comparator is similar to that of a sawtooth phase comparator. Saito and Suzuki [23] propose a novel carrier recovery circuit for coherent detection to be used in digital land mobile radio transmission which has two modes of operations and the circuit selects one of two operation modes according to the fading environment: Costas loop mode or adaptive carrier tracking

mode. They give the experimental results for GMSK and QPSK to demonstrate how this fast carrier tracking coherent detection technique improves the performance of coherent detection.

In literature it is possible to meet with the term "partially coherent detection" at several different books and papers. Viterbi [24], Van Trees [25] and Spilker [26] all use the term in the sense that perfect carrier phase cannot be obtained due to phase error in the system. Aulin and Sundberg refer to partially coherent detection as the weighted combination of optimum metrics for coherent and noncoherent detectors in [27], which in our work we deal with in a similar manner, where they applied it to CPM signals. Another version of partially coherent detection can be found in [28]. Here, Harold and Kingsbury again applied it to CPM signals but instead of using a PLL to track the phase of the carrier, by assuming only that the carrier phase is constant over a few symbol intervals, they incorporate phase estimation within the Viterbi Algorithm by processing a sequence of symbols.

1.3 Thesis Organization

In Chapter 2, the channel models considered in this thesis are introduced. These are AWGN channel with a noisy phase reference, Rician channel and Rician channel with a noisy phase reference. All the assumptions made in these models are explained.

In Chapter 3, after a description of PSK signals (BPSK and QPSK), their coherent, differential and multi-differential detection is explained. Analytical expressions for their performance in AWGN channels and Rician channels are given and bit error rate performance curves obtained by simulations are plotted and compared with the ones given in literature.

In Chapter 4, the description of partially coherent detection is given. Metric expressions are derived and applied to PSK signals. We derive the metric expressions both for ideal and distorted (time dispersive) channels. Then, considering the complexity of the expression for PSK signals, it is simplified by examining the expression

under two cases: high $\frac{E_b}{N_0}$ and low $\frac{E_b}{N_0}$. An interpretation of these metric expressions are given. The metric expression for the case of high $\frac{E_b}{N_0}$ is truncated under certain assumptions and simulated using a Monte Carlo technique. The BER performance of partially coherent detection of uncoded BPSK and QPSK signals obtained through these simulations are presented for different signal to noise ratios of carrier recovery loop and direct component power to diffuse component power ratios. Comparison with coherent and differential detection performances under same circumstances using the models introduced in Chapter 2 are also provided. The results obtained are interpreted.

Chapter 5 concludes the results of this work and suggestions for future research are listed.

Chapter 2

CHANNEL MODEL

In this chapter, channel models which incorporate some of the imperfections are presented. The models are based on three considerations. The first one is the case where the channel is an AWGN channel and the phase reference used is noisy. The second one is for slowly varying Rician fading channels where the phase variations due to fading can be tracked by the carrier recovery circuit and the AWGN noise introduces no phase noise on the carrier. Finally, the third one is the same as the second model but this time there is phase noise due to AWGN.

Contrary to classical textbook treatment, all coherent systems suffer from some phase jitter. This is due to the conflicting requirements of the circuits used in extracting the coherent carrier reference. For example, the use of PLL's are very common in communication systems employing coherent detection. One of the important components of the PLL is the loop filter.. The conflicting requirement on the design of the loop filter is that for rapid acquisition and large pull-in range, PLL should have a wideband, high gain characteristic. On the other hand, it is required that the local reference signal be shielded from noise and phase jitter on the input signal and this can be achieved by a low-gain narrowband filter. So in AWGN channels, in practice, some phase jitter in the reference signal is inevitable. Even if the rapid acquisition and large pull-in range were not a requirement, in mobile communications, the bandwidth of the loop filter would have to be wide enough to track the doppler shift in frequency

anyway. To get a more realistic evaluation of the performance of these systems, we have to consider this phase jitter. The first and third models were built considering this fact. Furthermore, especially in mobile communication systems where there is a line-of-sight (LOS) component, the channel has the characteristics of a Rician fading channel. Our second and third model were built to realize the fading characteristics of this channel.

2.1 AWGN Channel with a Noisy Phase Reference

In coherent communication systems, it is very important to accurately estimate the phase of the carrier, so that the incoming signal at the receiver can be demodulated by generating a replica of the carrier that was used to modulate an information bearing signal. One way of achieving this is by employing a PLL and this is what we assume being used[1]. Although there are analog, analog-digital (hybrid), discrete and digital PLLs, we base our analysis on the theory of analog PLL's. To have a better insight to the models and to see how well they represent the real practical situation, it is necessary at this point to have a brief look at how PLLs function.

The basic structure of analog PLL is given in Fig. 2.1. Phase detector compares the phase of the incoming signal with the phase of the signal at the output of the VCO. The output frequency of the VCO changes in a direction so as to reduce the phase difference of the incoming signal and the reference signal. Phase detector characteristics can be sinusoidal, triangular or sawtooth. Since it is the most common one, sinusoidal one will be considered here. In this case, the phase comparator is simply a multiplier. The PLL is said to be locked when the frequency of the VCO is exactly equal to the average frequency of the incoming signal. Basic PLL and its model is given in Fig. 2.2. In the model, additive noise is neglected. $\Gamma = \Gamma_1\sqrt{A}$ represents the total gain, i.e. gain of VCO and phase detector. The analysis of the

[1]This is not the only application of a PLL. In addition to demodulation, it is employed for synchronization, tracking and ranging. But our main interest is in its application in demodulation.

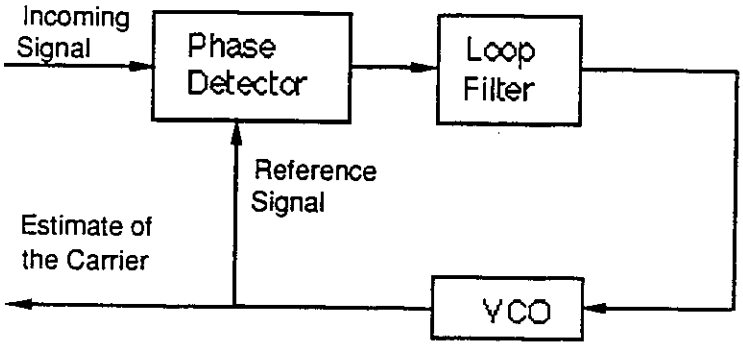

Figure 2.1: Basic configuration of a phase-locked loop.

PLL is considerably simplified if $\epsilon(t)$ is small. Then, since $\sin(\epsilon(t)) \approx \epsilon(t)$ for small $\epsilon(t)$, the sinusoidal nonlinearity is removed from the model. The new model is as shown in Fig. 2.3. This model gives the opportunity to analyze the PLL without much additional difficulty when the noise is present, since the Gaussian noise process is independent of the incoming signal and the system is linear.

Nonlinear model of a PLL when additive white Gaussian noise is considered is as shown in Fig. 2.4. Probability density function of the phase error satisfies the Fokker-Planck differential equation and the solution derived by Fokker-Planck techniques is given in [24] (which is well known to be Tikhonov density) as

$$p(\phi) = \frac{\exp(\xi \cos\phi)}{2\pi I_0(\xi)} \tag{2.1}$$

where $\xi = \frac{4A}{\Gamma N_0}$ is the signal to noise ratio (SNR) at the output of the PLL and $I_0(\cdot)$ is the modified Bessel function of order zero. For large SNR using the approximation

$$I_0(\xi) \approx \frac{\exp(\xi)}{\sqrt{2\pi\xi}}, \tag{2.2}$$

utilizing the identity $\cos\phi = 1 - 2\sin^2\frac{\phi}{2}$ and recognizing that ϕ is small at large SNRs, an approximate expression for the pdf of ϕ can be found as

$$p(\phi) \approx \frac{\exp(\frac{-\xi\phi^2}{2})}{\sqrt{\frac{2\pi}{\xi}}} \qquad \xi \gg 1 \tag{2.3}$$

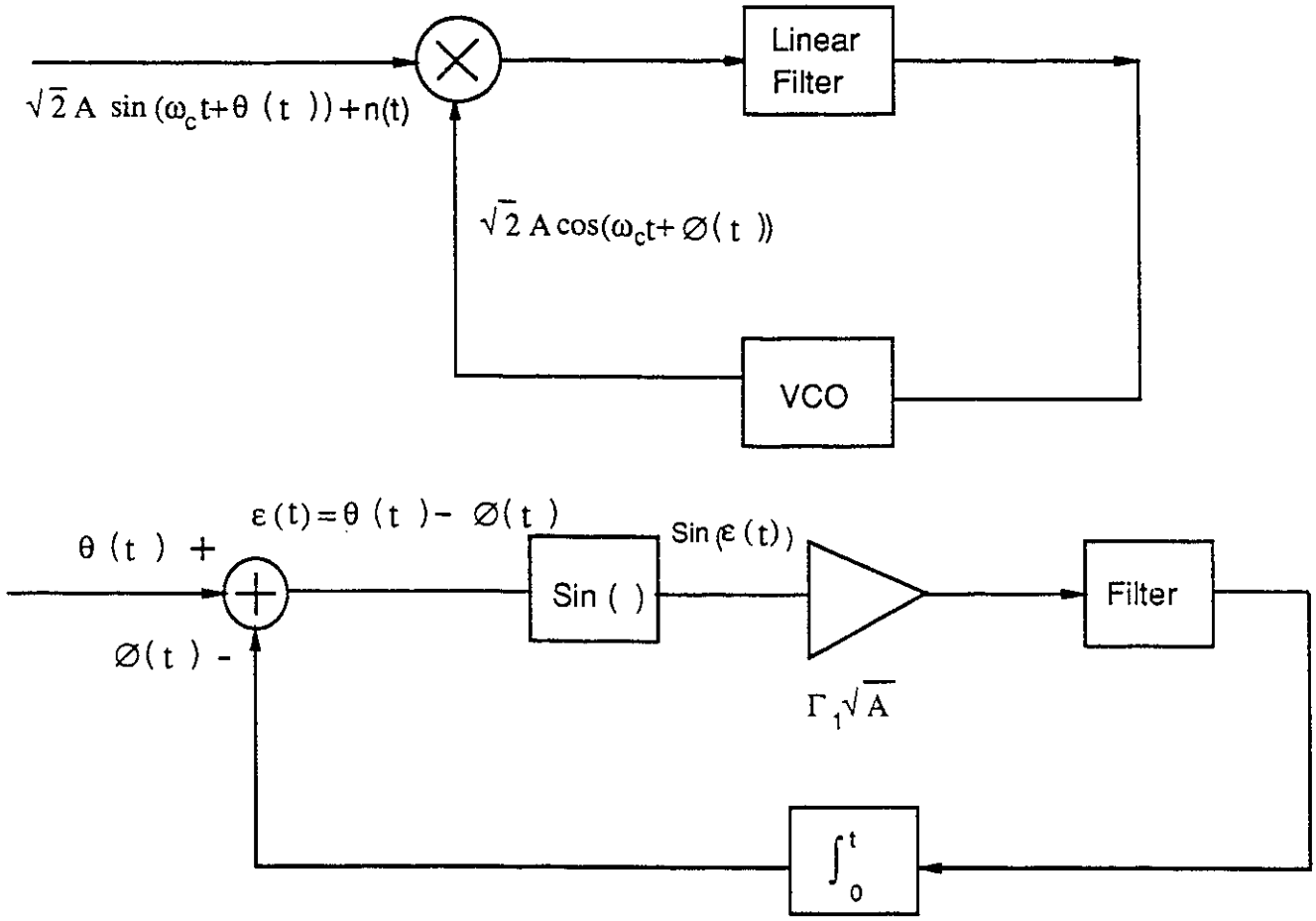

Figure 2.2: Basic PLL and its model.

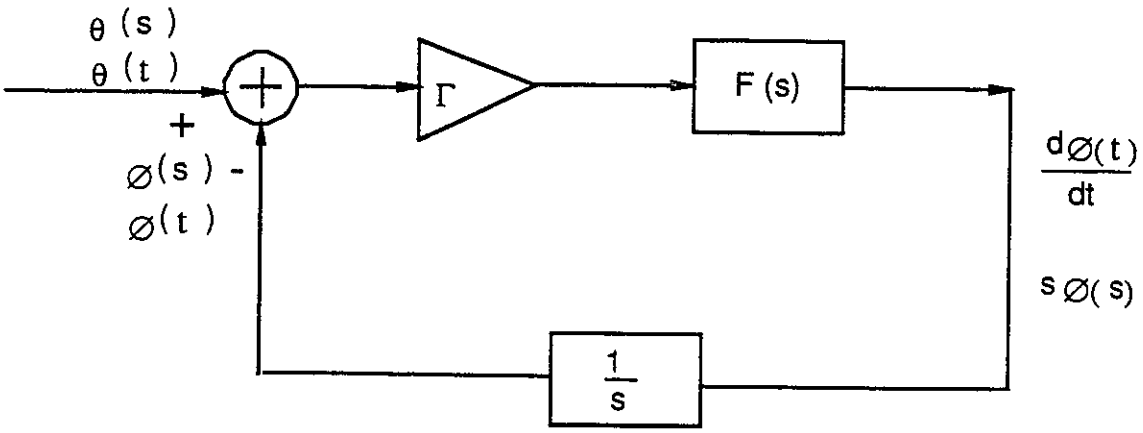

Figure 2.3: Linear model of PLL.

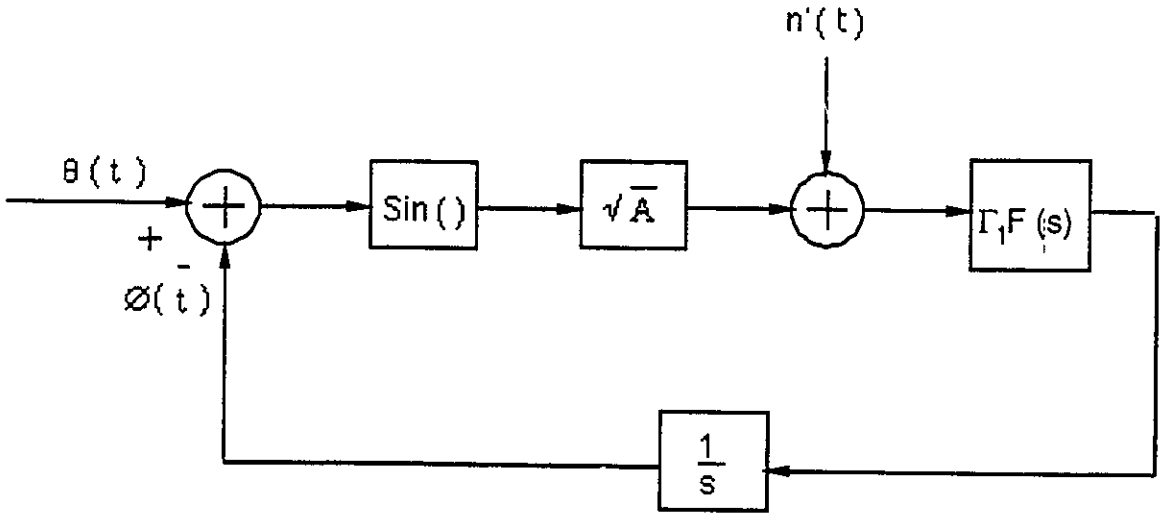

Figure 2.4: Model of PLL with AWGN.

which is a Gaussian pdf.

Our model for AWGN channel with phase error taken into account is shown in Fig. 2.5 with

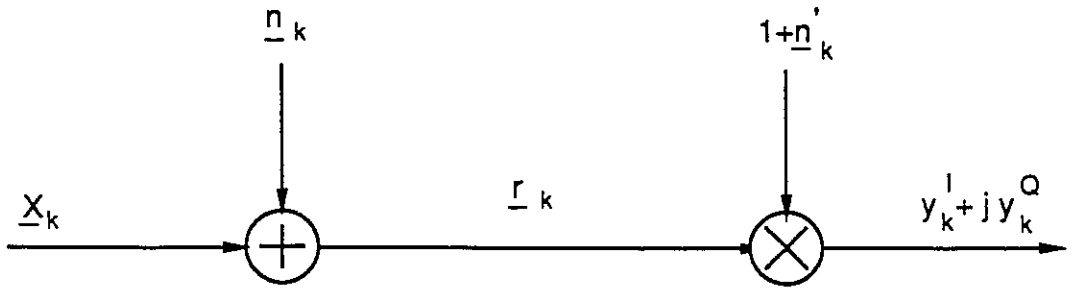

Figure 2.5: Model of AWGN channel with noisy phase reference.

$$\underline{x}_k = x_k^I + jx_k^Q \tag{2.4}$$

$$\underline{n}_k = n_k^I + jn_k^Q \tag{2.5}$$

$$\underline{r}_k = r_k^I + jr_k^Q \tag{2.6}$$

$$\underline{n'}_k = n'^I_k + jn'^Q_k \tag{2.7}$$

and

$$\underline{r}_k = \underline{x}_k + \underline{n}_k. \tag{2.8}$$

x_k^I and x_k^Q are the samples of the in-phase and quadrature components of the baseband equivalent of the transmitted signal, n_k^I and n_k^Q are the samples of the in-phase and quadrature components of the baseband equivalent of the bandpass Gaussian noise, r_k^I and r_k^Q are the samples of the in-phase and quadrature components of the baseband equivalent of the received signal and finally the multiplication with $(1 + \underline{n}'_k)$ is to implement the phase error introduced by imperfect estimation of the phase of the carrier

where n'^I_k and n'^Q_k are the samples of the in-phase and quadrature components of a narrowband Gaussian process. It has been shown in [29] (see Appendix I of [29]) that the pdf of the phase of a two dimensional vector $X = A + N_R + jN_I$ which represents a real constant A perturbed by a complex Gaussian process is asymptotically:

$$\lim_{\sigma^2 \to 0} P_v(u; \frac{A^2}{\sigma^2}) = \frac{\exp[(\frac{A^2}{\sigma^2})\cos(u)]}{2\pi I_0(\frac{A^2}{\sigma^2})} \tag{2.9}$$

where σ^2 is the variance of Gaussian random variables N_R, N_I and v is the phase of the vector X. The exact density function compared with the Tikhonov density function for $SNR = 0, 3$ and 6 dB are plotted in Fig. 1 of [29] as shown in Fig. 2.6. From the figures it can be observed that as SNR gets larger, the phase density function gets closer to Tikhonov pdf. For $SNR = 6$ dB, it is a very good approximation. So, we can conclude that the phase error at the PLL can accurately be implemented by multiplying the signal by $(1 + n'^I_k + jn'^Q_k)$ for $SNR \geq 5$ dB because this phase error will be reflected to the filtered received signal during demodulation process (since the signal will be multiplied by the estimate of the "carrier"). Another approach to verify the model is to show that the phase of $(1 + n'^I_k + jn'^Q_k)$ is Gaussian for high SNR. Since

$$\tan(\phi) = \frac{n'^Q_k}{1 + n'^I_k} \approx \frac{n'^Q_k}{1} = n'^Q_k \tag{2.10}$$

and at high SNR ϕ is small, then $\tan(\phi) \approx \phi$; and this shows that the density function of the phase of the vector is Gaussian. Nevertheless, from the model of the PLL with AWGN (Fig. 2.4), for the SNRs that are of interest to us the $\sin(\cdot)$ nonlinearity can be removed and the PLL can be viewed as a bandpass filter. In fact, for carrier recovery circuits in general, a bandpass filter is needed and in many applications a PLL is used as a bandpass filter (cf. [27, p. 411]). So, the model described above can be quite an accurate one for phase noise in many carrier recovery circuits.

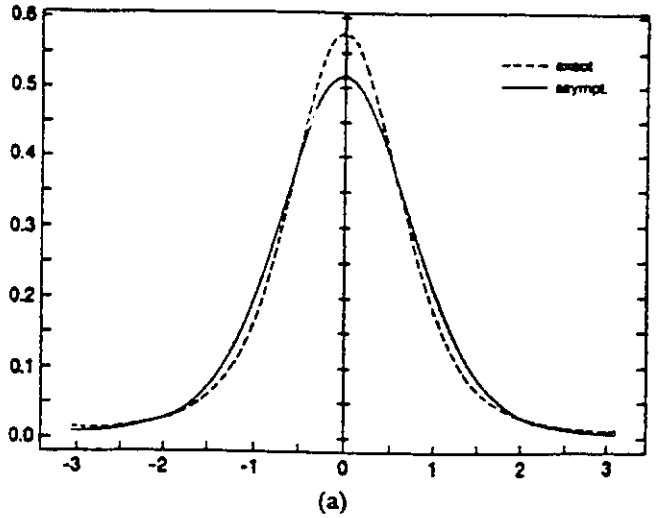

Figure 2.6: Exact and asymptotic (Tikhonov) pdf of phase of a vector perturbed by zero-mean Gaussian noise. (a) SNR=0 dB. (b) SNR=3 dB. (c) SNR=6 dB. [29]

2.2 Rician Channel Model

A major source of fading in communication systems is due to multiple transmission paths. If the received multipath signal is made up of numerous reflected components, it is noiselike and is called *diffuse*; if it is made up of one or two strong reflected rays, it is called *specular*. If the latter one is not reflected, it is called *line-of-sight (LOS)* or *direct* component. If the received signal is composed of a specular and a diffuse component, the envelope of the received signal is Rician distributed and it is called a *Rician fading channel*. If a specular component does not exist or is very weak compared to the diffuse component, the signal envelope has Rayleigh distribution and thus a *Rayleigh fading channel*. So, Rayleigh channel is a special case of Rician channel where the specular component is absent.

There are different measures that define the characteristics of a fading channel. Especially in mobile communications, due to the constantly changing environment, the signals that arrive via multiple paths at the receiving antenna are displaced in time and space (cf. [28, p. 18]). This will have an effect of lengthening the time alloted to discrete portion of the signal information and can cause signal smearing which is called delay spread. Furthermore, the arrival of two closely spaced frequencies with different time-delay spreads can make the statistical properties of the two multipath signals to be weakly correlated. The maximum frequency difference between frequencies having a strong potential for correlation is called *coherence bandwidth* [30]. If the signal bandwidth is much smaller than coherence bandwidth, then the fading is called *frequency nonselective*. Frequency nonselective fading appears as multiplicative distortion of the transmitted signal [31]. Then the diffuse component can be represented as the product of a complex zero-mean Gaussian process and the original transmitted signal component [2]. With the help of the information given above, the frequency nonselective Rician channel can be modeled as shown in Fig. 2.7. In this figure, $\underline{n}''_k = n''^I_k + jn''^Q_k$ with n''^I_k and n''^Q_k being the in-phase and quadrature components of a complex Gaussian process having variances $\sigma''^2_I = \sigma''^2_Q = \sigma''^2$ and $\underline{n}_k$ and

Figure 2.7: Complex baseband equivalent model of Rician Channels.

$\underline{r}_k$ are as defined in Eq. (2.5) and Eq. (2.6) respectively. The nature and strength of fading is determined by *K-factor (Rice factor)* which is the ratio of the power of direct component to the diffuse component, i.e.

$$K = \frac{1}{2\sigma''^2}. \tag{2.11}$$

where direct component power is assumed to be 1. Both $n''_I(t)$ and $n''_Q(t)$ are obtained by passing two independent Gaussian processes with one-sided power spectral densities N_0 through Butterworth lowpass filters with one sided equivalent noise bandwidths of B. Then, the average powers of $n''_I(t)$ and $n''_Q(t)$ are both

$$\sigma''^2 = N_0 B. \tag{2.12}$$

Fading amplitude $a(t) = \sqrt{(1 + n''_I(t))^2 + (n''_Q(t))^2}$ is Rician with pdf:

$$P(a) = \frac{a}{\sigma''^2} \exp(-\frac{a^2+1}{2p}) I_0(\frac{a}{p}) \quad . \tag{2.13}$$

A similar model is also given in [32].

2.3 Rician Channel With Noisy Phase Reference

Since noisy phase reference has an impact during the demodulation process, the channel model is same as shown in Fig. 2.7 and explained in the previous section.

We have two different models for the demodulation process. The models are shown in Figs. 2.8 and 2.9. In Model 1, it is assumed that the loop filter has such a narrow

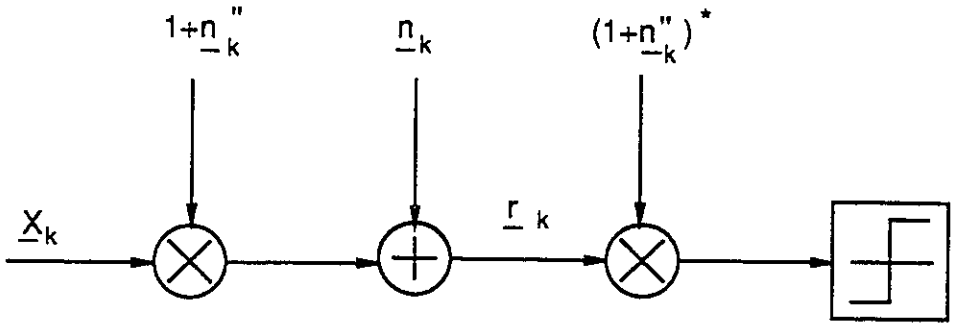

Figure 2.8: **Model 1** for the Rician channel and the demodulation process (perfect phase tracking).

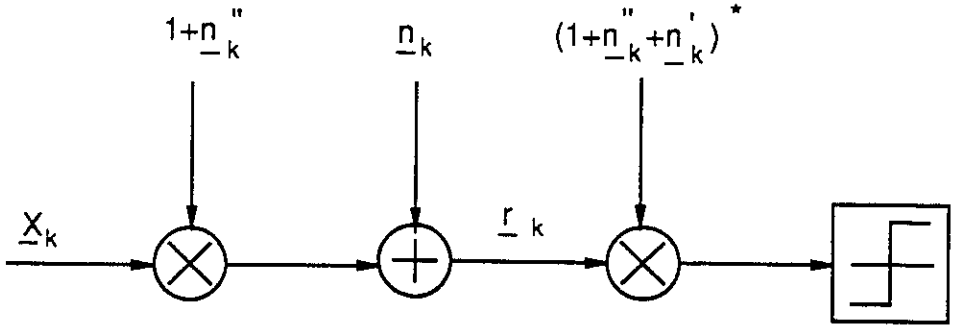

Figure 2.9: **Model 2** for the Rician channel and the demodulation process (noisy phase reference).

bandwidth that there is no phase error due to the Gaussian noise that has entered the system. In other words, the loop filter lets in no Gaussian noise and the estimate of the phase is perfect if fading is neglected. On the other hand, it is assumed that the loop filter bandwidth is wide enough to track the phase changes caused by fading perfectly. So, there is no phase error imposed on the system either due to Gaussian

noise or due to fading. The only distortion in the carrier is the amplitude fluctuations imposed by fading. This is the model assumed by many authors and is not realistic.

In the second model, we assume that the Gaussian noise that passes through the narrow bandwidth of the loop filter causes a phase error in the estimation of the carrier phase but the loop bandwidth is wide enough to track the changes in phase due to fading. At this point, we should mention that we are neglecting the cross product terms between the fading and the conjugate of the Gaussian process causing the phase error since both are small compared to the signal level. Also, it should be noticed that taking the conjugate of $n'_I + jn'_Q$ does not change the statistics of the process. At this point, we should define the SNR ξ at the output of the carrier recovery circuit:

$$\begin{aligned} \xi &= \frac{E\{(1+n''_I+jn''_Q)^2\}}{E\{(n'_I+jn'_Q)^2\}} = \frac{1+E\{n''^2_I\}+E\{n''^2_Q\}}{E\{n'^2_I\}+E\{n'^2_Q\}} \\ &= \frac{1+2\sigma''^2}{2\sigma'^2} = \frac{1+\frac{1}{K}}{2\sigma'^2} = \frac{K+1}{K}\frac{1}{2\sigma'^2} \end{aligned} \tag{2.14}$$

In the above equation, we observe that the signal power with fading is different from the signal power with no fading. This will also affect the signal energy per bit (E_b). The E_b when there is fading is related to E_b when there is no fading by the following relation:

$$E_{b_f} = E_{b_{nf}}\frac{K+1}{K} \tag{2.15}$$

As a last comment on the model 2, we observe that it reduces to the model of AWGN with noisy phase reference (Fig. 2.5) if the fading process is made zero and it reduces to Rician channel model (Fig. 2.7) when the Gaussian noise through the loop filter $(n'_I(t)+jn'_Q(t))$ is made zero.

2.4 Conclusions

In this chapter, channel models which take into account some imperfections were presented. Considering that all coherent systems suffer from some phase jitter, the first

model was for AWGN channels with a noisy phase reference. The second model was for Rician channels which many mobile communication channels can be represented with. Finally, the last model was for Rician channels with a noisy reference. It has been shown that although the models are simple, they are realistic. In the next two chapters, performance of PSK signals using these channel models will be evaluated.

Chapter 3

DETECTION OF PSK SIGNALS

In this chapter, after a brief description of PSK signals, the performance of uncoded BPSK and QPSK with coherent and differential (differentially coherent) detection in AWGN channels and slowly varying Rician channels will be examined. The coherent detection case for AWGN channels is simulated with and without phase noise. In Rician fading channel case, it is assumed that the carrier recovery circuit can track the changes in the phase of the carrier due to fading, but the phase reference is noisy because of the narrowband Gaussian noise that is let in by the filter. The simulation results will be compared with the ones available in literature. This will give us the opportunity to verify the correctness of our models.

3.1 Description of PSK Signals

PSK signals are used in many communication systems (especially in digital satellite communication) due to their relatively good power and bandwidth efficiencies.

Constellation points of M-ary PSK signals lie on a circle. Assuming equal phase difference between the constellation points, the signal can be represented as:

$$x(t) = \sqrt{2P_1}\cos(\omega_c t + \theta_m) \quad for \quad (m-1)T \leq t \leq mT \tag{3.1}$$

where θ_m represents information phases. θ_m can take the values $\frac{2\pi(i-1)}{M} \quad for \quad i = 1, \ldots, M$. M is the number of phases; it is 2 for BPSK, 4 for QPSK, 8 for 8PSK

and so on. Since with each symbol transmitted $\log_2 M$ bits are sent, increasing M, increases the bandwidth efficiency. Although larger values of $M \geq 8$ have greater bandwidth efficiency compared to biphase and quadriphase shift keying, they are less efficient in the use of power [26].

3.1.1 BPSK

For BPSK, θ_m is zero for binary zero and π for binary one. Let d_k represent the binary sequence of zeros and ones. Then the waveform is simply:

$$x(t) = \mp\sqrt{2P_1}\cos(\omega_c t) \quad kT_b < t \leq (k+1)T_b \quad \begin{cases} + & \text{for } d_k = 1 \\ - & \text{for } d_k = 0 \end{cases} \tag{3.2}$$

The block diagram of a BPSK transmitter is shown in Fig. 3.1. The differential

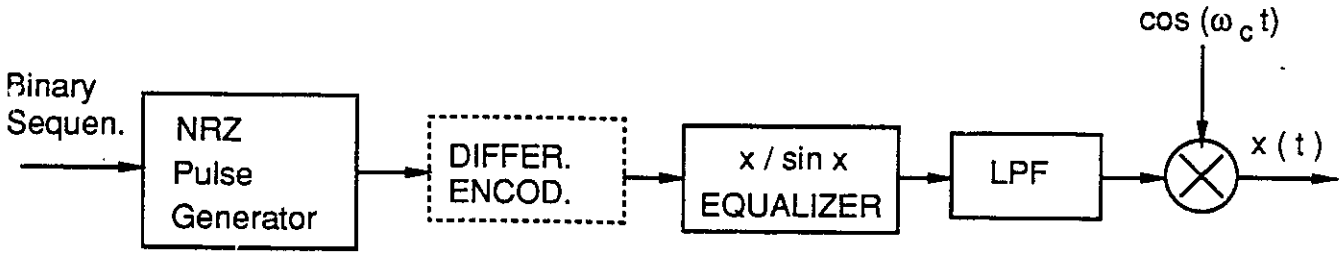

Figure 3.1: Block diagram of a BPSK transmitter.

encoder is needed if differential detection is employed at the receiver. It is optional if coherent detection is used. The reason for employing a differential encoder for coherent case is to prevent phase ambiguity in determining the phase of the carrier. The ambiguity is caused by the squaring process (the nonlinearity introduced) at the receiver for BPSK to extract the carrier phase from the received signal. A sync pattern (unique word) instead of differential encoding can also prevent this ambiguity. Unique word is a requirement in TDMA for frame synchronization anyway. For uncoded systems differential encoding approximately doubles the error rate because an error in the demodulated phase of the signal will cause a decoding error in two consecutive

intervals. But this factor of two corresponds to a relatively small loss in SNR [cf. [31], p.266]. For coded systems the performance is usually best if the differential encoder precedes the FEC coder and follows the decoder [cf. [26], p. 300].

3.1.2 QPSK

The signal constellation for QPSK is usually in one of the two forms that is shown in Fig. 3.2. In this case, the phase of the carrier is shifted by $\frac{\pi}{2}$ radian increments

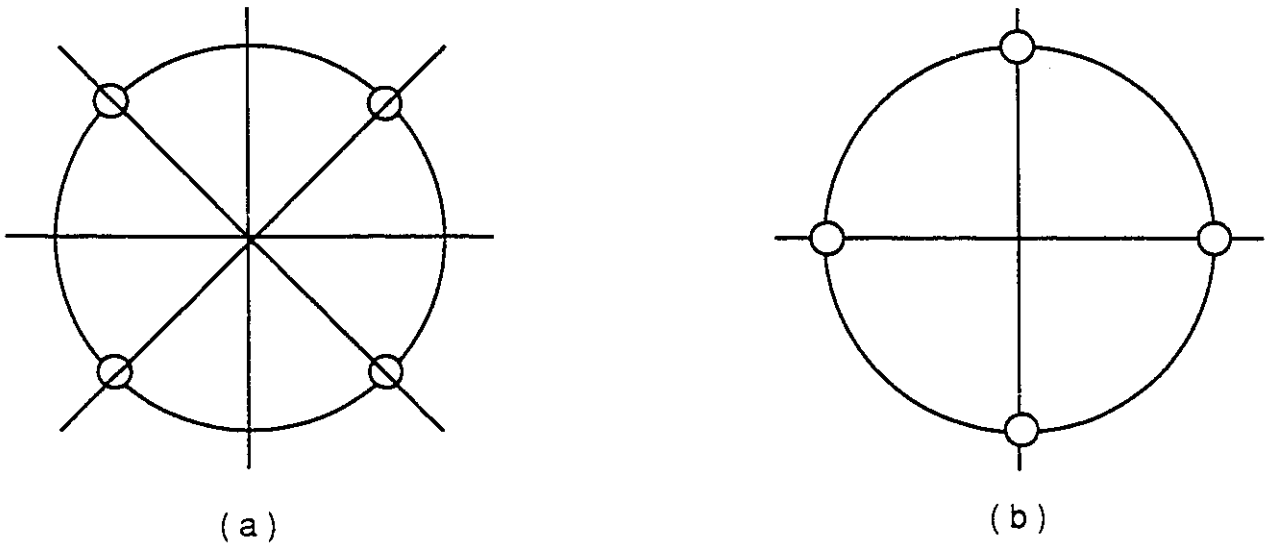

Figure 3.2: Signal constellations of QPSK.

for the quadrature part. Sequences from both channels are processed and the bit to symbol mapping is done according to Gray coding so that neighbouring symbols differ in one bit. This reduces the number of errors when erroneous decision is made in favor of one from the symbols which are the closest to the transmitted one. The phase ambiguity in QPSK is due to the fourth power nonlinearity and is $\frac{\pi}{2}$ radians.

3.2 Coherent Detection of PSK Signals

In coherent detection, the major task is to obtain a coherent reference to be used in demodulation. The carrier recovery can be achieved in alternate ways, also depending on the number of phases (M) employed. A matched filter detector can follow which is known to be optimal for ideal AWGN channels. If differential encoding is employed, a differential decoder will be needed at the receiver, to recover the original information. For applications where carrier phase noise effects are not severe, coherent detection performs better than noncoherent detection. Although phase deviations different than $\frac{2\pi}{M}$ (e.g. to obtain a residual carrier component) and different types (e.g. Offset Keyed QPSK (OKQPSK) to decrease the phase jumps in QPSK) of PSK signals can be employed, we will simply consider uncoded BPSK and QPSK with the signal constellation shown in Fig.3.2.

For BPSK, a typical receiver is a coherent matched filter receiver as shown in Fig. 3.3. The matched filter is an integrator if the pulse shape is rectangular (i.e.

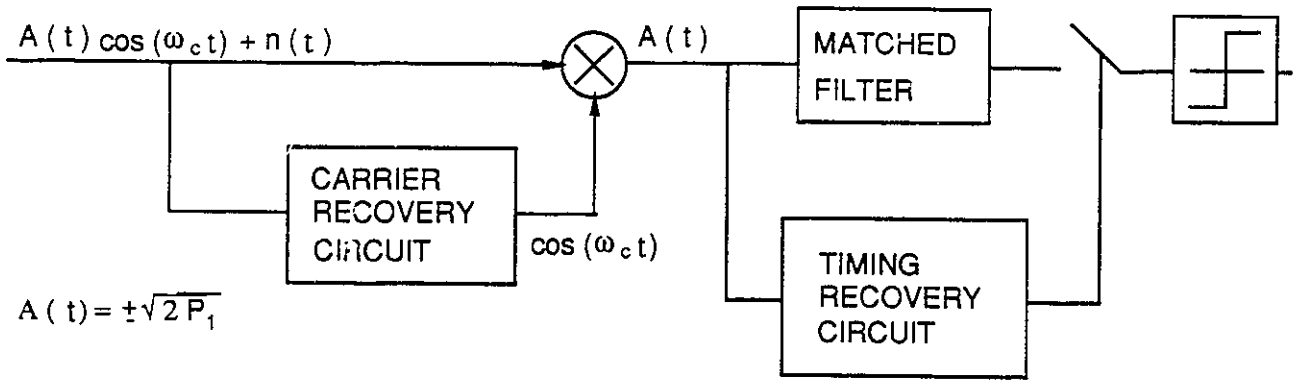

Figure 3.3: Block diagram of coherent matched filter BPSK receiver.

nonreturn-to-zero (NRZ) signal shaping is used). The integrator and its impulse

response is shown in Fig. 3.4. This structure is called integrate sample and dump filter

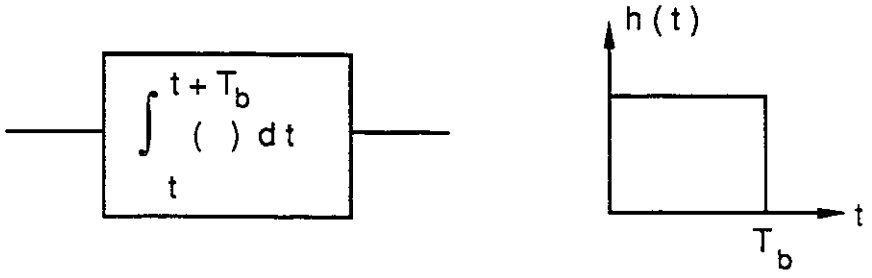

Figure 3.4: The integrate and dump filter and its impulse response.

and acts as a lowpass filter. Its output should be reset to zero after each sampling. For ISI free equally apportioned systems operating in a pure AWGN environment and under the assumption that carrier recovery and bit synchronization is perfect, the bit error rate performance of BPSK is given by the equation [31]

$$P_b = Q(\sqrt{\frac{2E_b}{N_0}}) \tag{3.3}$$

where

$$Q(x) = \frac{1}{\sqrt{2\pi}} \int_x^\infty \exp\{-\frac{y^2}{2}\} dy \tag{3.4}$$

and E_b, N_0 are the signal energy per bit and the one sided noise spectral density respectively. For differentially encoded and coherently decoded signals, this rate will double, i.e. $P_{de} = 2P_b$.

For QPSK, the receiver is made up of two matched filter receivers (operating on the inphase and quadrature channels) as shown in Fig. 3.5. The exact expression for symbol error probability of QPSK is given in [33] as

$$P_s = 2Q(\sqrt{\frac{2E_b}{N_0}}) - Q^2(\sqrt{\frac{2E_b}{N_0}}). \tag{3.5}$$

For Gray coding, the symbols at two adjacent phases will differ only in one bit and since most of the errors will be made by decoding the adjacent phase (at least for

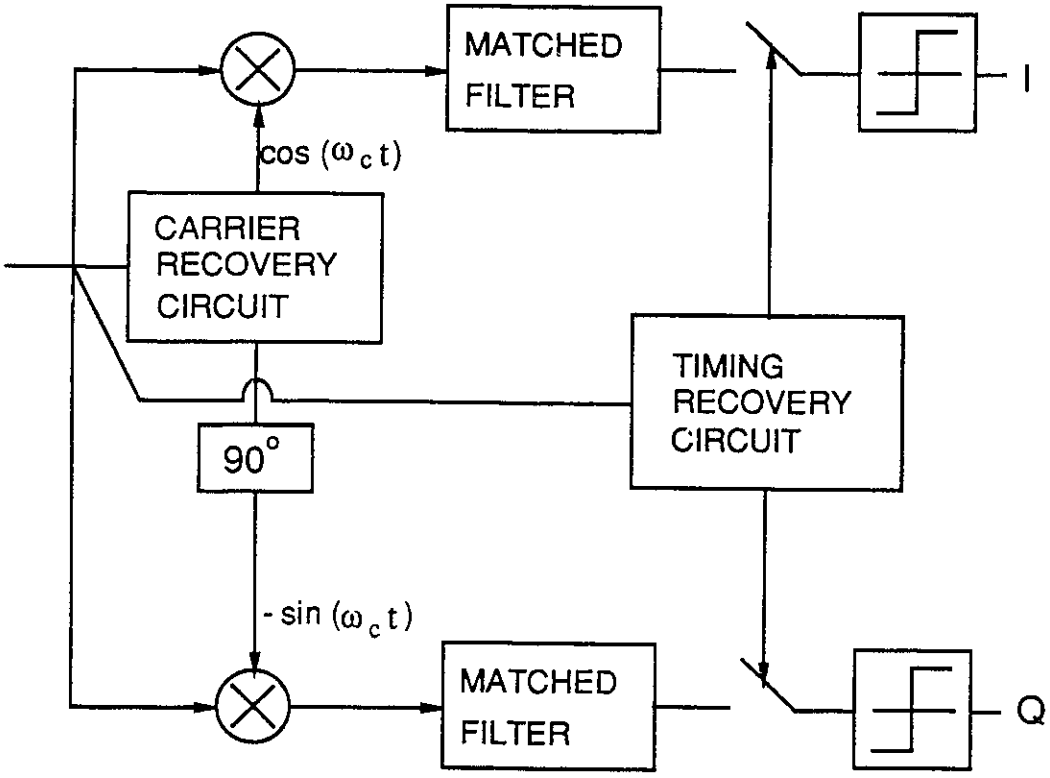

Figure 3.5: Block diagram of a matched filter QPSK receiver.

high $\frac{E_b}{N_0}$), the bit error probability will be approximately half of the symbol error probability. Also neglecting the $Q^2(\cdot)$ term which is small compared to $Q(\cdot)$ term, the bit error probability becomes

$$P_b = Q(\sqrt{\frac{2E_b}{N_0}}) \tag{3.6}$$

which is exactly the same as the one in the BPSK case. Preserving the same bit error rate, QPSK has the advantage of allowing a bit rate twice of BPSK in the same bandwidth.

The bit error rate performance curves of coherent BPSK, QPSK and Differentially Encoded BPSK (DECBPSK), QPSK (DECQPSK), both from the tables available in [34] (indicated as Lin. & Simon in the legend) and obtained by simulations are plotted in Fig. 3.6. This figure verifies that our simulation results closely match the theoretical performance.

3.2.1 Performance of PSK Signals in AWGN Channels With a Noisy Phase Reference

As mentioned in the introductory part of Chapter 2, PLLs used to track the phase of the carrier will let in some noise depending on their equivalent noise bandwidths. This will cause a phase error in the estimate of the carrier phase. For BPSK and QPSK the phase error ϕ, in the estimation of the carrier phase will result in a correlation loss of $\rho(\phi)$. Given the phase error ϕ, the probability of bit error is given in [35] as:

$$P_b = Q(\sqrt{\frac{2E_b}{N_0}}\rho(\phi)). \tag{3.7}$$

In the case of BPSK, let $A(t)\cos(\omega_c t+\theta)$ be the transmitted signal, with θ representing arbitrary phase of the carrier, and let the carrier recovery circuit provide the phase estimate of $\hat{\theta}$. Using the estimate $\hat{\theta}$ for demodulation gives:

$$\begin{aligned} s(t) &= A(t)\cos(\omega_c t+\theta)\cos(\omega_c t+\hat{\theta}) \\ &= \frac{1}{2}[A(t)\cos((\omega_c t+\theta)+(\omega_c t+\hat{\theta}))+A(t)\cos((\omega_c t+\theta)-(\omega_c t+\hat{\theta}))] \\ &= \frac{1}{2}A(t)\cos(2\omega_c t+\theta+\hat{\theta})+\frac{1}{2}A(t)\cos(\theta-\hat{\theta}). \end{aligned} \tag{3.8}$$

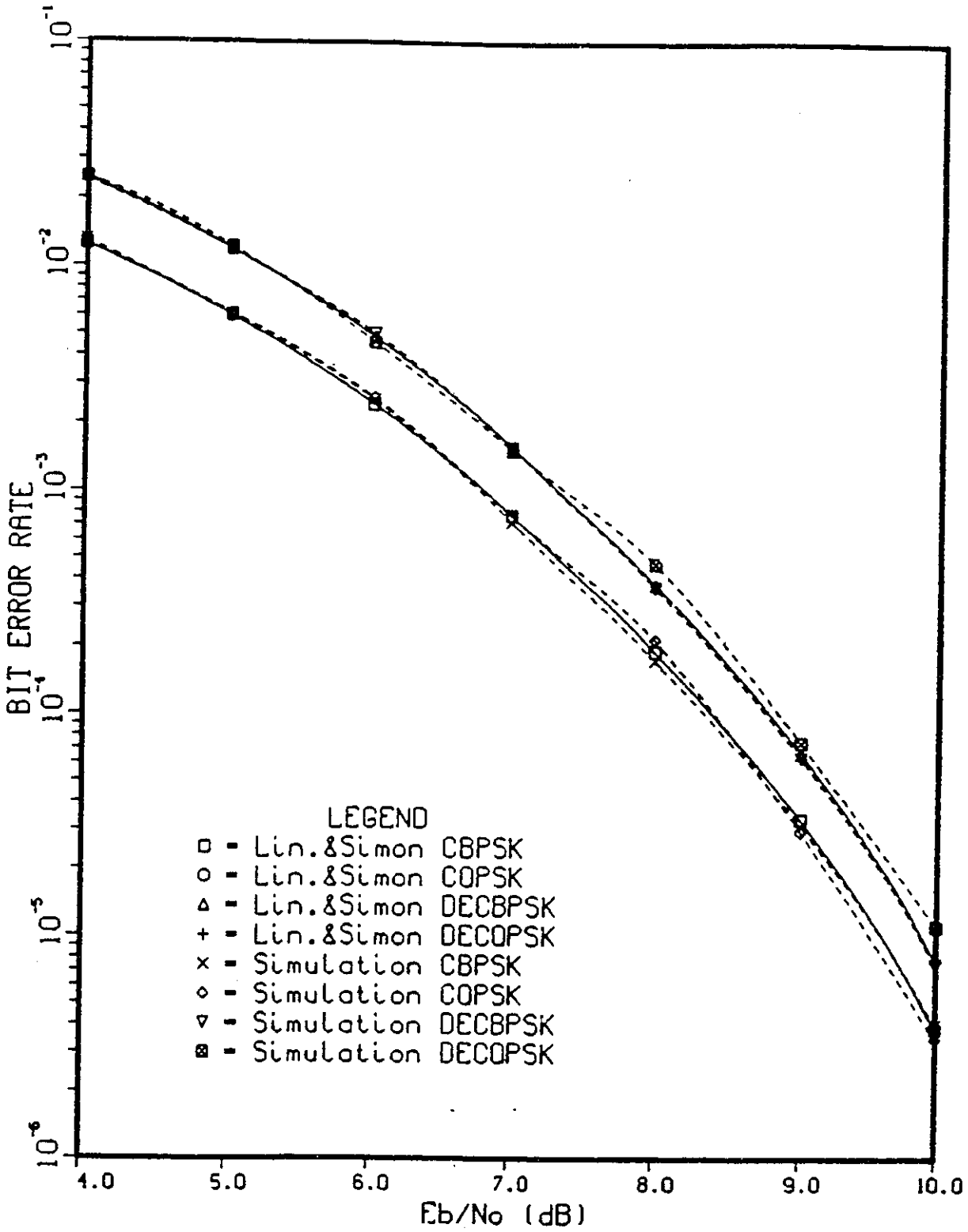

Figure 3.6: The BER performance curves for CBPSK, CQPSK and DECBPSK, DECQPSK. Lin.& Simon: [34].

The lowpass filtering will remove the $2\omega_c t$ component giving

$$s'(t) = \frac{1}{2}A(t)\cos(\theta - \hat{\theta}) = \frac{1}{2}A(t)\cos(\phi) \tag{3.9}$$

where $A(t) = \pm\sqrt{2P_1}$, P_1 representing the signal power. If the carrier phase estimation was perfect, we would end up with $\frac{1}{2}A(t)$. So the noisy phase reference introduces a correlation loss of $\cos\phi$.

For the QPSK case, quadrature form of the signal can be represented as

$$x(t) = A_I(t)\cos(\omega_c t + \theta) - A_Q(t)\sin(\omega_c t + \theta). \tag{3.10}$$

The inphase component of the demodulated signal will be

$$\begin{aligned} s_I(t) &= A_I(t)\cos(\omega_c t + \theta)\cos(\omega_c t + \hat{\theta}) - A_Q(t)\sin(\omega_c t + \theta)\cos(\omega_c t + \hat{\theta}) \\ &= \frac{1}{2}A_I(t)[\cos(2\omega_c t + \theta + \hat{\theta}) - \cos(\theta - \hat{\theta})] - \frac{1}{2}A_Q(t)[\sin(2\omega_c t + \theta + \hat{\theta}) \\ &\quad + \sin(\theta - \hat{\theta})]. \end{aligned} \tag{3.11}$$

After filtering out the double frequency terms, it becomes

$$s'_I(t) = \frac{1}{2}A_I(t)\cos(\theta - \hat{\theta}) - \frac{1}{2}A_Q(t)\sin(\theta - \hat{\theta}). \tag{3.12}$$

Similarly, the quadrature component

$$\begin{aligned} s_Q(t) &= A_I(t)\cos(\omega_c t + \theta)\sin(\omega_c t + \hat{\theta}) + A_Q(t)\sin(\omega_c t + \theta)\sin(\omega_c t + \hat{\theta}) \\ &= \frac{1}{2}A_Q(t)[\cos(\theta - \hat{\theta}) - \cos(2\omega_c t + \theta + \hat{\theta})] + \frac{1}{2}A_I(t)[\sin(\theta - \hat{\theta}) \\ &\quad - \sin(2\omega_c t + \theta + \hat{\theta})] \end{aligned} \tag{3.13}$$

which after lowpass filtering becomes

$$s'_Q(t) = \frac{1}{2}A_Q(t)\cos(\theta - \hat{\theta}) + \frac{1}{2}A_I(t)\sin(\theta - \hat{\theta}). \tag{3.14}$$

The second terms in Eqs.3.12 and 3.14 are also known as crosstalk. For the NRZ case, since $A_I(t) = \pm A_Q(t)$, we can rewrite the inphase and quadrature components as

$$\begin{aligned} s'_I(t) &= \frac{1}{2}A_I(t)[\cos\phi \pm \sin\phi] \\ s'_Q(t) &= \frac{1}{2}A_Q(t)[\cos\phi \mp \sin\phi]. \end{aligned} \tag{3.15}$$

It is clearly seen that as one channel component voltage level is changed by a factor $\cos\phi + \sin\phi$, the other one is changed by a factor $\cos\phi - \sin\phi$. Since the source is equiprobable and the pdf of ϕ is symmetric around zero, the probability of error can be calculated by adding the probability of error for each case and taking the average. Then, the bit error probability for a given phase error is

$$P_b(\phi) = \frac{1}{2}[Q(\sqrt{\frac{2E_b}{N_0}}(\cos\phi + \sin\phi)) + Q(\sqrt{\frac{2E_b}{N_0}}(\cos\phi - \sin\phi))]. \tag{3.16}$$

The bit error probabilities can be calculated by multiplying these conditional probabilities with the pdf given in Eq. 2.1 and integrating over the possible range of phase error $(\mathrm{mod}(2\pi))$. Thus, the final expressions become

$$P_{b,BPSK} = \int_{-\pi}^{\pi} Q(\sqrt{\frac{2E_b}{N_0}}\cos\phi)\frac{\exp(\xi\cos\phi)}{2\pi I_0(\xi)}d\phi, \tag{3.17}$$

$$\begin{aligned} P_{b,QPSK} &= \frac{1}{2}\int_{-\pi}^{\pi} Q(\sqrt{\frac{2E_b}{N_0}}(\cos\phi + \sin\phi))\frac{\exp(\xi\cos\phi)}{2\pi I_0(\xi)}d\phi \\ &\quad + \frac{1}{2}\int_{-\pi}^{\pi} Q(\sqrt{\frac{2E_b}{N_0}}(\cos\phi - \sin\phi))\frac{\exp(\xi\cos\phi)}{2\pi I_0(\xi)}d\phi. \end{aligned} \tag{3.18}$$

These probabilites have been calculated by numerical integration and provided (having ξ as a parameter) in [35]. These curves along with the curves obtained by simulation are plotted in Figs. 3.7 and 3.8.

For the simulations, the model introduced in section 2.1 was used. The noise components n'_I and n'_Q were obtained by passing n_I and n_Q through a fourth order Butterworth filter taking $BT = 0.01$. The power of $n'_I + jn'_Q$ was normalized to unity. Depending on the ξ value desired, the power was denormalized by a corresponding constant.

From the curves for BPSK, it can be clearly seen that especially for $\xi = 8$ dB there is 2.4 dB difference between the curve presented in the reference and the curve obtained through simulations at $\frac{E_b}{N_0} = 10$ dB. The powers involved in the process were checked one by one and the difference could not be resolved. This difference is 1.2

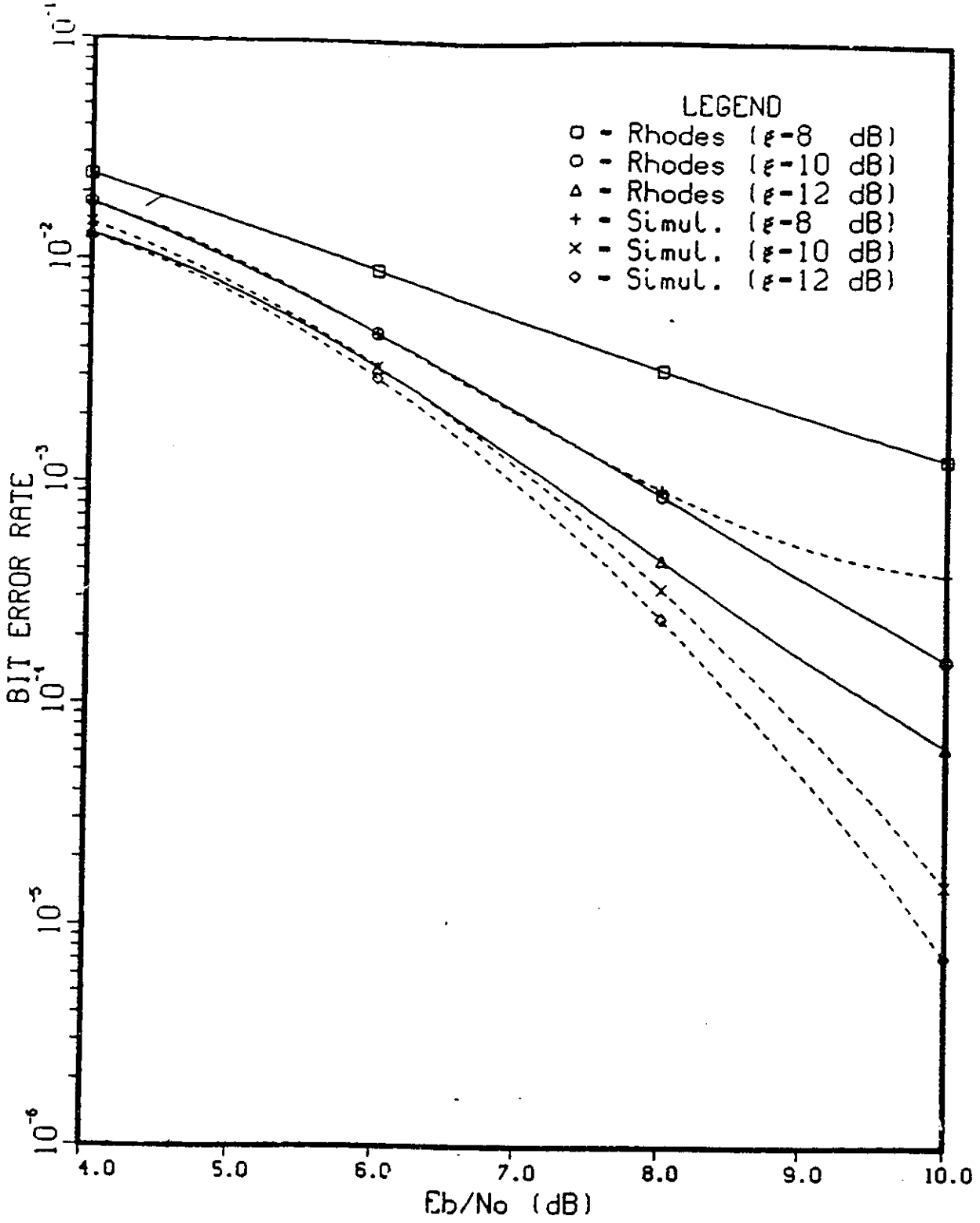

Figure 3.7: BER performance of coherent BPSK in AWGN channels with a noisy phase reference. Rhodes: [35], ξ is the loop SNR.

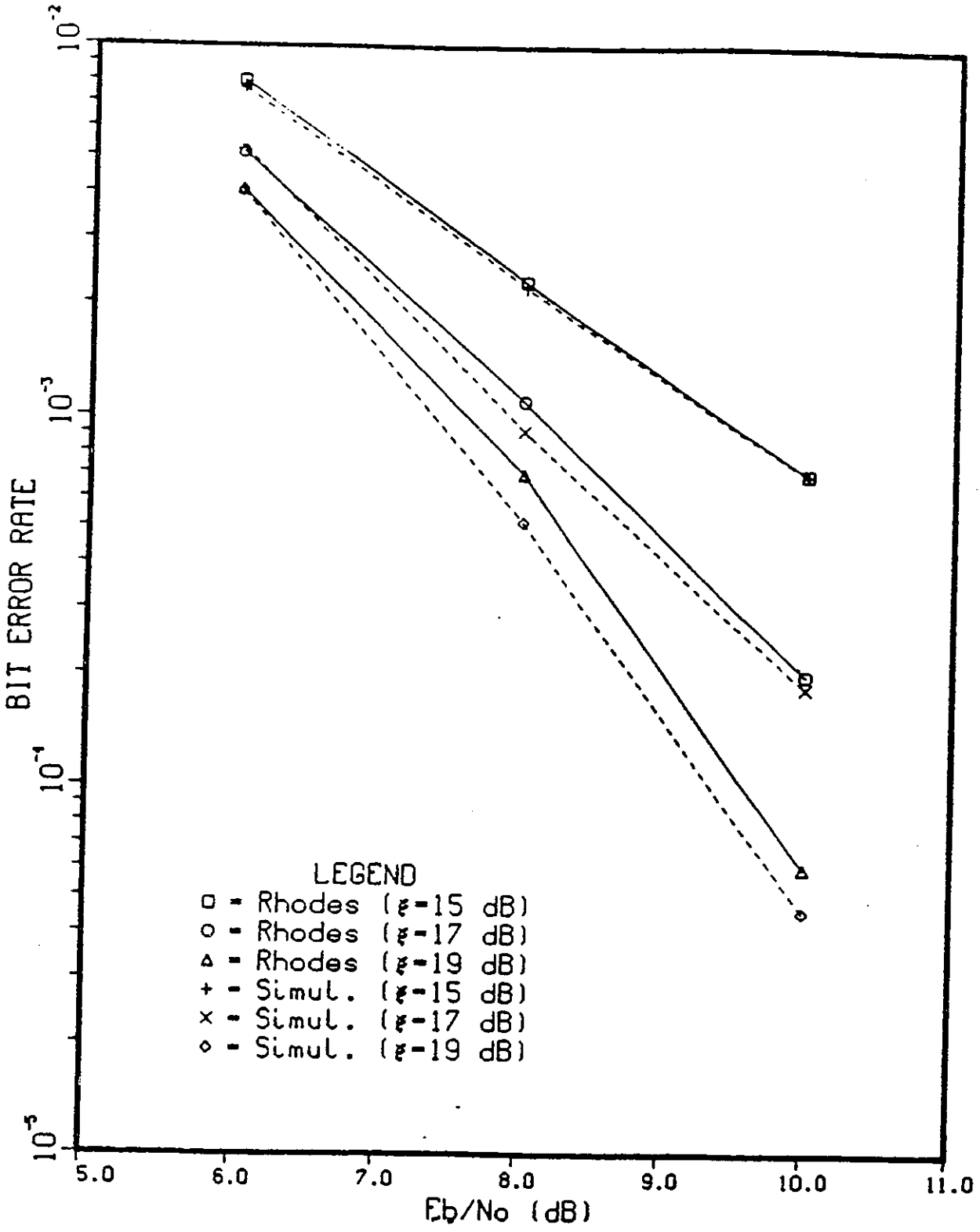

Figure 3.8: BER performance of QPSK in AWGN channels with a noisy phase reference. Rhodes: [35], ξ is the loop SNR.

dB for $\xi = 12$ dB. It is very difficult to explain completely the reasons behind the differences. One factor that is causing some difference is the BT product which was chosen to be 0.01 in the simulations. Since the probability that the phase error at the beginning of the process will be in the close neighbourhood of zero is much higher than it to be far from zero and the block length is taken to be 4096 symbols, it may be that for a long period of time the phase error imposed on the demodulated signal is stuck around zero due to the slow variations in the phase error. BPSK will obviously be more affected from this factor due to the larger angle between its constellation points. In other words, larger values of phase error are needed to have decision errors in BPSK, compared to QPSK systems. Another factor to be considered is that some difference will always be observed between analytical results and simulation results. Finally, the small inaccuracies in modelling will contribute to the differences between the two results. For the QPSK case, the simulation curves match the curves given in the reference quite well. Nevertheless, since all the simulations were run using the same normalized samples of the same filtered Gaussian process, the simulation results presented in Chapter 4 that compare coherent, differential, multidifferential and partially coherent detection BER performances will not be affected much due to their relativeness. They will be quite accurate for the QPSK case.

3.2.2 Performance of PSK Signals in Rician Channels with Noisy Phase Reference

For slow fading Rician channels, an analytical expression for the bit error probability is derived in [2] for BPSK. The probability of bit error assuming a constant fading amplitude a and a certain phase error ϕ is given by the expression

$$P_b(\phi, a) = Q(\sqrt{\frac{2E_b}{N_0}} a \cos\phi). \tag{3.19}$$

The unconditional bit error probability is then expressed as

$$P_b = \int_0^\infty \int_{-\pi}^{\pi} P_b(\phi, a) P(\phi|a) f(a) d\phi da \tag{3.20}$$

where

$$P(a) = \frac{a}{p}\exp\{-\frac{a^2+1}{2p}\}I_0(\frac{a}{p}) \quad a > 0 \tag{3.21}$$

as given in Eq. 2.13 and

$$P(\phi|a) = \frac{\exp\{a\xi_0\cos\phi\}}{2\pi I_0(a\xi_0)} \quad |\phi| < \pi. \tag{3.22}$$

ξ_0 is the nominal loop SNR which would exist in the absence of fading, i.e., $\xi = a\xi_0$. Substituting Eq. 3.19, 3.21 and 3.22 into Eq. 3.20 gives

$$P_b = \int_0^\infty \int_{-\pi}^{\pi} Q(\sqrt{\frac{2E_b}{N_0}}a\cos\phi)\frac{\exp\{a\xi_0\cos\phi\}}{I_0(a\xi_0)}\frac{a}{p}\exp\{-\frac{a^2+1}{2p}\}I_0(\frac{a}{p})d\phi da. \tag{3.23}$$

Since the effective loop SNR conditioned on a is $\xi = a\xi_0$, and $\frac{1}{2p} = K$, defining $y = \frac{a^2}{2p} = Ka^2$ we obtain

$$\begin{aligned} P_b &= \frac{\exp(-K)}{2\pi}\int_0^\infty \int_{-\pi}^{\pi} Q(\sqrt{\frac{2E_b}{N_0}\frac{y}{K}}\cos\phi)\frac{\exp\{\sqrt{\frac{y}{K}}\xi_0\cos\phi\}}{I_0(\sqrt{\frac{y}{K}}\xi_0)}\frac{1}{\sqrt{Ky}} \\ &\quad \exp(-y)I_0(2\sqrt{Ky})d\phi dy. \end{aligned} \tag{3.24}$$

The performance curves are obtained by taking the nominal loop SNR ξ_0 as a parameter (unlike the simulations where effective loop SNR ξ is taken as a parameter). The BER performance curves with the results given in [2] for BPSK is plotted in Fig. 3.9 and the QPSK BER performance curves with ξ taken as a parameter are plotted in Fig. 3.10. Since the signal to noise ratio used in the reference (ξ_0, i.e., nominal SNR) and the one used in the simulations (effective ξ) are different, it is not appropriate to make a comparison. For QPSK, a reference for comparison purposes could not be found. From the figure, it can be observed that QPSK is not only severely affected from the phase noise but also sits on error floors, i.e., after a certain $\frac{E_b}{N_0}$ value, no matter how much $\frac{E_b}{N_0}$ increases, there is no decrease in BER.

3.3 Conventional Differential Detection

Differentially coherent detection of Phase-Shift-Keyed (DPSK) signals assume that the phase of the carrier does not change for a period of two symbol intervals. Since the

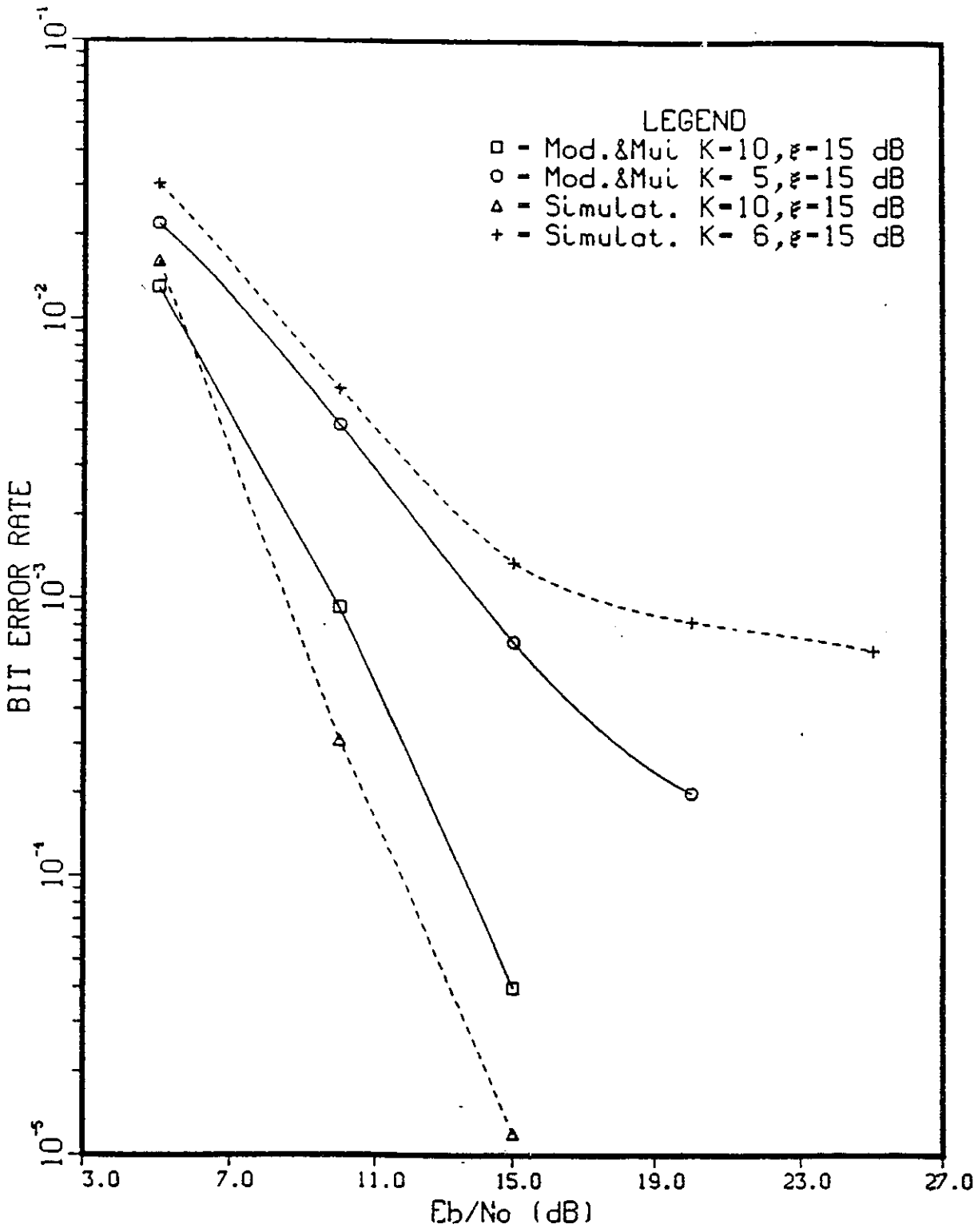

Figure 3.9: BER performance of coherent BPSK in Rician channels with a noisy phase reference for $K = 5$, 6, 10 and $\xi = 15$dB. Mod. & Mui: [2], ξ is the loop SNR.

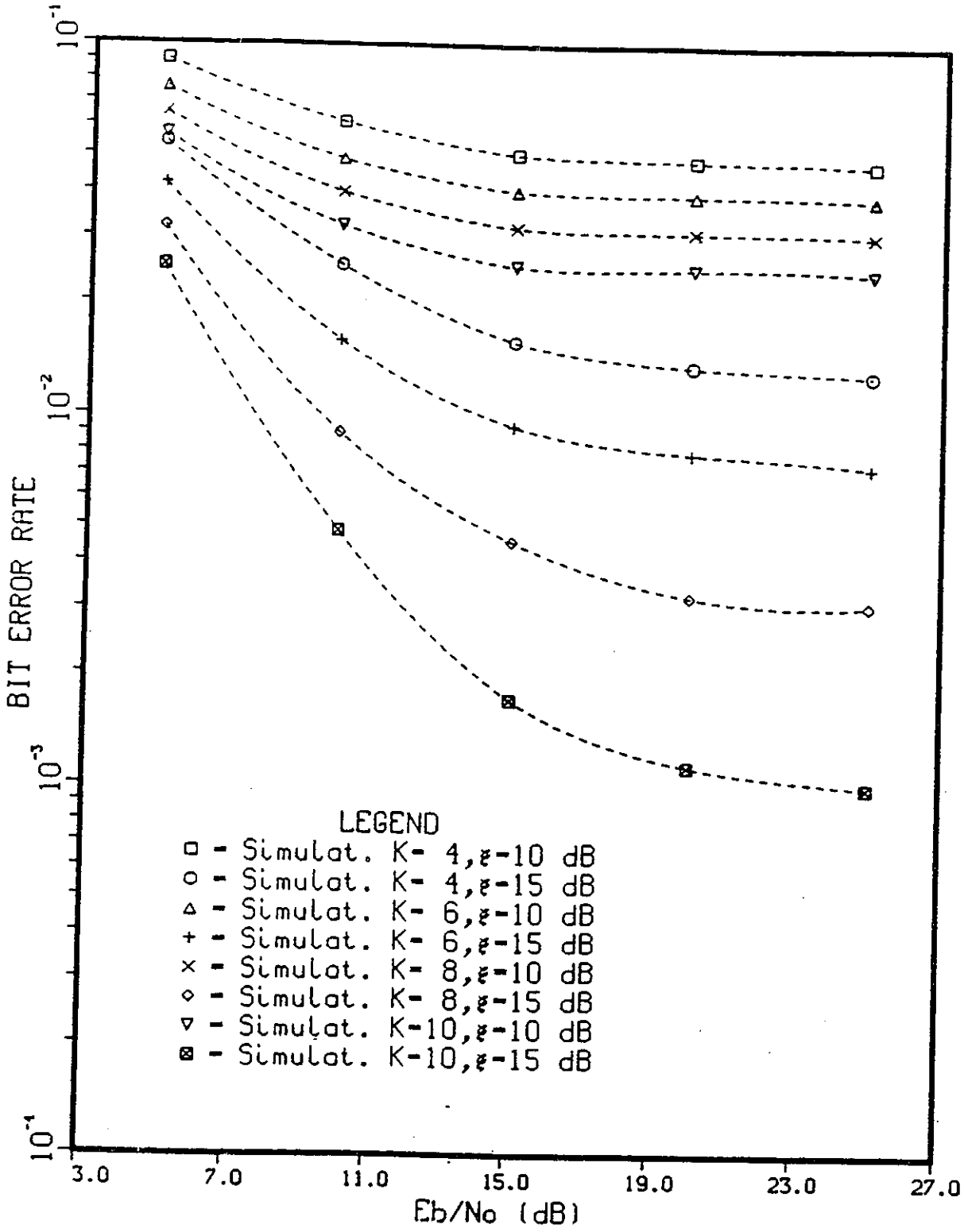

Figure 3.10: BER performance of coherent QPSK in Rician channels with a noisy phase reference for $K = 4, 6, 8, 10$ and $\xi = 10$ and 15dB. ξ is the loop SNR.

information phases are encoded not in absolute phases but rather in the difference of transmitted phases, the demodulation and decoding can be performed by multiplying the received signal with the one symbol delayed version of itself. The block diagram of a binary DPSK receiver is as shown in Fig. 3.11 and the two DQPSK receivers corresponding to the constellations shown in Fig. 3.2 are as shown in Fig. 3.12 (a) and (b) respectively. Assuming that the two consecutive samples of the received

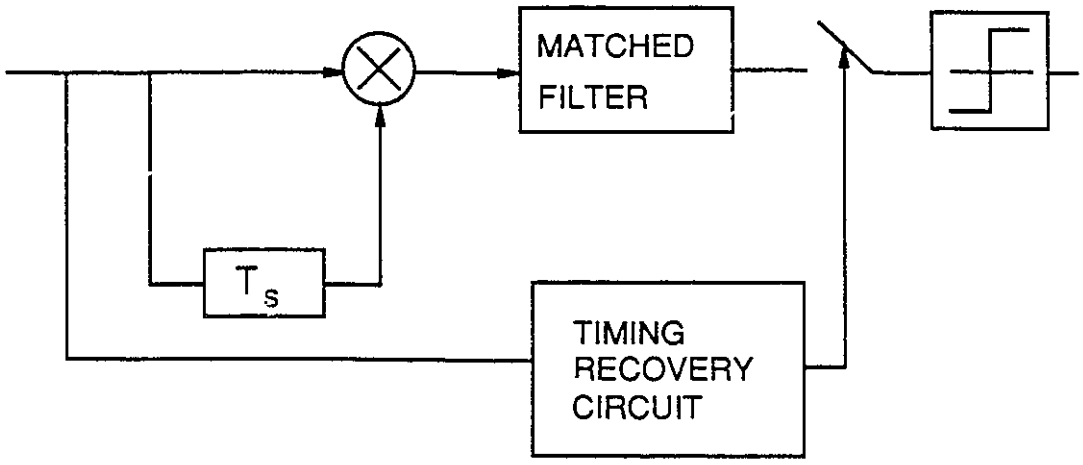

Figure 3.11: Block diagram of a DBPSK receiver.

signal in AWGN channels at $t = (k-1)T$ and $t = kT$ are $x_{k-1} = d_{k-1} + n_{k-1}$ and $x_k = d_k + n_k$ respectively, the multiplication of the samples will give

$$x_k x_{k-1} = d_k d_{k-1} + d_k n_{k-1} + d_{k-1} n_k + n_k n_{k-1}. \tag{3.25}$$

Due to the involvement of two signal times noise terms and a noise times noise term, differential detection will be inferior compared to coherent detection if the only disturbance is AWGN. In other cases, e.g. when there is fading, their performances might be comparable or even better depending on how valid the assumption of carrier phase being constant in two symbol intervals and the severity of the existing phase noise.

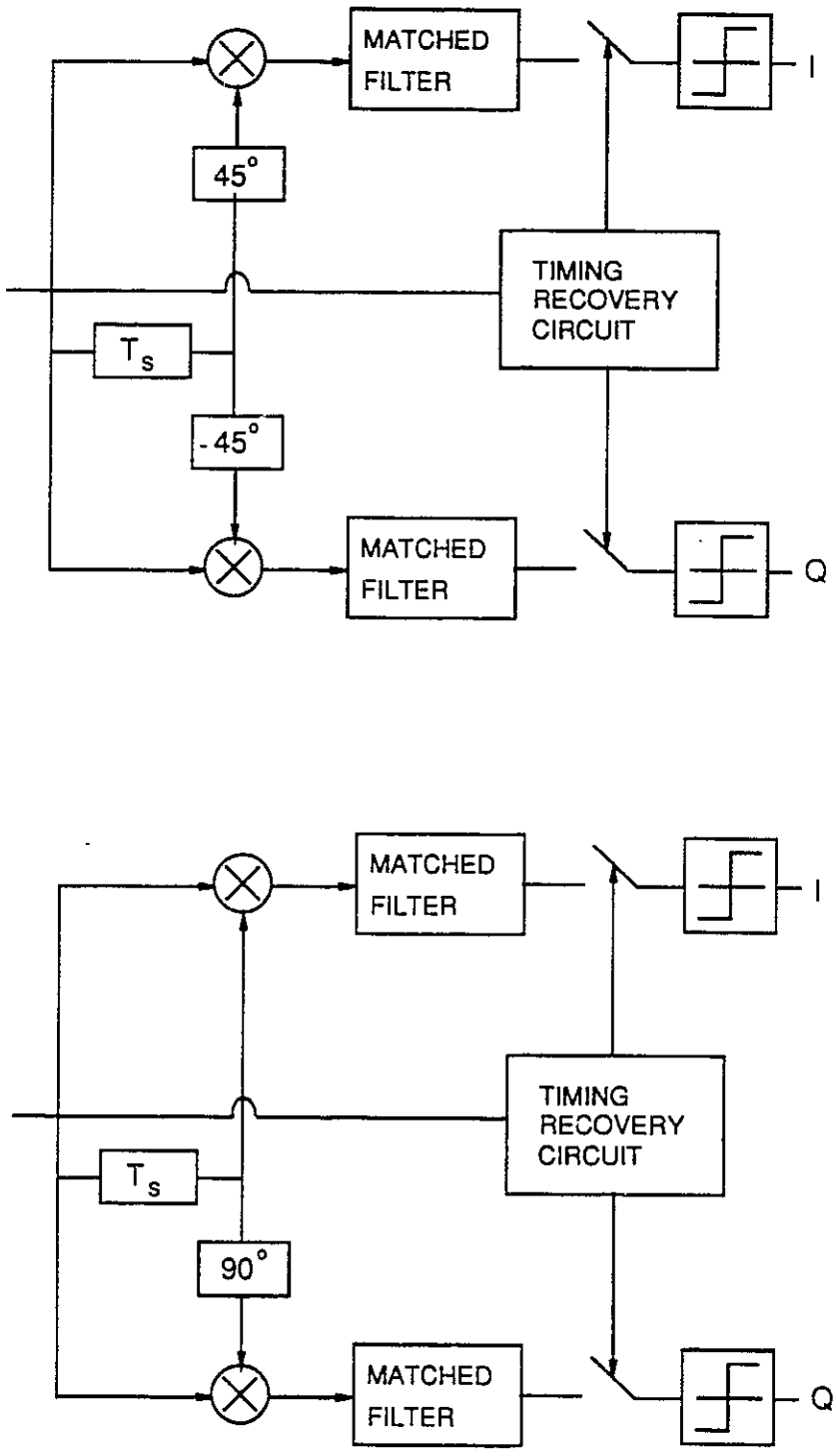

Figure 3.12: DQPSK receivers for signal constellations in Fig. 3.2 (a) and (b) respectively.

3.3.1 Performance of DPSK Signals in AWGN Channels

Probability of bit error for DBPSK is given in [31] as:

$$P_b = \frac{1}{2}\exp\{-\frac{E_b}{N_0}\} \tag{3.26}$$

and for DQPSK is given as

$$P_b = Q(a,b) - \frac{1}{2}I_0(ab)\exp[-\frac{1}{2}(a^2+b^2)] \tag{3.27}$$

where $Q(\cdot,\cdot)$ is the generalized Q function (Marcum Q function) which is defined as

$$Q(a,b) = \exp\{-(a^2+b^2)\}\sum_{k=0}^{\infty}(\frac{a}{b})^k I_k(ab) \quad (\ b > a > 0\ ), \tag{3.28}$$

where $I_k(\cdot)$ is the k^{th} order modified Bessel function of the first kind and the parameters a and b are defined as:

$$\begin{aligned} a &= \sqrt{\frac{2E_b}{N_0}(1-\frac{1}{\sqrt{2}})} \\ b &= \sqrt{\frac{2E_b}{N_0}(1+\frac{1}{\sqrt{2}})}. \end{aligned} \tag{3.29}$$

The bit error rate performances of DBPSK and DQPSK for the values given in tables in [34] and also obtained by our simulations are plotted in Fig. 3.13 and Fig. 3.14 respectively. The BER performances obtained through simulations and the ones given in the reference agree very well. The performance of DBPSK is within 0.5 dB compared to coherent BPSK for $\frac{E_b}{N_0} = 10$ dB whereas it is 2.5 dB for DQPSK. The reason for the degradation to be less for DBPSK is that the phases are at 0^o and 180^o, so only the real part of the decision variable is considered [31]. Another point of interest in DBPSK is that the degradation decreases considerably as $\frac{E_b}{N_0}$ gets higher. For DQPSK, there is no significant change in degradation as a function of $\frac{E_b}{N_0}$.

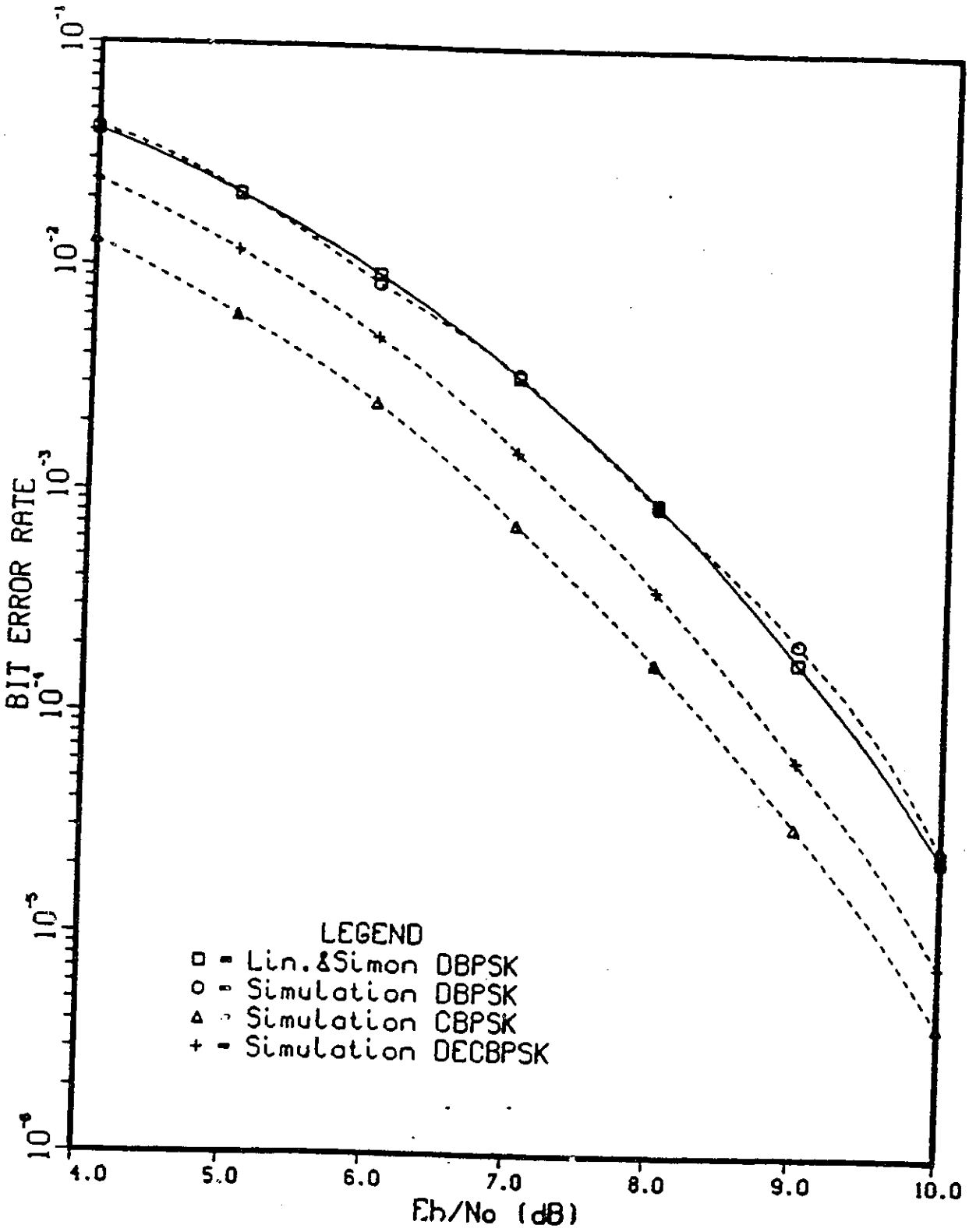

Figure 3.13: BER performance of DBPSK, CBPSK and DECBPSK in AWGN channels. Lin.& Simon: [34].

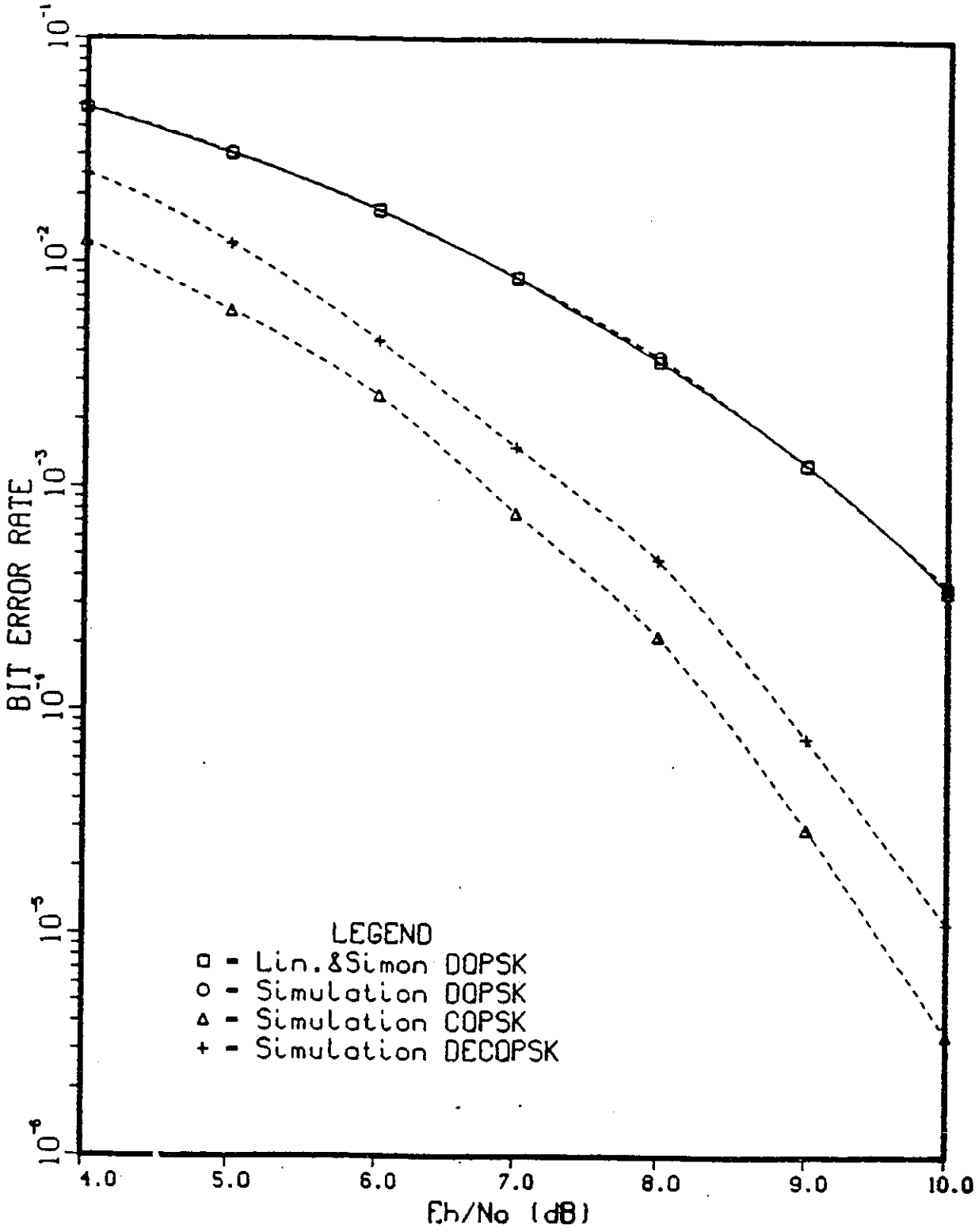

Figure 3.14: BER performance of DQPSK, CQPSK and DECQPSK in AWGN channels. Lin.& Simon: [34].

3.3.2 Performance of DPSK Signals in Slowly Varying Rician Channels

The probability of bit error for DBPSK in slowly varying Rician channels is given in [36] as:

$$P_b = Q(a,b) - \frac{1}{2}[1 + \sqrt{\frac{D}{D+1}}] \exp\{-\frac{a^2+b^2}{2}\} I_0(ab) \tag{3.30}$$

where

$$\begin{aligned} a &= \{\frac{K(1+2D-2\sqrt{D(1+D)}}{2(1+D)}\}^{\frac{1}{2}} \\ b &= \{\frac{K(1+2D+2\sqrt{D(1+D)}}{2(1+D)}\}^{\frac{1}{2}} \end{aligned} \tag{3.31}$$

S and D are the powers of the direct and diffuse components, and they are related to K-factor by $K = \frac{S}{D}$. BER performances for different K-factors from Fig. 2.4 of the same reference calculated from the above equation along with the ones obtained through simulations are plotted in Fig. 3.15. The BER performance curves of the reference and the corresponding simulation results are reasonably close for $K = 4$ dB and $K = 6$ dB. For $K = 8$ and $K = 10$ dB, the curves are close until (including) $\frac{E_b}{N_0} =$ 15 dB, but for higher $\frac{E_b}{N_0}$ values, the BER performance curves from the simulations start having a much better performance compared to the ones given in the reference. The main reason for the difference is that the Gaussian distributed sequence generated by the library function in the computer is not ideal, i.e., the tails do not extend to infinity. When the variance of the density function is very small, to have enough samples at the tails become crucial. For small K-factors, since fading process is dominant at high $\frac{E_b}{N_0}$ and the variance of the Rayleigh distribution (which is obtained from filtered Gaussian process) is large, the difference between the results given in the reference and obtained through simulations is not large. When the variance of the Rayleigh distribution becomes very small, having or not having enough samples at the tails become significant. Also. the BER performance curves given in the reference are obtained from analytical results and the BT product may play a role in the difference.

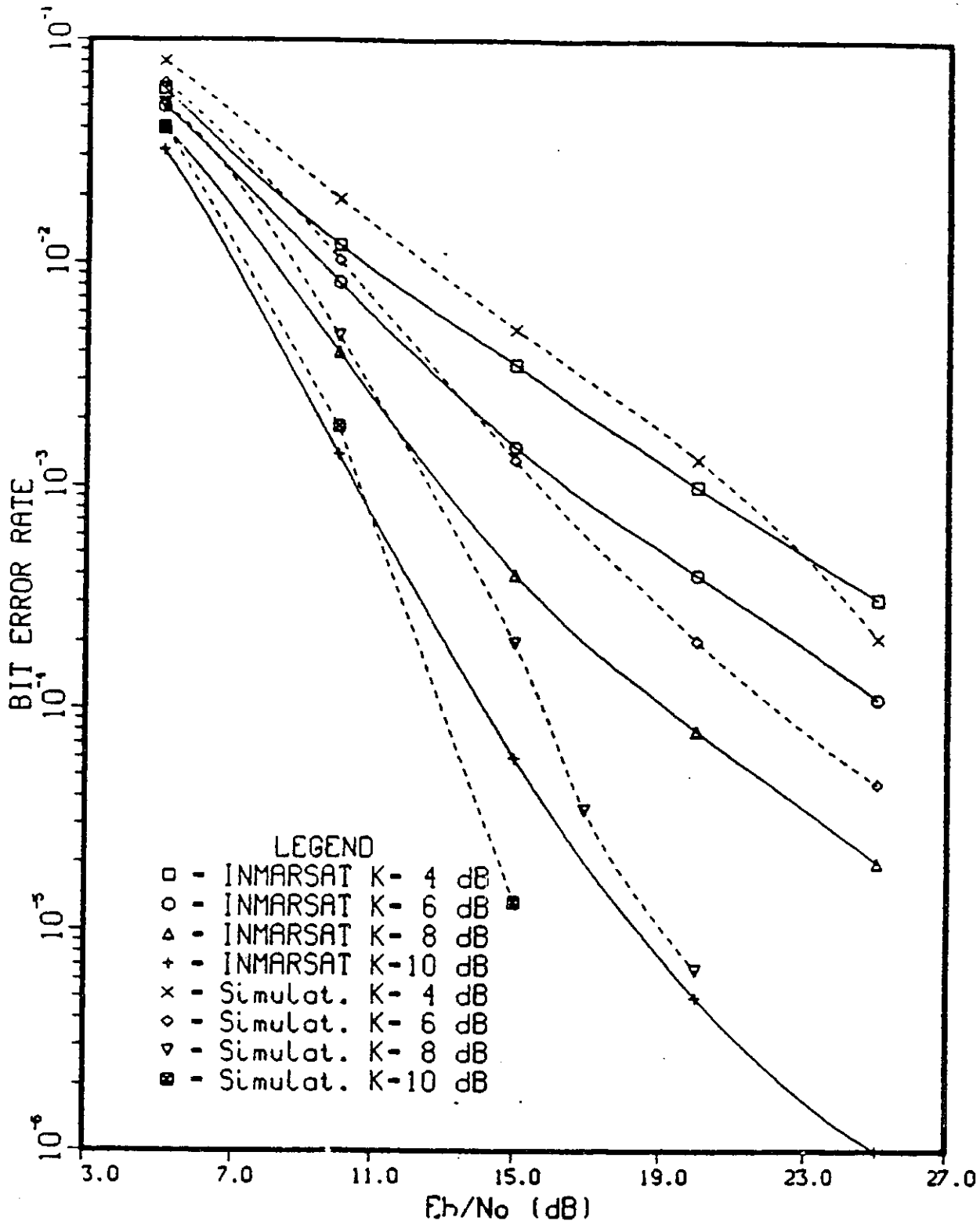

Figure 3.15: BER performance of DBPSK in slowly varying Rician channels. INMARSAT: [36].

For the DQPSK case, the simulation results are given in Fig. 3.16 along with the curve obtained from [19] for 10 dB. Since this time the our simulation results are compared to the simulation results presented in the reference and the BT products considered in both are exactly the same, the curves match quite well. Nevertheless, as mentioned before, the comparisons of the BER performances of different detection techniques in Chapter 4 all depend on same processes. Thus, the factors affecting the differences between the analytical and simulation results will diminish.

3.4 Multidifferential Detection

The first work on multidifferential detection is that of Chow and Ho [41], which was followed by Masamura *et. al.* [42] and Samejima *et. al.* [43]. In these works, the outputs of multiple differential detectors were used (in a hard decision form) in an error correcting scheme called non-redundant error corrections. This error correction scheme is making use of a self-encoding process, inherent in the multiple differential detectors which use delays longer than the symbol period. Later on, the works published in [44-50] provided symbol-by-symbol receivers and sequence estimators based on the use of multiple differential detectors. In these papers, multidifferential detection was applied to uncoded as well as trellis coded signals. Later on, Makrakis *et. al.* in [38],[51], and [52] derived the structure of optimal noncoherent detection and multiple differential detection. They have extended the concept of noncoherent detection to time dispersive environments. Also in [53] and [54], they have shown how the multiple differential detection applies to the optimal detection of signals in faded channels. Finally, recently Divsalar and Simon in [37], [55] came up with very similar structures and verified the results of the previous authors.

The concept of multidifferential detection can be simply explained as follows. If the phase of the carrier is constant over k symbol intervals, then the receiver can be implemented by multiplying the received signal separately by $T_s, 2T_s, 3T_s, \ldots, (k-1)T_s$ delayed version of the received signal and correlating each product to the all

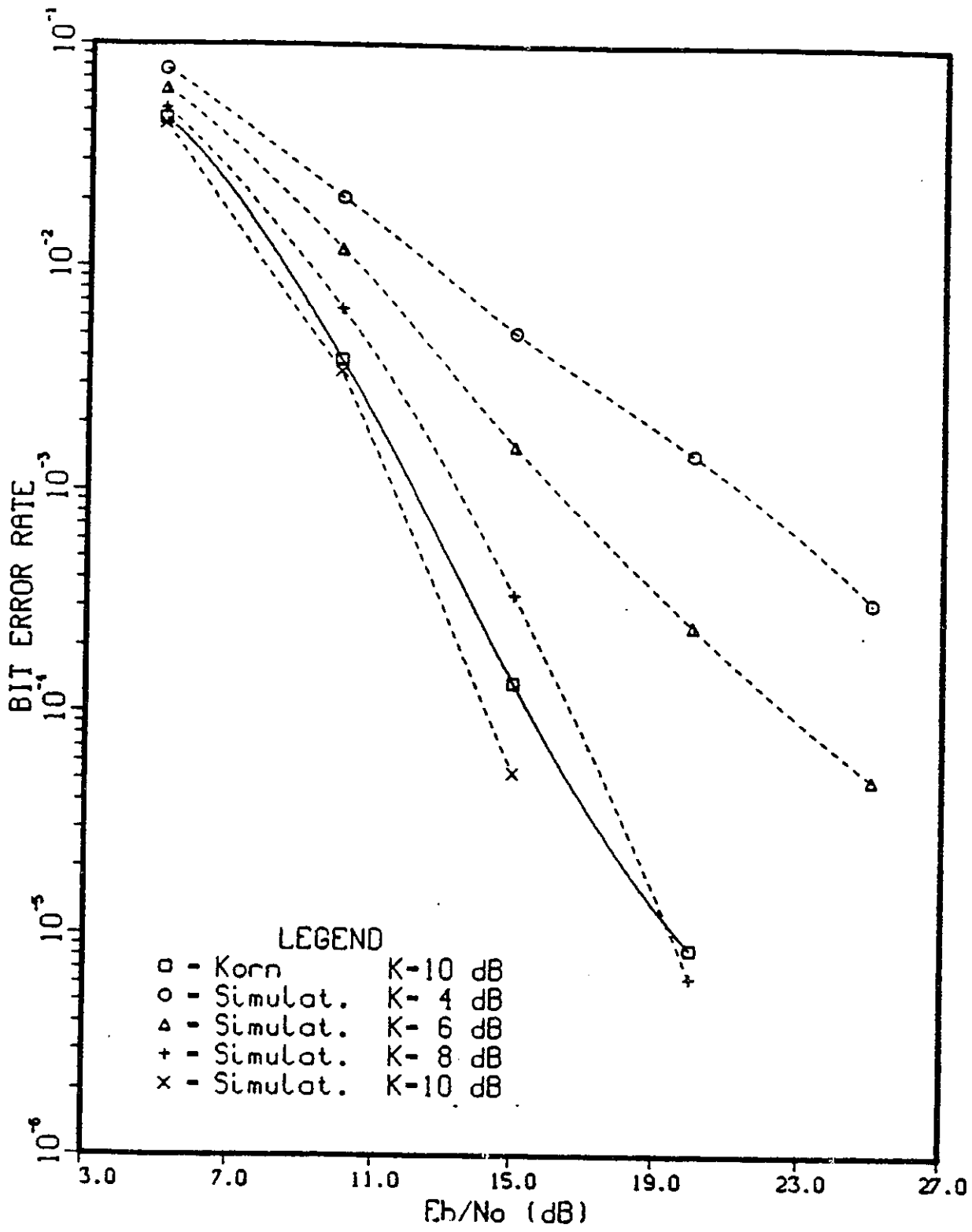

Figure 3.16: BER performance of DQPSK in slowly varying Rician channels. Korn: [19].

possible products of symbols (all possible phases) and make a decision accordingly. The decision can be made for one phase only or for $(k-1)$ phases. Let us assume that the samples of the received signals in k^{th}, $(k-1)^{th}$ and $(k-2)^{th}$ intervals are respectively

$$\begin{aligned} y_k &= e^{j(\omega_c t+\theta+\Delta\theta_k)} + n_k \\ y_{k-1} &= e^{j(\omega_c t+\theta+\Delta\theta_{k-1})} + n_{k-1} \\ y_{k-2} &= e^{j(\omega_c t+\theta+\Delta\theta_{k-2})} + n_{k-2}, \end{aligned} \tag{3.32}$$

where $\Delta\theta_m$'s are the differential information phases, θ is the phase of the carrier which is assumed to be constant over three symbol intervals. If we neglect the noise samples, the products $y_k y_{k-1}^*$, $y_{k-1}y_{k-2}^*$ and $y_k y_{k-2}^*$ will give $e^{j(\Delta\theta_k-\Delta\theta_{k-1})}$, $e^{j(\Delta\theta_{k-1}-\Delta\theta_{k-2})}$ and $e^{j(\Delta\theta_k-\Delta\theta_{k-2})}$ respectively. It is clearly seen that multiplying the signal sample in a certain symbol interval by the conjugate of the signal sample received in a previous symbol interval (and assuming that the carrier phase does not change in an interval covering the three symbol intervals which is the main principle behind differential detection) does not only demodulate the received signal, but also performs differential decoding. Considering this fact, the above procedure can be better expressed with the following decision rule:

Let c_l's be the possible symbols that could be sent in the l^{th} symbol interval. Then, decide on phases $\arg\{c_k c_{k-1}^*\}$ (and $\arg\{c_{k-1}c_{k-2}^*\}$) for c_k, c_{k-1},c_{k-2} combination which makes

$$Re\{(y_k y_{k-1}^*)(c_k c_{k-1}^*)^*\} + Re\{(y_k y_{k-2}^*)(c_k c_{k-2}^*)^*\} + Re\{(y_{k-1}y_{k-2}^*)(c_{k-1}c_{k-2}^*)^*\}$$

maximum [37].

Multiplying the signal products (e.g. $y_k y_{k-1}^*$) by all possibilities of conjugates of corresponding symbol products (e.g. $(c_k c_{k-1}^*)^*$) cross correlates it to the possible corresponding symbol products. The decision is made in favour of symbol(s) which provides maximum correlation. If in the above decision metric, only the first term is considered, the detection simply becomes conventional differential detection. The

whole expression is for 1 and 2 symbol differential detection (denoted as $1+2$). Using the identity, $Re\{\alpha_1\alpha_2^*\} = Re\{\alpha_1\}Re\{\alpha_2\} + Im\{\alpha_1\}Im\{\alpha_2\}$ where α_1 α_2 are complex variables, an equivalent version of the decision metric given above can be expressed as

$$Re\{y_k y_{k-1}^*\}Re\{c_k c_{k-1}^*\} + Im\{y_k y_{k-1}^*\}Im\{c_k c_{k-1}^*\} + Re\{y_k y_{k-2}^*\}Re\{c_k c_{k-2}^*\}$$
$$+Im\{y_k y_{k-2}^*\}Im\{c_k c_{k-2}^*\} + Re\{y_{k-1} y_{k-2}^*\}Re\{c_{k-1} c_{k-2}^*\} + Im\{y_{k-1} y_{k-2}^*\}Im\{c_{k-1} c_{k-2}^*\},$$

which in turn is used as the decision metric for both multidifferential detection and as a part of partially coherent detection decision metric.

3.4.1 Performance of Multidifferential PSK Signals in AWGN Channels

In literature, some results on the performance of multidifferential detection has been reported [37,38]. The simulation results for $1 + 2$ symbol differential detection case in [37] along with our simulation results are plotted in Fig. 3.17 for BPSK and in Fig. 3.18 for QPSK. The curves of the reference and the curves obtained through simulations match quite well. Since the figures of the reference are very small, they could not be read very accurately. This is one of the reasons for the difference in between them. Another point is that the authors make decisions block by block, i.e., they process three symbols using the decision metric given in Section 3.4 and decide on two phases. Then they proceed to the next block which has only its first symbol in common with the previous block's last symbol, whereas in the simulations the block was shifted one symbol at each decision and the decision was made on one phase only.

The simulation results show that BER performance of conventional differential detection in AWGN channels can be improved by increasing the number of differential detectors used. In [37,38], it has been shown that, as the number of differential detectors used approach infinity, the BER performance of multidifferential detection approach the performance of coherent detection in AWGN channels, although, it has also been shown that increasing the number of differential detectors by one beyond a

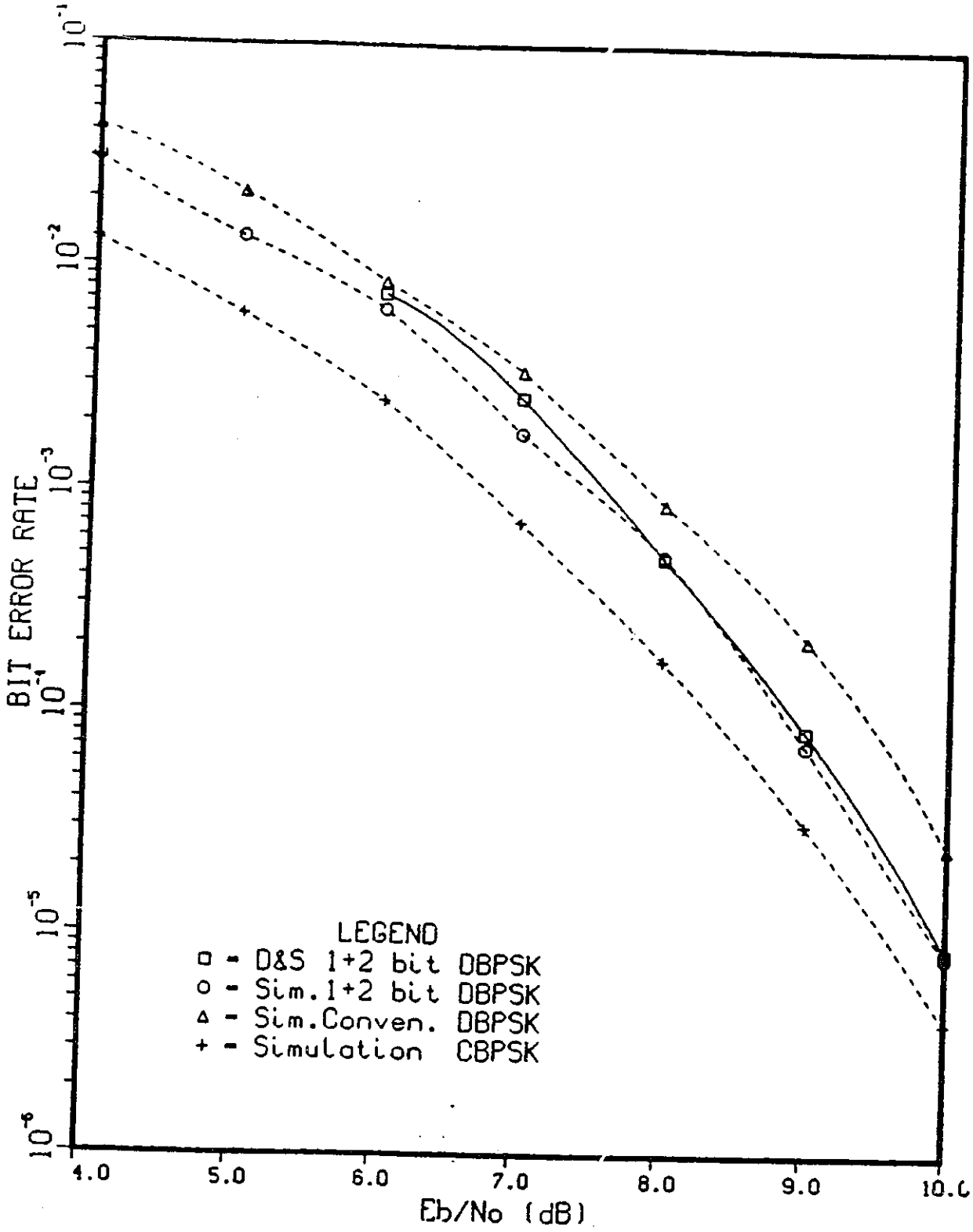

Figure 3.17: BER performance of 1+2 differential detection of BPSK in AWGN channels. D& S: [37].

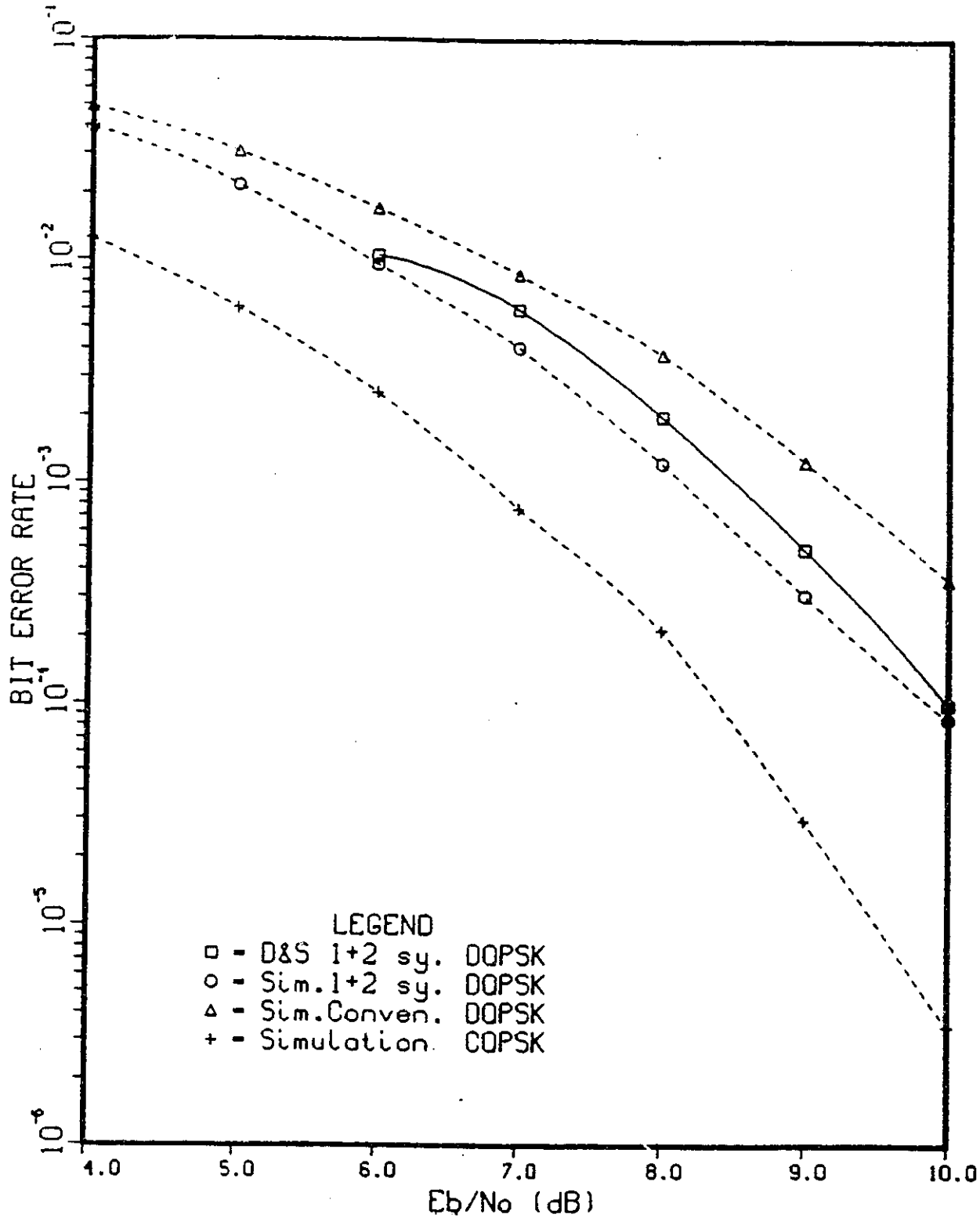

Figure 3.18: BER performance of 1+2 differential detection of QPSK in AWGN channels. D& S: [37].

few contributes relatively small to the improvement of the performance. In [38] and [56], it has also been shown that while for the uncoded schemes 2 or 3 differential detectors are enough to provide practically all the available gain, for coded schemes a larger number of detectors is required in order to approach to the best performance possible. Considering that most of the gain is reached within a small number of detectors and taking into account the large reduction in complexity we achieve by limiting the detectors used to a small number, we decided to consider a scheme based only on two (the 1 and 2-symbol delay) detectors used in a Viterbi decoding scheme.

3.4.2 Performance of Multidifferential Detection of PSK Signals in Slowly Varying Rician Channels

The BER performance of $1+2$ symbol differential detection of BPSK and QPSK in slowly varying Rician channels ($BT = 0.01$) obtained by simulation are as shown in Fig. 3.19 and 3.20 respectively.

For BPSK case, we observe that $1+2$ differential detection is slightly inferior compared to conventional differential detection for $K = 4$ dB and for high $\frac{E_b}{N_0}$ values. The improvement is larger as K gets larger for both BPSK and QPSK. This was as we expected. Since the channel is slowly varying fading channel, when fading dominates AWGN, the additional differential detector does not provide much further information about the phase of the carrier. So, the improvement, if any, is small. When fading is weak, the AWGN becomes more important and since the samples of the Gaussian process are uncorrelated, considering the phase difference between the previous successive symbols and the phase difference in two symbol intervals in the likelihood process provides more information compared to strong fading case. So, the improvement is larger.

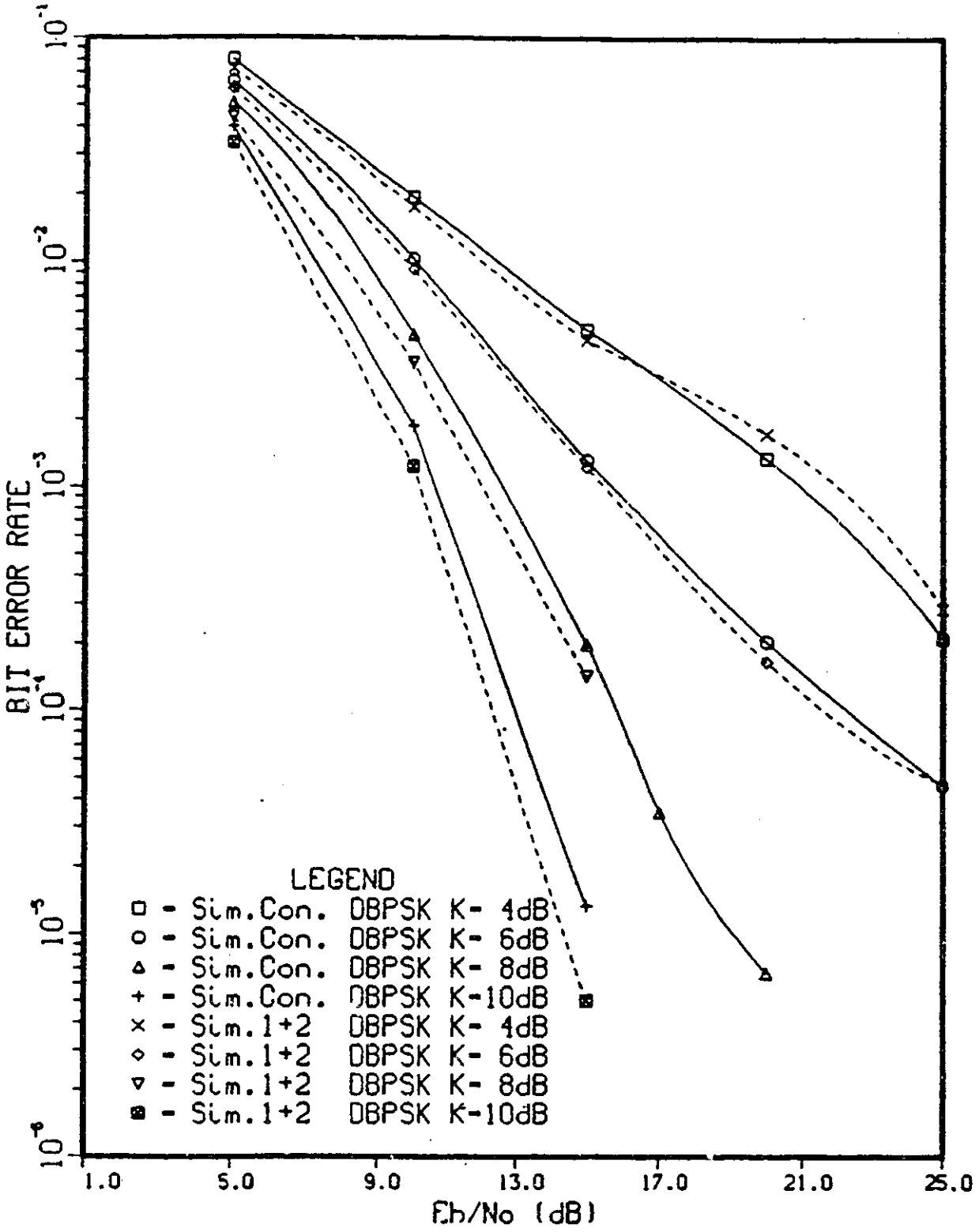

Figure 3.19: BER performance of 1+2 differential detection of BPSK in Rician channels.

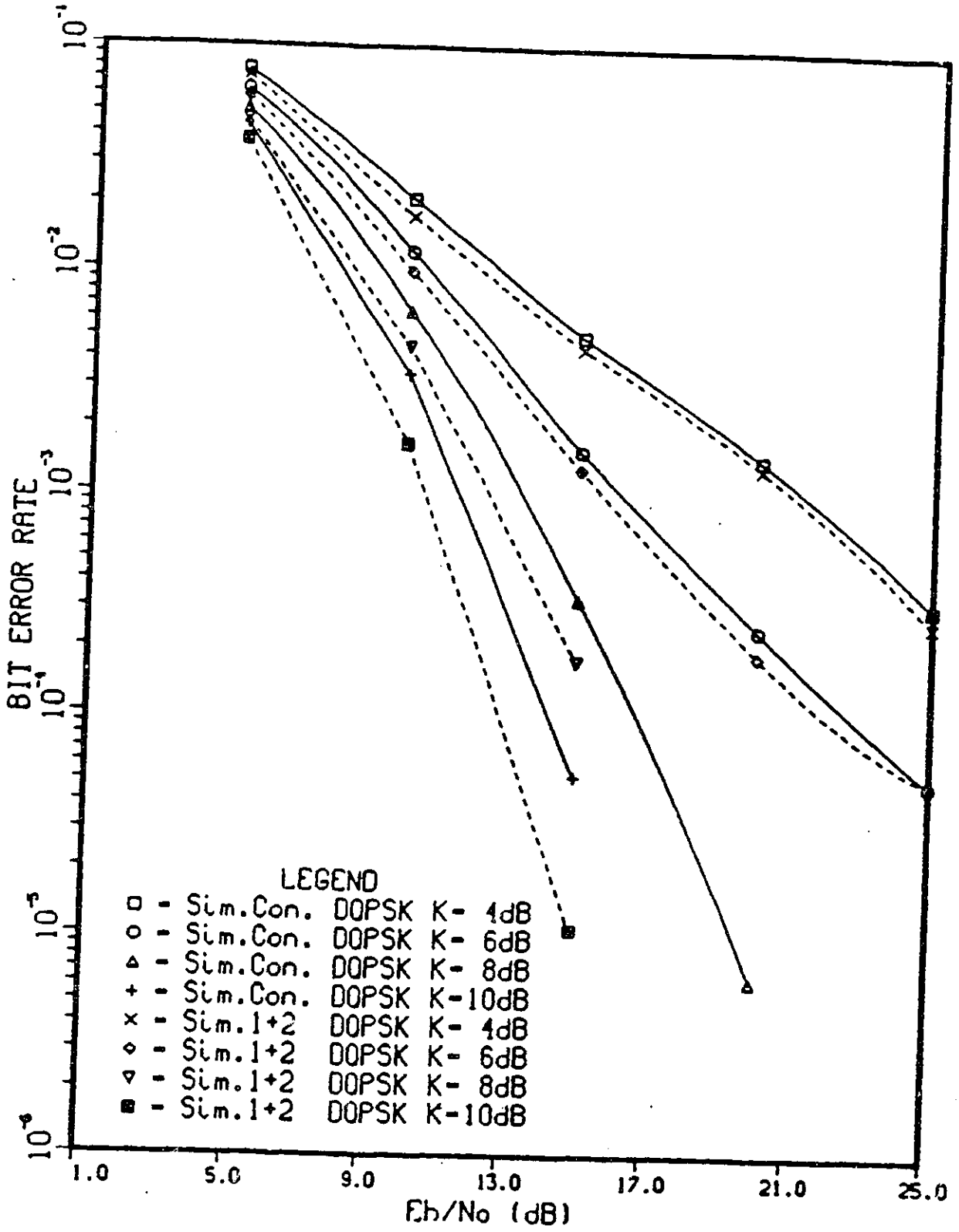

Figure 3.20: BER performance of 1+2 differential detection of QPSK in Rician channels.

3.5 Conclusion

In this chapter, we first showed that the simulation programs are functioning for detection of PSK signals by checking the BER performances of coherent, differential and multidifferential detection in AWGN channels. Then, we tried to verify the reliability of our models by applying them to the detection of uncoded BPSK and QPSK signals. Only in the case of coherent detection of BPSK with a noisy phase reference, the BER performances obtained analytically in the reference was significantly different than the performance obtained through our simulations. If this case is excluded, the simulation results show that the models we used represent the channels considered reasonably well.

Chapter 4

PARTIALLY COHERENT DETECTION

In this chapter, the metric expressions for partially coherent detection[1] are derived and they are applied to PSK signals. Then, metric expressions are obtained for low and high $\frac{E_b}{N_0}$ cases, and the one for high $\frac{E_b}{N_0}$ is truncated to simplify the receiver structure. Viterbi decoding is employed to have maximum likelihood detection by using the truncated metric expression for $\frac{E_b}{N_0}$ case. The simulation results are presented using the channel models given in Chapter 2 (slowly varying Rician fading channels with and without noisy phase reference under the assumption that the carrier recovery circuit can track the phase variations due to fading) for coherent, conventional differential, 1+2 differential and partially coherent detection of uncoded BPSK and QPSK signals. Also, the simulation results are presented and interpreted.

4.1 Derivation of the Metric Expressions

The block diagram of the transmitter for the communication system under consideration is as shown in Fig. 4.1. In Chapter 3, we discussed the symbol by symbol detection of PSK signals. In this chapter the decision laws are based on sequence

[1] Recall from Section 1.2 that in this thesis by *partially coherent* we are referring to the use of the decoding metric expression which is a weighted combination of optimum metrics for coherent and noncoherent detectors in the detection process.

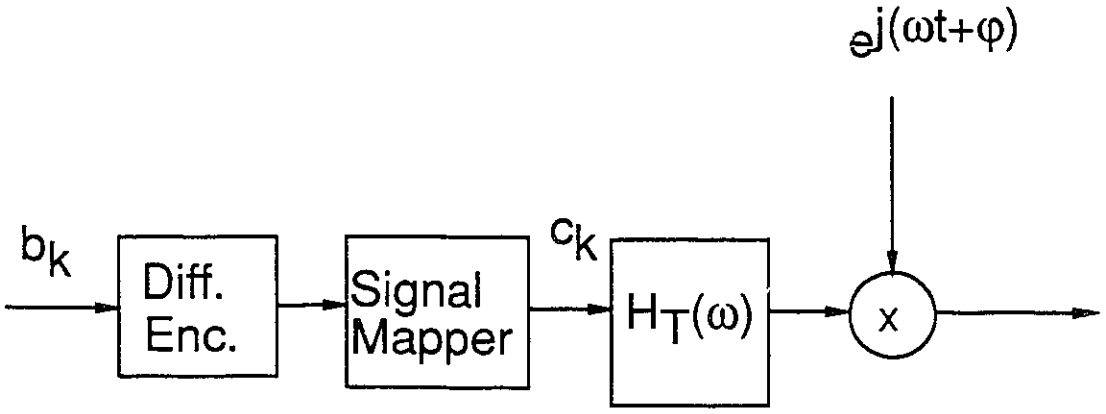

Figure 4.1: Block diagram of the transmitter.

estimation, and for this reason describing the transmitted and received signals using vector notation is more convenient. The transmitter is made up of two parts, the encoding unit and the modulator. The encoding unit translates the binary information sequence $\bar{B} = [b_1, b_2, ..., b_{N-1}]$, by signal mapping and differential encoding into a sequence of symbols $\bar{C}(\bar{A}) = [c_0, c_1, ..., c_{Z-1}]$ with c_k being complex and N and Z being integers where $N = Z$ for BPSK and $N = 2Z$ for QPSK. The symbols c_k are fed into the modulator. The modulator output can be expressed as:

$$x_{tr}(\bar{C}(\bar{A}), t) = x_{tr,B}(\bar{C}(\bar{A}), t)e^{j(\omega_c t+\psi)} \tag{4.1}$$

where ω_c is the carrier frequency, ψ is the initial phase of the modulator and $x_{tr,B}(\bar{C}(\bar{A}), t)$ is the complex baseband representation of the transmitted signal. The signal $x_r(t)$ at the input of the receiver can be expressed as:

$$x_r(t) = x_B(\bar{C}(\bar{A}), t)e^{j(\omega_c t+\psi)} + n(t) \tag{4.2}$$

where $n(t)$ is the white Gaussian noise with a one-sided spectral density of N_o, and

$$x_B(\bar{C}(\bar{A}), t) = x_{tr,B}(\bar{C}(\bar{A}), t) \otimes h_{c,B}(t) \ , \tag{4.3}$$

$$h_{c,B}(t) = h_c(t)e^{-j\omega_c t} \tag{4.4}$$

$x_{tr,B}(\bar{C}(\bar{A}),t)$ and $h_{c,B}(t)$ are the baseband equivalents of the signal $x_{tr}(\bar{C}(\bar{A}),t)$ and channel response $h_c(t)$ respectively. In Eq. (4.3), $\otimes$ defines the convolution operation. Since initial phase ψ is unknown to the receiver, its estimate $\hat{\psi}$ has to be obtained for example by employing a nonlinearity in cascade with a PLL. Eq. 2.1 can be rewritten for the steady-state phase error of the estimate $\widehat{\Delta\psi} = \psi - \hat{\psi}$ as

$$\mathbf{P}_{\widehat{\Delta\psi}(\xi)}(u) = \begin{cases} \frac{1}{2\pi I_0(\xi)} e^{\xi \cos u} & \mid u \mid \leq \pi \\ 0 & \text{otherwise.} \end{cases} \tag{4.5}$$

The pdf of the received signal, given the transmitted signal is (cf. [33], p. 317):

$$P(x_r(t)|x_B(\bar{C}(\bar{A}),t),\psi) =$$
$$\frac{1}{(2\pi)^{\frac{Z}{2}}\sigma^Z} \exp\{-\frac{1}{2N_0}\|x_r(t) - x_B(\bar{C}(\bar{A}),t)e^{j(\omega_c t+\psi)}\|^2\} \tag{4.6}$$

where $\|y(t)\|$ is the norm of vector $y(t)$, which is defined as $\int_{-\infty}^{\infty} |y(t)|^2 dt$ and $\sigma^2 = N_0$ is the variance of the real or imaginary part of the Gaussian noise. Expanding the expression given in Eq. (4.6) and collecting the constant terms under K_1, we get

$$P(x_r(t)|x_B(\bar{C}(\bar{A}),t),\psi) =$$
$$K_1 \exp\{-\frac{1}{2N_0}(\|x_r(t)\|^2 + \|x_B(\bar{C}(\bar{A}),t)\|^2)\}$$
$$\exp\{-\frac{1}{N_0} Re[e^{j(\omega_c t+\psi)} < x_r(t), x_B(\bar{C}(\bar{A}),t) >^*]\} \tag{4.7}$$

where $< x, y >$ is the inner product of vectors x and y and is equal to $\int_{-\infty}^{\infty} y(t)x^*(t)dt$. Using the definition of norm, the inner product and the relation $< x, y >^* = < y, x >$, the expression becomes

$$P(x_r(t)|x_B(\bar{C}(\bar{A}),t),\psi) =$$
$$K_1 \exp\{-\frac{1}{2N_0}\int_{t_L}^{t_U} |x_r(\tau)|^2 d\tau\} \exp\{-\frac{1}{2N_0}\int_{t_L}^{t_U} |x_B(\bar{C}(\bar{A}),\tau)|^2 d\tau\}$$
$$\exp\{-\frac{1}{N_0} Re\{e^{j(\omega_c t+\psi)} \int_{t_L}^{t_U} x_B(\bar{C}(\bar{A}),\tau)x_r^*(\tau)d\tau\}\} \tag{4.8}$$

where t_L and t_U represent the limits of the integration process and their values depend on the spreading of the signal $x_B(\bar{C}(\bar{A}),t)$. $P(x_r(t)|x_B(\bar{C}(\bar{A}),t),\psi)$ can be calculated from the above equation through integration with respect to $\widehat{\Delta\psi}$ (i.e.,

$P(x_r(t)|x_B(\bar{C}(\bar{A}),t),\psi) = \int_{-\pi}^{\pi} P(x_r(t)|x_B(\bar{C}(\bar{A}),t),\psi) P_{\widehat{\Delta\psi(\xi)}}(u)du)$. Performing the integration provides us the following expression:

$$
\begin{aligned}
&P(x_r(t)|x_B(\bar{C}(\bar{A}),t),\psi) = \\
&K_1 \exp\{-\tfrac{1}{2N_0}\int_{t_L}^{t_U}|x_r(\tau)|^2 d\tau\} \exp\{-\tfrac{1}{2N_0}\int_{t_L}^{t_U}|x_B(\bar{C}(\bar{A}),\tau)|^2 d\tau\} \\
&\tfrac{1}{2\pi I_0(\xi)}\int_{-\pi}^{\pi} e^{\xi\cos u}(\exp\{-\tfrac{1}{N_0}Re\{e^{j(\omega_c t+\psi)}\int_{t_L}^{t_U} x_B(\bar{C}(\bar{A}),\tau)x_r^*(\tau)d\tau\}\})du \\
&= K_1 \exp\{-\tfrac{1}{2N_0}\int_{t_L}^{t_U}|x_r(\tau)|^2 d\tau\} \exp\{-\tfrac{1}{2N_0}\int_{t_L}^{t_U}|x_B(\bar{C}(\bar{A}),\tau)|^2 d\tau\} \\
&\tfrac{1}{2\pi I_0(\xi)}\int_{-\pi}^{\pi} \exp\{(-\tfrac{1}{N_0})(\xi N_0\cos u + Re\{e^{j(\omega_c t+\psi)}\int_{t_L}^{t_U} x_B(\bar{C}(\bar{A}),\tau)x_r^*(\tau)d\tau\})\})du \\
&= K_1 \exp\{-\tfrac{1}{2N_0}\int_{t_L}^{t_U}|x_r(\tau)|^2 d\tau\} \exp\{-\tfrac{1}{2N_0}\int_{t_L}^{t_U}|x_B(\bar{C}(\bar{A}),\tau)|^2 d\tau\} \\
&\tfrac{1}{2\pi I_0(\xi)}\int_{-\pi}^{\pi} \exp\{Re\{\tfrac{\xi N_0 e^{ju}}{N_0}\} + Re\{\tfrac{1}{N_0}e^{j(\omega_c t+\psi)}[\int_{t_L}^{t_U} x_B(\bar{C}(\bar{A}),\tau)x_r^*(\tau)d\tau]\}]\}du \\
&= K_1 \exp\{-\tfrac{1}{2N_0}\int_{t_L}^{t_U}|x_r(\tau)|^2 d\tau\} \exp\{-\tfrac{1}{2N_0}\int_{t_L}^{t_U}|x_B(\bar{C}(\bar{A}),\tau)|^2 d\tau\} \\
&\qquad \tfrac{1}{2\pi I_0(\xi)}\int_{-\pi}^{\pi} \exp[Re\{\frac{e^{ju}\xi N_0 + e^{j(\omega_c t+\psi)}[\int_{t_L}^{t_U} x_B(\bar{C}(\bar{A}),\tau)x_r^*(\tau)d\tau]}{N_0}\}]du \\
&= K_1 \exp\{-\tfrac{1}{2N_0}\int_{t_L}^{t_U}|x_r(\tau)|^2 d\tau\} \exp\{-\tfrac{1}{2N_0}\int_{t_L}^{t_U}|x_B(\bar{C}(\bar{A}),\tau)|^2 d\tau\} \\
&\tfrac{1}{2\pi I_0(\xi)}\int_{-\pi}^{\pi} \exp[Re\{e^{ju}(\tfrac{\xi N_0}{N_0} + e^{-ju}e^{j(\omega_c t+\psi)}[\int_{t_L}^{t_U} x_B(\bar{C}(\bar{A}),\tau)x_r^*(\tau)d\tau])\}du. \qquad (4.9)
\end{aligned}
$$

Replacing the parameter u with $\psi - \hat{\psi}$, the equation becomes

$$
\begin{aligned}
&P(x_r(t)|x_B(\bar{C}(\bar{A}),t),\psi) = \\
&K_1 \exp\{-\tfrac{1}{2N_0}\int_{t_L}^{t_U}|x_r(\tau)|^2 d\tau\} \exp\{-\tfrac{1}{2N_0}\int_{t_L}^{t_U}|x_B(\bar{C}(\bar{A}),\tau)|^2 d\tau\} \\
&\tfrac{1}{2\pi I_0(\xi)}\int_{-\pi}^{\pi} \exp[Re\{e^{ju}(\tfrac{\xi N_0}{N_0} + \tfrac{e^{j(\omega_c t+\hat{\psi})}}{N_0}[\int_{t_L}^{t_U} x_B(\bar{C}(\bar{A}),\tau)x_r^*(\tau)d\tau])\}du \quad . \qquad (4.10)
\end{aligned}
$$

From the definition of the modified Bessel functions [33]

$$
I_0(|\alpha|) = \frac{1}{2\pi}\int_{-\pi}^{\pi} \exp\{Re\{e^{j\phi}\alpha^*\}\}d\phi. \qquad (4.11)
$$

Substituting Eq. 4.11 into Eq. 4.10, we get

$$
\begin{aligned}
P(x_r(t)|x_B(\bar{C}(\bar{A}),t),\hat{\psi}) \;=\; & \frac{K_1}{2\pi I_0(\xi)} \exp\{-\frac{1}{2N_0}\int_{t_L}^{t_U}|x_r(\tau)|^2 d\tau\} \\
& \exp\{-\frac{1}{2N_0}\int_{t_L}^{t_U}|x_E(\bar{C}(\bar{A}),\tau)|^2 d\tau\} \\
& I_0(\frac{|\int_{t_L}^{t_U}(x_r(t)e^{-j(\omega_c t+\hat{\psi})})x_B^*(\bar{C}(\bar{A}),t)dt + \xi N_o|}{N_0}).
\end{aligned}
$$

(4.12)

The maximum likelihood receiver chooses as the most probable sequence, the one which maximizes $P(x_r(t)|x_B(\bar{C}(\bar{A}),t),\hat{\psi})$. Since the term $(\int_{t_L}^{t_U}|x_r(t)|^2dt)$ is independent of the transmitted sequence $\bar{C}(\bar{A})$, it does not affect the decision rule. Considering this fact, we end up with the following decision metric expression (to be maximized) :

$$\exp\{-(\frac{1}{2N_o}(\int_{t_L}^{t_U}|x_B(\bar{C}(\bar{A}),\tau)|^2d\tau)\}I_0(\frac{|\int_{t_L}^{t_U}x_r(\tau)e^{-j(\omega_c\tau+\hat{\psi})}x_B^*(\bar{C}(\bar{A}),\tau)d\tau+\xi N_o|}{N_o}).$$

(4.13)

The expression of Eq. (4.13) consists of an exponential term and a zero order modified Bessel function term. The implementation of a receiver based on this metric would be quite complex, therefore, it will be useful if it can be approximated by lower complexity structures. In the following paragraphs asymptotically optimal structures of the receiver for high and low E_b/N_o with lower complexity are provided.

Before examining the cases of low $\frac{E_b}{N_o}$ and high $\frac{E_b}{N_o}$, we should mention that in [38], the metric expressions for noncoherent detection are derived. The metric expressions derived above is a generalization of the noncoherent case. When $\xi = 0$, as the pdf of phase error reduces to uniform density function, the metric expressions get reduced to the ones for noncoherent case.

Low E_b/N_o Case

The exponential and modified Bessel functions can be expressed through the following time series expansions:

$$e^x = \sum_{l=0}^{\infty}\frac{x^l}{l!} \quad \text{and} \quad I_o(x) = \sum_{i=0}^{\infty}\frac{x^{2i}}{2^{2i}(i!)^2}\ . \tag{4.14}$$

Using these formulas with Eq. (4.13), we get

$$[1+(-\frac{1}{2N_0}\int_{t_L}^{t_U}|x_B(\bar{C}(\bar{A}),\tau)|^2d\tau)+\frac{1}{2}\frac{1}{4N_0^2}(\int_{t_L}^{t_U}|x_B(\bar{C}(\bar{A}),\tau)|^2d\tau)^2+\ldots]$$
$$[1+\frac{1}{4}\frac{1}{N_0^2}|\int_{t_L}^{t_U}x_r(\tau)e^{-j(\omega_c\tau+\hat{\psi})}x_B^*(\bar{C}(\bar{A}),\tau)d\tau+\xi N_0|^2+\ldots]\ . \tag{4.15}$$

Defining

$$INT(x_B(\bar{C}(\bar{A}),t)) = \frac{1}{2}\int_{t_L}^{t_U} |x_B(\bar{C}(\bar{A}),\tau)|^2 d\tau \tag{4.16}$$

and

$$IRE(x_r(t), x_B(\bar{C}(\bar{A}),t)) = \int_{t_L}^{t_U} x_r(\tau) e^{-j(\omega_c\tau+\hat{\psi})} x_B^*(\bar{C}(\bar{A}),\tau) d\tau \tag{4.17}$$

and neglecting the terms containing the term N_0 raised to the power higher than two in the denominator (since at low $\frac{E_b}{N_0}$, N_0 is large, division by high powers of N_0 will give very small values compared to the rest of the terms), Eq. 4.15 becomes

$$1 + \frac{|IRE(x_r(t), x_B(\bar{C}(\bar{A}),t)) + \xi N_0|^2}{4N_0^2} - \frac{1}{N_0} INT(x_B(\bar{C}(\bar{A}),t)) + \frac{1}{2N_0^2} INT^2(x_B(\bar{C}(\bar{A}),t)). \tag{4.18}$$

The constant term 1 can be neglected since it will not affect the decision rule. Also, multiplying every term by N_0 will not change the decision rule. After the above procedure, the metric expression becomes:

$$\frac{|IRE(x_r(t), x_B(\bar{C}(\bar{A}),t)) + \xi N_0|^2}{4N_0} - INT(x_B(\bar{C}(\bar{A}),t)) + \frac{1}{2N_0} INT^2(x_B(\bar{C}(\bar{A}),t)) \tag{4.19}$$

Since

$$\begin{aligned}\frac{|IRE(x_r(t), x_B(\bar{C}(\bar{A}),t)) + \xi N_0|^2}{4N_0} = {} & \frac{|IRE(x_r(t), x_B(\bar{C}(\bar{A}),t))|^2}{4N_0} + \frac{|\xi N_0|^2}{4N_0} \\ & + \xi N_0 \frac{Re\{IRE(x_r(t), x_B(\bar{C}(\bar{A}),t))\}}{2N_0}\end{aligned} \tag{4.20}$$

ignoring the second term which is a constant and common to all received signals, we get

$$\begin{aligned}\frac{|IRE(x_r(t), x_B(\bar{C}(\bar{A}),t))|^2}{4N_0} & + \xi N_0 \frac{Re\{IRE(x_r(t), x_B(\bar{C}(\bar{A}),t))\}}{2N_0} \\ & - INT(x_B(\bar{C}(\bar{A}),t)) + \frac{INT^2(x_B(\bar{C}(\bar{A}),t))}{2N_o}.\end{aligned} \tag{4.21}$$

When $INT(x_B(\bar{C}(\bar{A}),t))$ is dependent on $\bar{C}(\bar{A})$, it remains in the decoding process (this is the case of a time dispersive channel). As E_b/N_o becomes smaller, the two terms having N_o at the denominator become negligible. The decoding metric in this case becomes:

$$-INT(x_B(\bar{C}(\bar{A}),t)) + \frac{\xi}{2}[Re\{IRE(x_r(t), x_B(\bar{C}(\bar{A}),t))\}]. \tag{4.22}$$

As ξ (i.e., the signal to noise ratio of the carrier recovery loop) becomes larger, the term $[IRE(x_r(t), x_B(\bar{C}(\bar{A}),t))]$ becomes dominant in the decoding process. On the contrary, as ξ becomes smaller, the effect of $[IRE(x_r(t), x_B(\bar{C}(\bar{A}),t))]$ becomes smaller and for $\xi = 0$ (which corresponds to the non-coherent case) this term disappears completely. This results in a decision which is independent from the received signal. Regardless of what the received signal is, the decoder will always decode the sequence(s) which happens to provide the maximum value for $-INT(x_B(\bar{C}(\bar{A}),t))$. When $\xi = 0$, the pdf given in Eq.4.5 will equal to $\frac{1}{2\pi}$, which is a uniform density function. In addition, since the signal to noise ratio is low, the received signal will carry almost no information regarding to the transmitted signal. So, the receiver will have its decision based on not the received signal but the whole sequence. Because of the low signal to noise ratio, the signal is practically covered completely by noise. Since there is no apriori knowledge of the signal carrier phase, the receiver observes practically noise without having an information to extract a useful signal out of it. In this case, the safest decision is to choose the signal that happens to have the highest energy content from all the possible signals that can be generated from the different combinations of the information sequence.

High E_b/N_o Case

For high E_b/N_o, the following approximation of the modified Bessel function can be used :

$$I_o(|z|) \simeq \frac{1}{\sqrt{2\pi|z|}} e^{|z|} \quad \text{for} \quad |z| > 3. \tag{4.23}$$

We define

$$\begin{aligned} INT(1) &= INT(x_B(\bar{C}(\bar{A}_1),t)) \\ INT(2) &= INT(x_B(\bar{C}(\bar{A}_2),t)) \\ IRE(1) &= IRE(x_{r_1}(t),x_B(\bar{C}(\bar{A}_1),t)) \\ IRE(2) &= IRE(x_{r_2}(t),x_B(\bar{C}(\bar{A}_2),t)). \end{aligned} \tag{4.24}$$

For two different possible sequences $\bar{C}(\bar{A}_1)$, $\bar{C}(\bar{A}_2)$ and received signals $x_{r_1}(t)$, $x_{r_2}(t)$ (and by using the approximation for modified Bessel function given above), we end up with the following decision metric:

$$\begin{aligned} &\exp(-\frac{1}{N_0}INT(1))\frac{1}{\sqrt{2\pi}\sqrt{\frac{|IRE(1)+\xi N_0|}{N_0}}}\exp(\frac{|IRE(1)+\xi N_0|}{N_0})\underset{2}{\overset{1}{\gtrless}} \\ &\exp(-\frac{1}{N_0}INT(2))\frac{1}{\sqrt{2\pi}\sqrt{\frac{|IRE(2)+\xi N_0|}{N_0}}}\exp(\frac{|IRE(2)+\xi N_0|}{N_0}). \end{aligned} \tag{4.25}$$

where $\underset{2}{\overset{1}{\gtrless}}$ means that the decision will be made in favor of sequence 1 (i.e. $\bar{C}(\bar{A}_1)$) if the term appearing to the left of $\underset{2}{\overset{1}{\gtrless}}$ is larger than the term appearing to the right of it and *vice versa*. Equivalently,

$$\frac{\frac{1}{\sqrt{2\pi}\sqrt{\frac{|IRE(1)+\xi N_0|}{N_0}}}}{\frac{1}{\sqrt{2\pi}\sqrt{\frac{|IRE(2)+\xi N_0|}{N_0}}}}\exp\{\frac{|IRE(1)+\xi N_0|-|IRE(2)+\xi N_0|-INT(1)+INT(2)}{N_0}\}\underset{2}{\overset{1}{\gtrless}}1 \tag{4.26}$$

Taking the natural logarithm of both sides, we have

$$\frac{N_0\ln\frac{\sqrt{|IRE(2)+\xi N_0|}}{\sqrt{|IRE(1)+\xi N_0|}}+|IRE(1)+\xi N_0|-|IRE(2)+\xi N_0|-INT(1)+INT(2)}{N_0}\underset{2}{\overset{1}{\gtrless}}0 \tag{4.27}$$

or

$$N_0 \ln \frac{\sqrt{|IRE(2)+\xi N_0|}}{\sqrt{|IRE(1)+\xi N_0|}} + |IRE(1)+\xi N_0| - |IRE(2)+\xi N_0|$$

$$-INT(1) + INT(2) \underset{2}{\overset{1}{\gtrless}} 0. \tag{4.28}$$

Neglecting the first term, since the product N_0 is small and reorganizing the expression gives:

$$|IRE(1)+\xi N_0| - INT(1) \underset{2}{\overset{1}{\gtrless}} |IRE(2)+\xi N_0| - INT(2) \quad . \tag{4.29}$$

In other words, the asymptotically optimal decoding metric is

$$-INT(x_B(\bar{C}(\bar{A}),t)) + |IRE(x_r(t), x_B(\bar{C}(\bar{A}),t)) + \xi N_o|. \tag{4.30}$$

Comparing Eqs. (4.13) and (4.30), we see that (4.30) does not contain exponential and Bessel functions. Also the need to provide scaling according to the noise has disappeared.

So far, the derived metric expressions are general and can apply to any phase modulated signal. Now, we will apply these metric expressions to PSK signals. In the PSK format c_k has the form $c_k = e^{j\phi_k}$. The possible values of ϕ_k are equal to $\phi_k = \frac{2i\pi}{M}$ $(0 \leq i \leq M-1)$ with $M = 2^q$ being the number of points in the PSK constellation (M-PSK). The symbols c_k enter the premodulation filter $H_T(\omega)$ (Fig. 4.1) with an impulse response of $h_T(t)$. The output of $H_T(\omega)$ is given by :

$$x_{tr,B}(\bar{C}(\bar{A}),t) = \sum_{k=0}^{Z-1} c_k h_T(t-kT) \tag{4.31}$$

The transmitted signal after passing through the channel becomes:

$$x(\bar{C}(\bar{A}),t) = x_B(\bar{C}(\bar{A}),t)e^{j(\omega_c t+\psi)} = \sum_{k=0}^{Z-1} c_k h_E(t-kT)e^{j(\omega_c t+\psi)} \tag{4.32}$$

with $h_E(t) = h_T(t) \otimes h_{c,B}(t)$ representing the overall baseband impulse response of the transmitter and the channel. The frequency response of $h_E(t)$ is $H_E(\omega)$. Substituting

Eq.(4.32) into Eq.(4.13), we get

$$\exp\{-\frac{1}{2N_0}\int_{t_L}^{t_U}(\sum_{k=0}^{Z-1}c_k h_E(\tau-kT))(\sum_{l=0}^{Z-1}c_l^* h_E^*(\tau-lT))d\tau\}$$
$$I_0(\frac{|\int_{t_L}^{t_U}x_r(t)e^{-j(\omega_c t+\hat{\psi})}(\sum_{k=0}^{Z-1}c_k^* h_E^*(\tau-kT))d\tau+\xi N_0|}{N_0}). \tag{4.33}$$

For the argument of the exponential term above, reversing the order of integration and summation, it becomes:

$$-\frac{1}{2N_0}\sum_{k=0}^{Z-1}\sum_{l=0}^{Z-1}c_k c_l^*\int_{t_L}^{t_U}h_E(\tau-kT)h_E^*(\tau-lT)d\tau. \tag{4.34}$$

Since $h_k = h(kT)$ and

$$h_{k-l} = h((k-l)T) = \int_{t_L}^{t_U}h_E^*(\tau)h_E((k-l)T+\tau)d\tau, \tag{4.35}$$

the change of variables $\alpha = \tau + kT$ and $d\alpha = d\tau$ leads to

$$h_{k-l} = \int_{t_L}^{t_U}h_E^*(\alpha-kT)h_E(\alpha-lT)d\alpha. \tag{4.36}$$

Replacing the integral term in Eq.(4.34) accordingly, the argument of the exponential term becomes:

$$-\frac{1}{2N_0}\sum_{k=0}^{Z-1}\sum_{l=0}^{Z-1}c_k c_l^* h_{k-l}. \tag{4.37}$$

Eq. 4.37 can be rewritten in the form

$$-\frac{1}{2N_0}(\sum_{k=0}^{Z-1}|c_k|^2 h_0+\underbrace{\sum_{k=0}^{Z-1}\sum_{l=0}^{Z-1}}_{k\neq l}c_k c_l^* h_{k-l}). \tag{4.38}$$

Since $\sum_{k=0}^{Z-1}|c_k|^2 h_0$ is common to all received signals ($|c_k|^2 = |c_i|^2$ for all k and i), it can be neglected. The rest can be expressed as

$$-\frac{1}{2N_0}(\sum_{k=1}^{Z-1}\sum_{l=k}^{Z-1}(c_l c_{l-k}^* h_k + c_l^* c_{l-k} h_k^*)). \tag{4.39}$$

For the argument of the modified Bessel function in Eq. (4.33), change of the order of integration and summation will give:

$$\frac{|\sum_{k=0}^{Z-1}\int_{t_L}^{t_U} x_\tau(\tau)e^{-j(\omega_c t+\hat{\psi})}h_E^*(\tau-kT))dt\ c_k^*+\xi N_0|}{N_0}. \tag{4.40}$$

Since

$$y(t)=\int_{-\infty}^{\infty}(x_\tau(\tau)e^{-j(\omega_c\tau+\hat{\psi})})h_E^*(\tau-t)d\tau. \tag{4.41}$$

where $y(t)$ can be derived by demodulating $x_\tau(t)$ (the process described by the term $(x_\tau(t)e^{-j(\omega_c t+\hat{\psi})})$) and afterwards passing it through a filter $H_R(\omega)$ matched to $H_E(\omega)$ and $y_k=y(kT)$, the argument of the modified Bessel function becomes:

$$\frac{|\sum_{k=0}^{Z-1}y_k c_k^*+\xi N_0|}{N_0}. \tag{4.42}$$

So, the decoder metric for PSK signals becomes:

$$\exp\{-\frac{1}{2N_o}(\sum_{k=1}^{Z-1}\sum_{l=k}^{Z-1}(c_l c_{l-k}^* h_k+c_l^* c_{l-k}h_k^*))\}I_0(\frac{|\sum_{k=0}^{Z-1}y_k c_k^*+\xi N_o|}{N_o}) \tag{4.43}$$

For low $\frac{E_b}{N_0}$ case, since

$$\begin{aligned} INT(x_B(\bar{C}(\bar{A}),t)) &= \frac{1}{2}\sum_{k=1}^{Z-1}\sum_{l=k}^{Z-1}(c_l c_{l-k}^* h_k+c_l^* c_{l-k}h_k^*) \\ &= \sum_{k=1}^{Z-1}\sum_{l=k}^{Z-1}Re\{c_l c_{l-k}^* h_k\} \end{aligned} \tag{4.44}$$

and

$$IRE(x_\tau(t),x_B(\bar{C}(\bar{A}),t))=\sum_{k=0}^{Z-1}y_k c_k^*\ , \tag{4.45}$$

substituting them into Eq.(4.22) we get:

$$\sum_{k=1}^{Z-1}\sum_{l=k}^{Z-1}Re\{c_l c_{l-k}^* h_k\}+\frac{\xi}{2}[\sum_{k=0}^{Z-1}Re\{y_k c_k^*\}]. \tag{4.46}$$

For high $\frac{E_b}{N_0}$, the metric expression becomes:

$$-\sum_{k=1}^{Z-1}\sum_{l=k}^{Z-1} Re\{c_l c_{l-k}^* h_k\} + |\sum_{k=0}^{Z-1} y_k c_k^* + \xi N_o|. \tag{4.47}$$

When $H_E(\omega)$ has the spectral shaping of a square root Nyquist I filter, (i.e., $h_0 = 1$ and $h_k = 0 \ \ \forall k \neq 0$) only the modified Bessel function term remains in the metric of Eq. (4.43). At this point, considering the monotonic nature of the modified Bessel function, we can transfer the maximization of the function itself to the maximization of its argument, i.e.,

$$\Re(\bar{y}, \bar{C}(\bar{A})) = |\sum_{k=0}^{Z-1} y_k c_k^* + \xi N_o|. \tag{4.48}$$

Note that, the decoder based on Eq. (4.48) is optimal only for PSK signals and under Nyquist filtering and equal apportioning conditions.

An alternative (equivalent) way of implementing the receiver can be achieved by squaring the decoding metric expression given in Eq.(4.48), in which case we get:

$$\begin{aligned}
[\Re(\bar{y}, \bar{C}(\bar{A}))]^2 &= |\sum_{k=0}^{Z-1} y_k c_k^* + \xi N_o|^2 \\
&= (Re\{\sum_{k=0}^{Z-1} y_k c_k^*\} + \xi N_0)^2 + (Im\{\sum_{k=0}^{Z-1} y_k c_k^*\})^2 \\
&= (\sum_{k=0}^{Z-1} Re\{y_k c_k^*\})^2 + (\sum_{k=0}^{Z-1} Im\{y_k c_k^*\})^2 + 2\xi N_0 \sum_{k=0}^{Z-1} Re\{y_k c_k^*\} + (\xi N_0)^2 \\
&= \sum_{k=0}^{Z-1} (Re\{y_k c_k^*\})^2 + \sum_{k=0}^{Z-1} (Im\{y_k c_k^*\})^2 + 2\sum_{k=1}^{Z-1}\sum_{l=0}^{k-1} Re\{y_k c_k^*\} Re\{y_l c_l^*\} \\
&\quad +2\sum_{k=1}^{Z-1}\sum_{l=0}^{k-1} Im\{y_k c_k^*\} Im\{y_l c_l^*\} + 2\xi N_0 \sum_{k=0}^{Z-1} Re\{y_k c_k^*\} + (\xi N_0)^2
\end{aligned} \tag{4.49}$$

Since

$$\begin{aligned}
\sum_{k=0}^{Z-1} (Re\{y_k c_k^*\})^2 + \sum_{k=0}^{Z-1} (Im\{y_k c_k^*\})^2 &= \sum_{k=0}^{Z-1} |y_k c_k^*|^2 = \sum_{k=0}^{Z-1} |y_k|^2 |c_k^*|^2 \\
&= \sum_{k=0}^{Z-1} |y_k|^2 |c_k|^2
\end{aligned} \tag{4.50}$$

and $|c_k|^2 = 1$, this term will not affect the decision along with the constant term $(\xi N_0)^2$ and so they can both be dropped from the metric expression. Dividing the rest by two, the metric expression becomes:

$$\sum_{k=1}^{Z-1}\sum_{l=0}^{k-1} Re\{y_k c_k^*\}Re\{y_l c_l^*\} + \sum_{k=1}^{Z-1}\sum_{l=0}^{k-1} Im\{y_k c_k^*\}Im\{y_l c_l^*\} + \xi N_0 \sum_{k=0}^{Z-1} Re\{y_k c_k^*\}. \quad (4.51)$$

Using the identity

$$\begin{aligned} &Re\{c_1 c_2^*\}Re\{c_3 c_4^*\} + Im\{c_1 c_2^*\}Im\{c_3 c_4^*\} \\ &= Re\{c_1 c_3^*\}Re\{c_2 c_4^*\} + Im\{c_1 c_3^*\}Im\{c_2 c_4^*\} \end{aligned} \quad (4.52)$$

(c_1, c_2, c_3, and c_4 being complex variables), the metric expression can be rewritten as:

$$\sum_{k=1}^{Z-1}\sum_{l=0}^{k-1} Re\{y_k y_l^*\}Re\{c_k c_l^*\} + \sum_{k=1}^{Z-1}\sum_{l=0}^{k-1} Im\{y_k y_l^*\}Im\{c_k c_l^*\} + \xi N_0 \sum_{k=0}^{Z-1} Re\{y_k c_k^*\}. \quad (4.53)$$

Defining a new variable $m = k - l$, replacing l by $k - m$ and rearranging the limits, we get:

$$\begin{aligned} \sum_{k=1}^{Z-1}\sum_{m=1}^{k} Re\{y_k y_{k-m}^*\}Re\{c_k c_{k-m}^*\} \quad &+ \quad \sum_{k=1}^{Z-1}\sum_{m=1}^{k} Im\{y_k y_{k-m}^*\}Im\{c_k c_{k-m}^*\} \\ &+ \quad \xi N_0 \sum_{k=0}^{Z-1} Re\{y_k c_k^*\}. \end{aligned} \quad (4.54)$$

The block diagram of the receiver based on the metric expression given above is shown in Fig. 4.2.

In the metric expression, we recognize that the last term stands for coherent detection and is multiplied by the weight ξN_0, which in fact shows that there is more weight given to this term as the signal to noise ratio at the output of the carrier recovery circuit increases. It is obvious that the coherent detection term becomes dominant as ξ increases. The first two terms stand for multidifferential detection. It was shown in [37] and [38] that increasing the number of differential detectors infinitely will lead the BER performance of multidifferential detection to approach

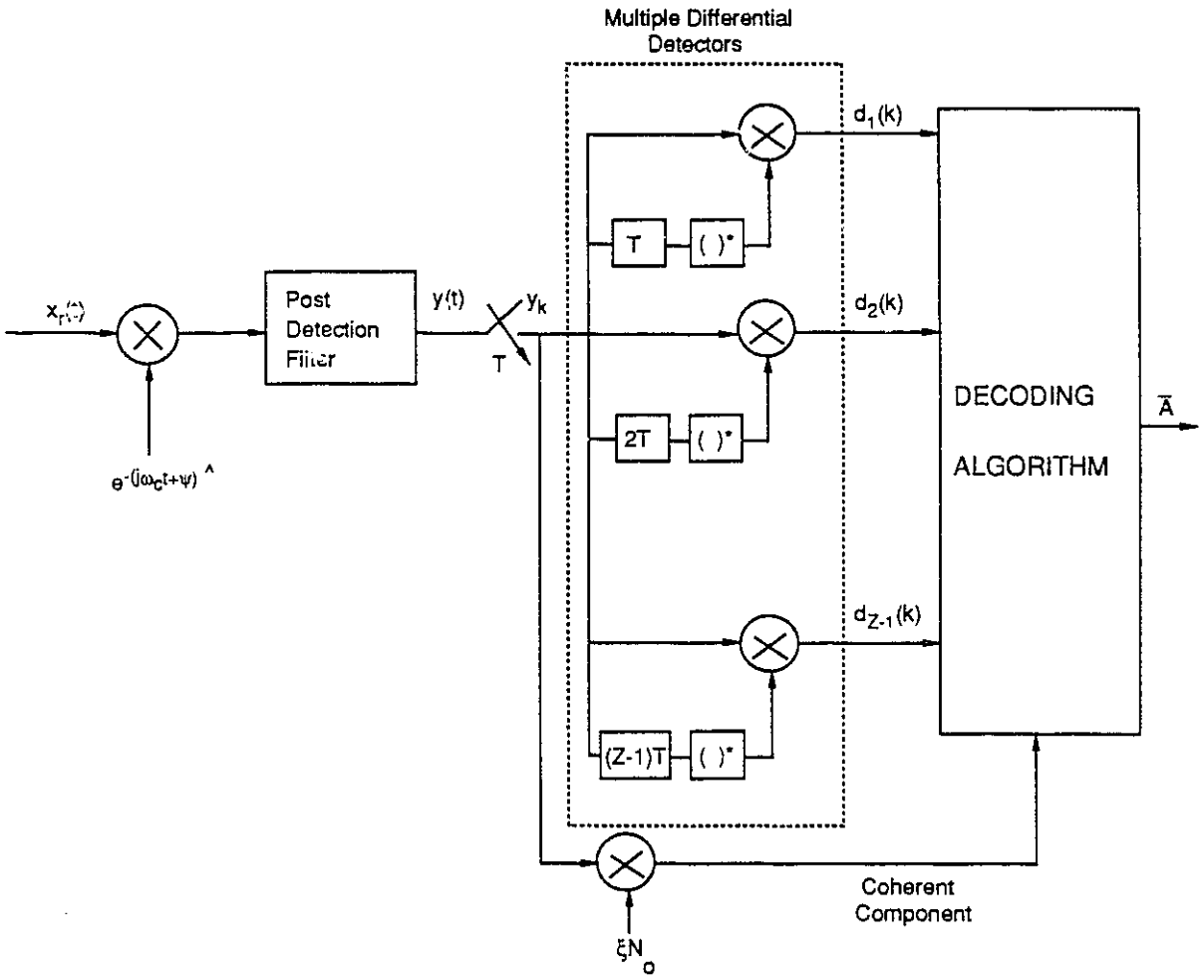

Figure 4.2: Block diagram of partially coherent PSK receiver based on the metric expression in Eq (4.54).

the performance of coherent detection in AWGN channels. It was also shown in the same paper that the incremental improvement obtained by increasing the number of differential detectors by one beyond a few of them would be negligible. Considering these facts, we decided to truncate multidifferential detectors with delay elements more than $2T$, i.e., only the T, $2T$ differential detectors are used, and employ Viterbi decoding to make decisions. In this case, the decision metric expression becomes:

$$\begin{aligned} & Re\{y_k y_{k-1}^*\} Re\{c_k c_{k-1}^*\} + Im\{y_k y_{k-1}^*\} Im\{c_k c_{k-1}^*\} \\ + \; & Re\{y_k y_{k-2}^*\} Re\{c_k c_{k-2}^*\} + Im\{y_k y_{k-2}^*\} Im\{c_k c_{k-2}^*\} \\ + \; & Re\{y_{k-1} y_{k-2}^*\} Re\{c_{k-1} c_{k-2}^*\} + Im\{y_{k-1} y_{k-2}^*\} Im\{c_{k-1} c_{k-2}^*\} \\ + \; & \xi N_0 Re\{y_k c_k^*\}. \end{aligned} \tag{4.55}$$

Implementation of the metric expression given above requires that the states be defined as $c_k c_{k-m}^*$. Since each state is defined by a combination of two symbols, each state will consist of a combination of two bits for BPSK and a combination of four bits for QPSK. This will lead to a four state trelllis diagram for BPSK and a sixteen state trellis diagram for QPSK. So, the trellis diagrams for BPSK and QPSK can be shown as in Fig.4.3 and Fig.4.4 respectively.

4.2 Performance of Partially Coherent Detection in AWGN Channels With a Noisy Phase Reference

Simulation programs using the trellis diagrams shown in Fig.4.3 and Fig.4.4 were run for a decoding depth of 16, and $BT = 0.01$ for both the fading process and the loop filter, i.e., the 3dB bandwidth of the loop filter was taken to be the same as Doppler bandwidth. Bits or symbols were processed in blocks of 4096 and the programs were run for each $\frac{E_b}{N_0}$ value until 100 bit errors were observed except for the cases where the bit error rate goes below 10^{-5} in which case the number of bits in error were minimum 48. In [39], it has been shown that $\frac{70}{P_b}$ samples per simulation run are required to be

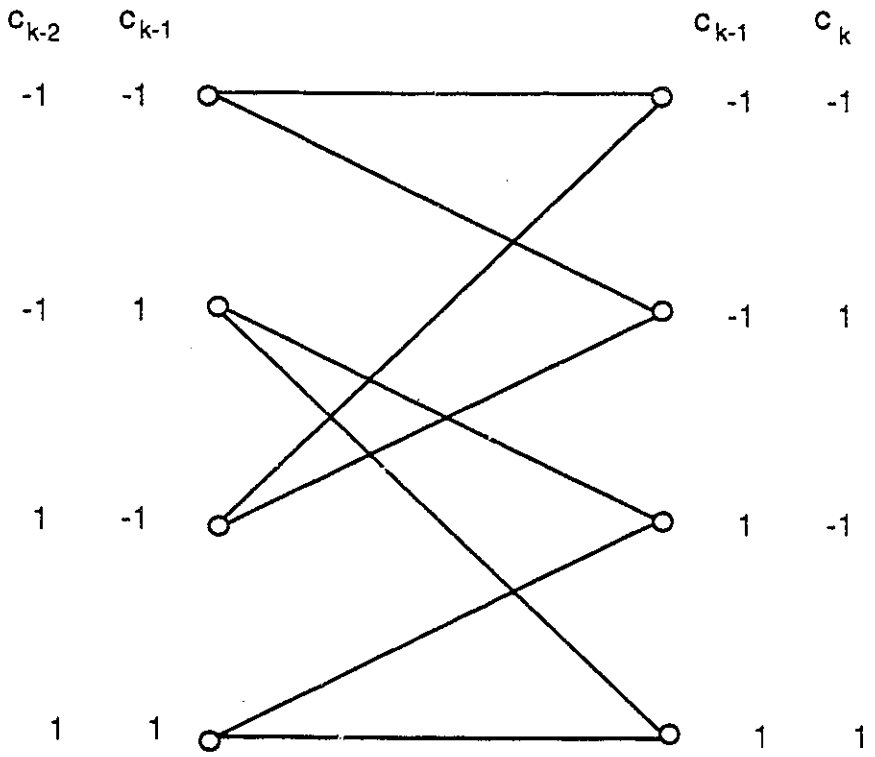

Figure 4.3: Trellis diagram used in the simulations for partially coherent detection of BPSK.

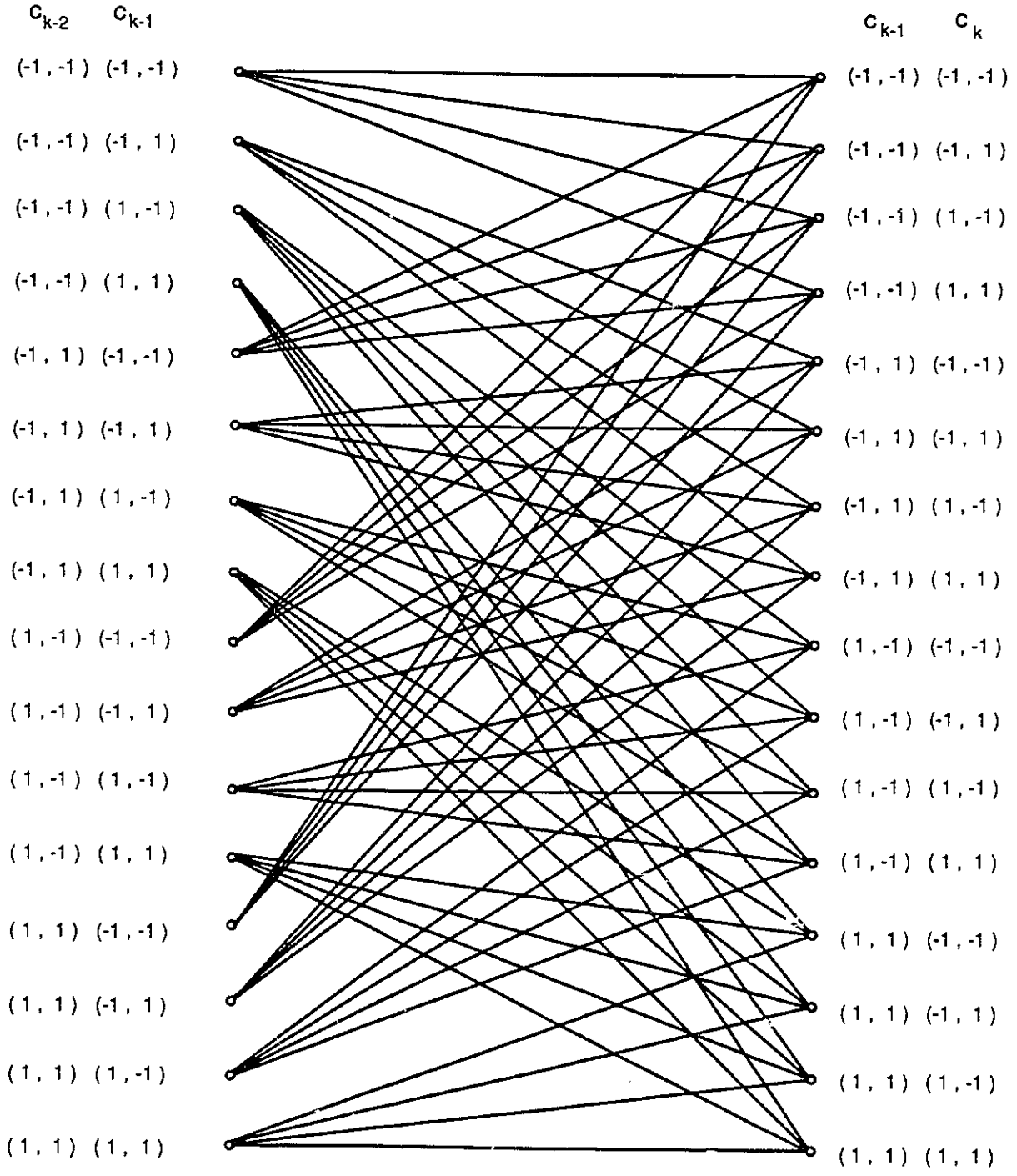

Figure 4.4: Trellis diagram used in the simulations for partially coherent detection of QPSK.

processed within the interval $[0.8P_b, \quad 1.2P_b]$ for a confidence of 95 percent. Also, in [40], it has been shown that $\frac{10}{P_b}$ samples per simulation run are required to be processed within the interval $[\frac{1}{3}P_b, \quad 1\frac{2}{3}P_b]$ with 95 percent confidence. So, the number of bits (symbols) processed during each simulation run meet the conditions given in these references.

The BER performance of BPSK for loop SNR $\xi = 10$dB and of QPSK for $\xi = 15$dB in AWGN channels with a noisy phase reference compared to coherent and $(1 + 2)$ differential detection are given in Figs.4.5 and 4.6 respectively. The loop filter 3dB bandwidth and symbol duration product was taken as $BT = 0.01$ for both cases.

First of all, when the two graphs are compared, it is apparent that, although the ξ is higher for the QPSK case, at $\frac{E_b}{N_0} = 10$dB, the BER performance coherent QPSK is almost an order of magnitude ($BER \approx 10^{-3}$ for QPSK and $\approx 10^{-4}$ for BPSK) inferior compared to BPSK This large difference in BER indicates how severely QPSK is affected by the noisy phase reference due to the fact that the phase difference between the neighbouring signal points in QPSK is half that of BPSK. Furthermore, common to both graphs, we observe that the performance curve of coherent detection crosses over the performance curves of $(1 + 2)$ differential and partially coherent detection. Since at low $\frac{E_b}{N_0}$ additive Gaussian noise is the dominating factor affecting the performances, coherent detection has a better performance than $(1+2)$ differential detection. As we go to higher $\frac{E_b}{N_0}$, since there is no attempt to estimate the phase of the carrier in differential detection, the performance of differential detection is better than coherent detection whereas the latter one severely degrades due to the dominating effect of phase noise.

When the performances of $(1 + 2)$ differential detection and partially coherent detection are compared, for the BPSK case, the BER performance of $(1+2)$ differential detection and partially coherent detection are almost identical (slightly better at lower values of $\frac{E_b}{N_0}$ and same for higher values). Recalling that the BER performances of coherent and $(1+2)$ differential detection are within 1 dB (Fig. 3.17), this result is not surprising. Furthermore, the BER performance curves get as close as 0.3 dB at $\frac{E_b}{N_0} =$

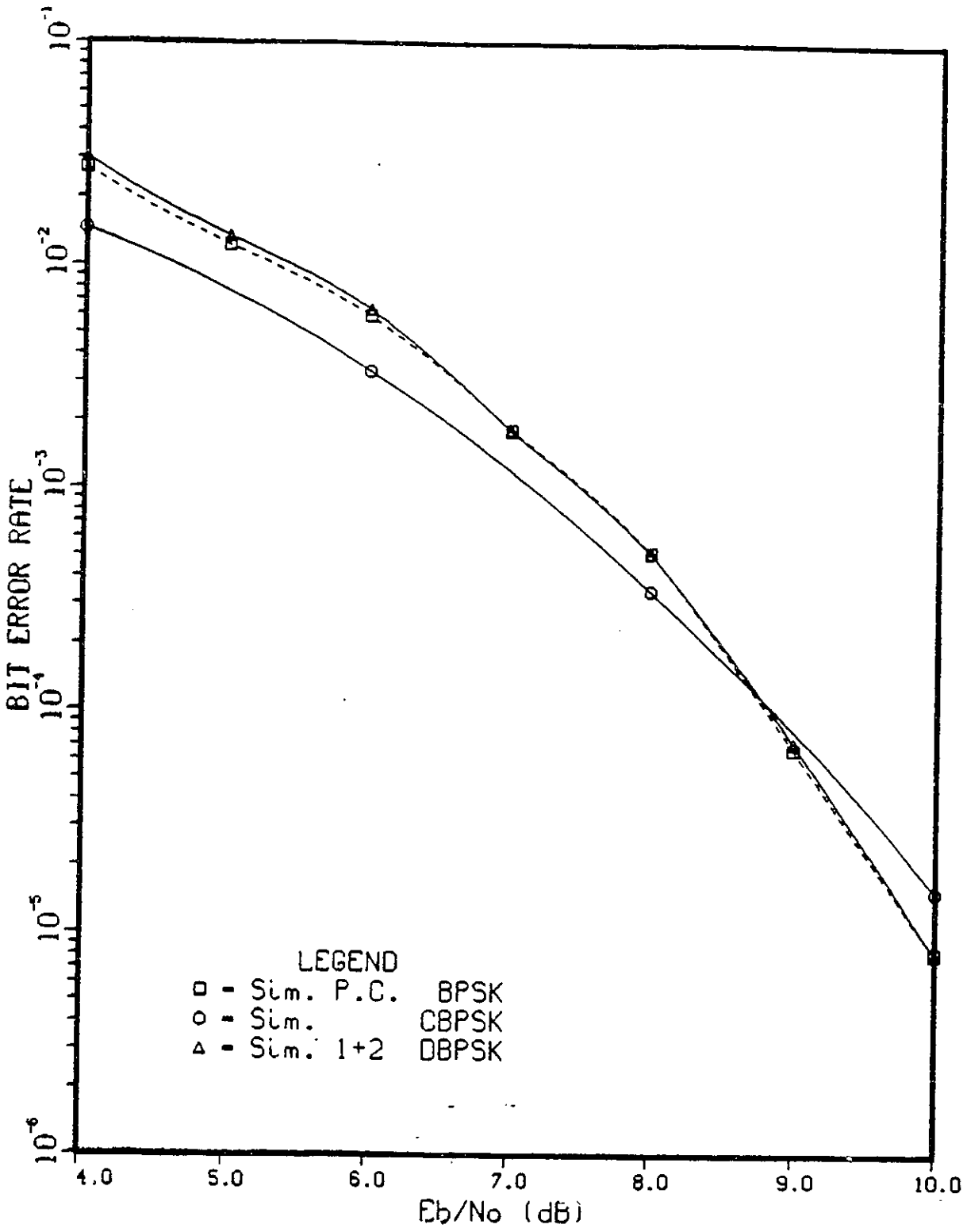

Figure 4.5: BER performance of partially coherent detection of BPSK in AWGN channels with a noisy phase reference for loop SNR $\xi = 10$dB and $BT = 0.01$.

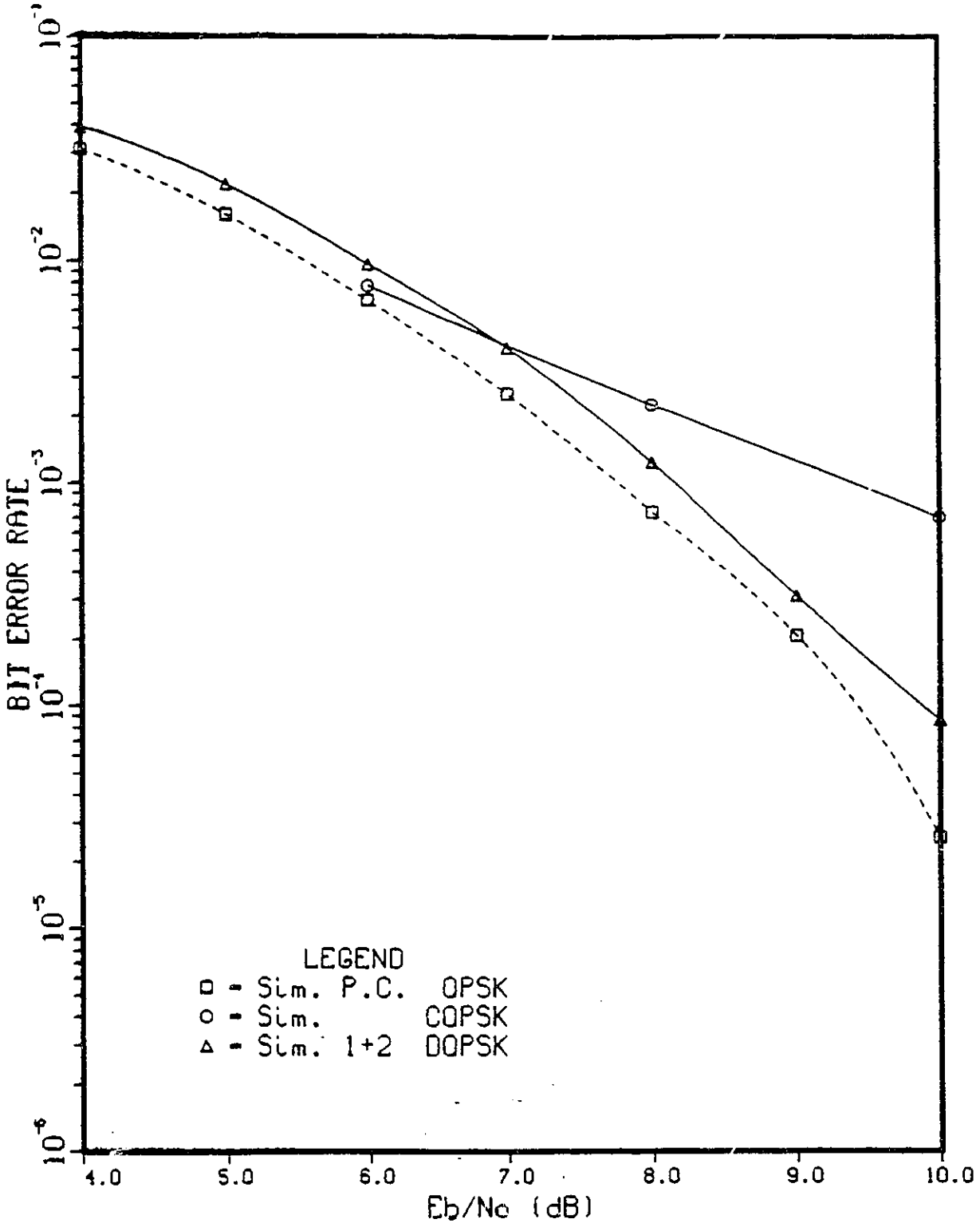

Figure 4.6: BER performance of partially coherent detection of QPSK in AWGN channels with a noisy phase reference for loop SNR $\xi = 15$dB and $BT = 0.01$.

10 dB. Considering the degradation of the coherent component of partially coherent detection due to the noisy phase reference and the fact that N_0 is getting smaller which is the only factor affecting the performance of multidifferential detection, actually this result was expected. It should also be considered that the metric expression applied is the truncated version of the one for the case of high $\frac{E_b}{N_0}$. At lower values of $\frac{E_b}{N_0}$, the coefficient of the coherent term (ξN_0) within the metric expression is large, causing coherent term to dominate where the performance of coherent detection is better compared to $(1+2)$ DBPSK. But the benefit from the domination of coherent term is significantly reduced due to the fact that the metric expression used is obtained under the assumption of high $\frac{E_b}{N_0}$.

For the QPSK case, partially coherent detection is 0.5dB better than $(1+2)$ differential detection at $\frac{E_b}{N_0} = 10$dB and the gain is increasing as $\frac{E_b}{N_0}$ increases. Since the difference in the performances of coherent detection and $(1+2)$ differential detection is higher (1.5dB at $\frac{E_b}{N_0} = 10$dB) compared to the corresponding difference for BPSK, and since $\xi = 15$dB, even at high values of $\frac{E_b}{N_0}$, the coefficient of the coherent term is relatively large (> 3 at $\frac{E_b}{N_0} = 10$dB) and causes the improvement in the performance.

4.3 Performance of Partially Coherent Detection in Slowly Varying Rician Channels

In order to have an idea about the effect of noisy phase reference in slowly varying Rician channels, we will have a brief look at the performances of partially coherent detection and coherent detection, using Model 1 of Section 2.3 where it was assumed that the loop filter bandwidth is wide enough to track the changes in phase due to the fading, but that the filter is not letting in the additive Gaussian noise. Although this model is not realistic, it was used to make comparisons.

As typical examples, the BER performances of coherent and partially coherent BPSK and QPSK for $K = 6$dB and $\xi = 15$dB using both models of Section 2.3 are as in Figs.4.7 and 4.8 respectively.

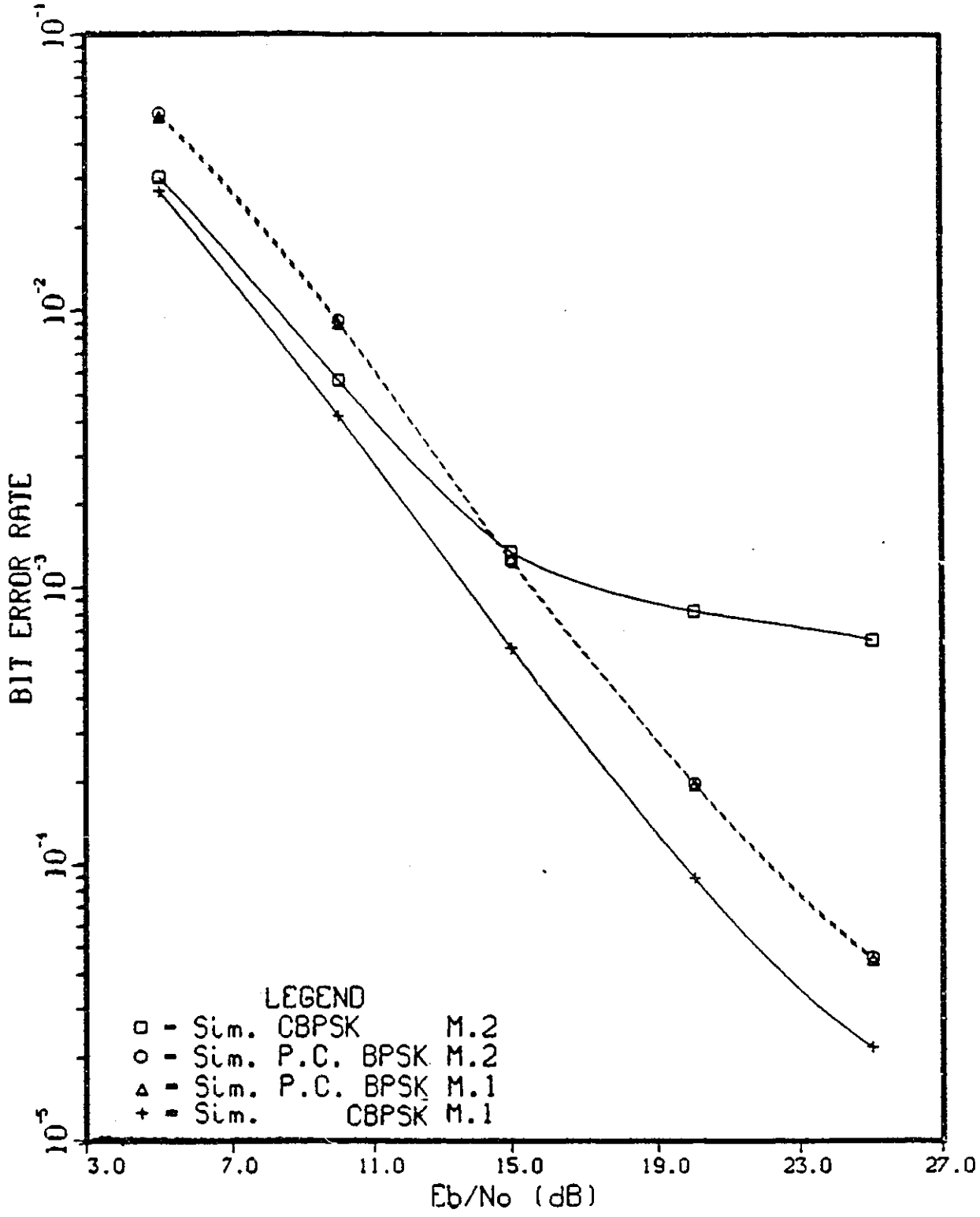

Figure 4.7: BER performances of coherent and partially coherent detection of BPSK in Rician channels using Model 1 (M.1) and Model 2 (M.2) of Section 2.3, for $K = 6$dB, loop SNR $\xi = 15$dB and $BT = 0.01$.

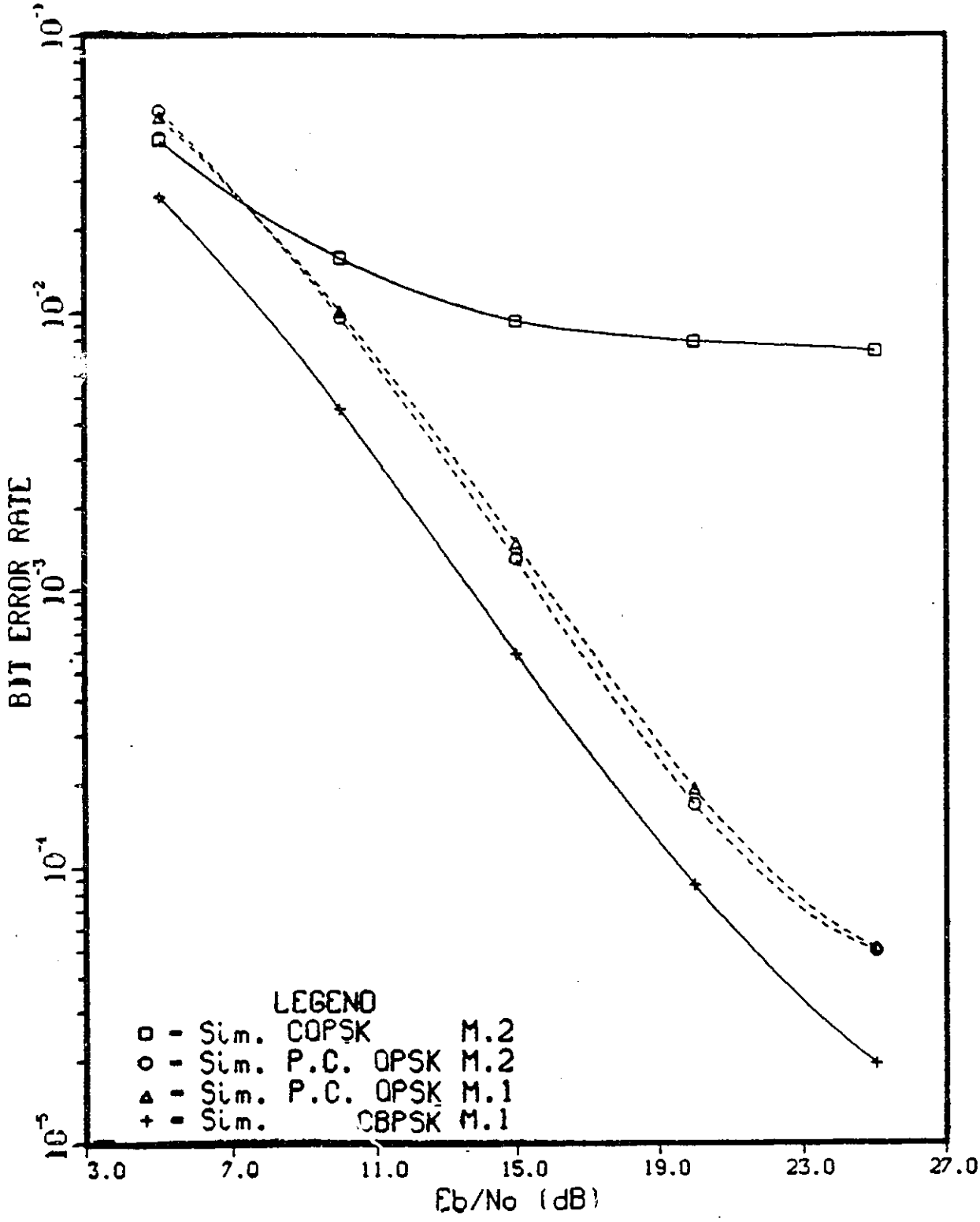

Figure 4.8: BER performances of coherent and partially coherent detection of QPSK in Rician channels using Model 1 (M.1) and Model 2 (M.2) of Section 2.3, for $K =$ 6dB, loop SNR $\xi = 15$dB and $BT = 0.01$.

In both of the graphs, when noisy phase reference is taken into account, coherent detection tails off and sits on error floors which is much lower for BPSK as expected. Performances of partially coherent detection for both models almost overlap in both of the graphs. If we consider that $K = 6$dB which means that fading is quite strong and on the contrary, $\xi = 15$dB which means that the signal to noise ratio of the loop filter is high and also taking into account that coherent detection is only 1dB better than $1 + 2$ differential detection for BPSK and 1.2dB better for QPSK, the reason for the close performances can be explained. Unfortunately, it was not possible to go beyond $\frac{E_b}{N_0} = 15$dB, when $K = 10$dB due to the low BER's reached. It would be unrealistic if the ξ would have been taken to be very low because the phase variations due to fading is very slow and not very large.

The BER performance of BPSK and QPSK in slowly varying Rician channels using Model 2 given in Section 2.3 and for K-factor values 6 and 10dB and loop SNR values $\xi = 10$ and 15dB are presented in comparison to coherent and $1+2$ differential detection in Fig.4.9 through Fig.4.16.

In neither BPSK, nor in QPSK case, the performance of partially coherent detection does not have any significant improvement compared to 1+2 differential detection. For BPSK, this was expected because there was no improvement even in AWGN channels with a noisy phase reference where the metric expressions were derived (see Fig. 4.5). For QPSK case, since even for $K = 6$dB, the direct component power is 4 times the diffuse component power, and the samples of filtered Gaussian processes used in the models for both to implement the noisy phase reference and the Rician fading are very strongly correlated, even the conventional differential detection can perform almost as well as partially coherent detection. Another factor that should be considered is that the original metric expression derived for high $\frac{E_b}{N_0}$ suggests that the received symbols be decoded in blocks. Although this implementation would complicate the decoding process, even relatively short block lengths might give a better performance.

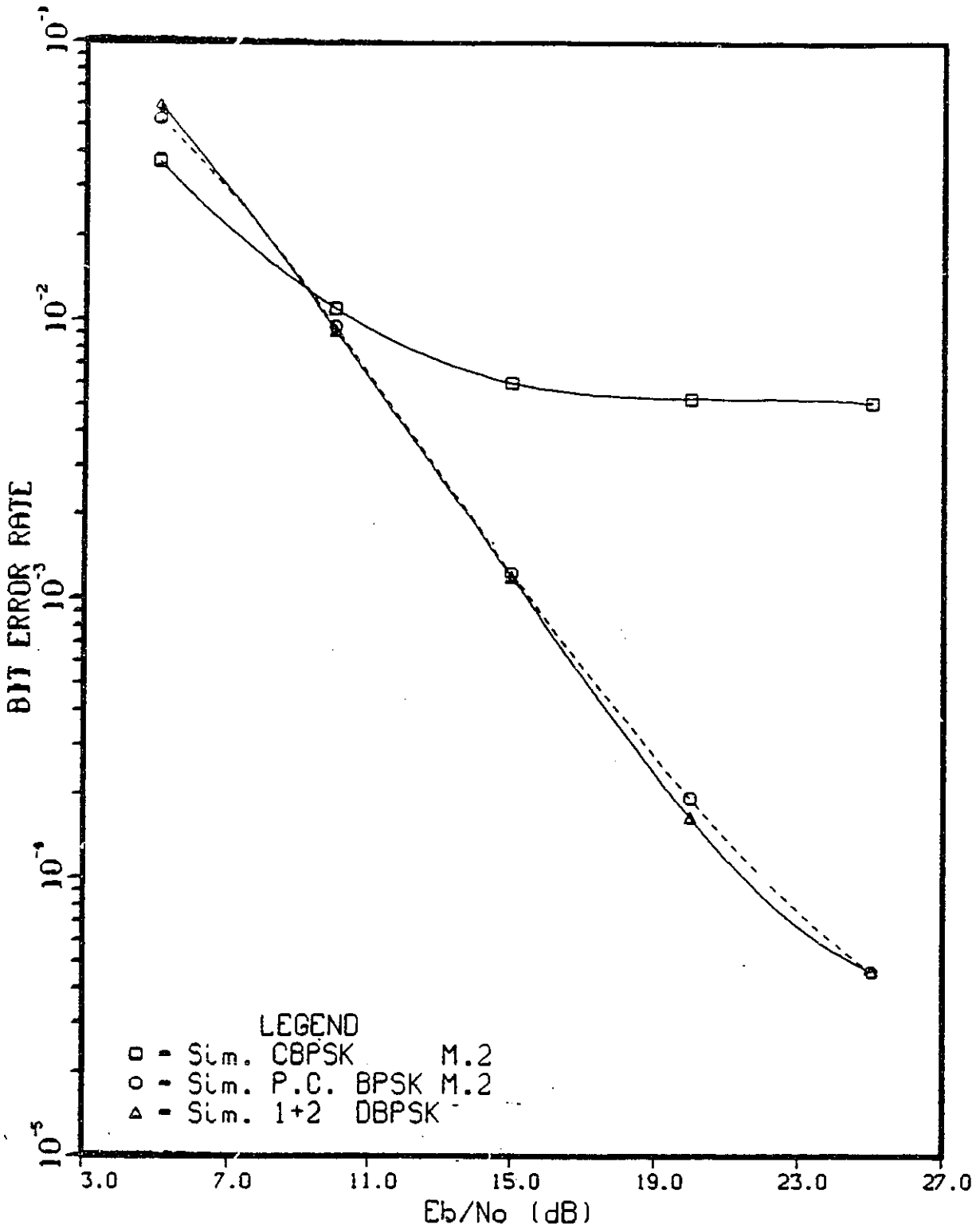

Figure 4.9: BER performance of partially coherent detection of BPSK in Rician channels using Model 2 (M.2) of Section 2.3, for $K = 6$dB, loop SNR $\xi = 10$dB and $BT = 0.01$.

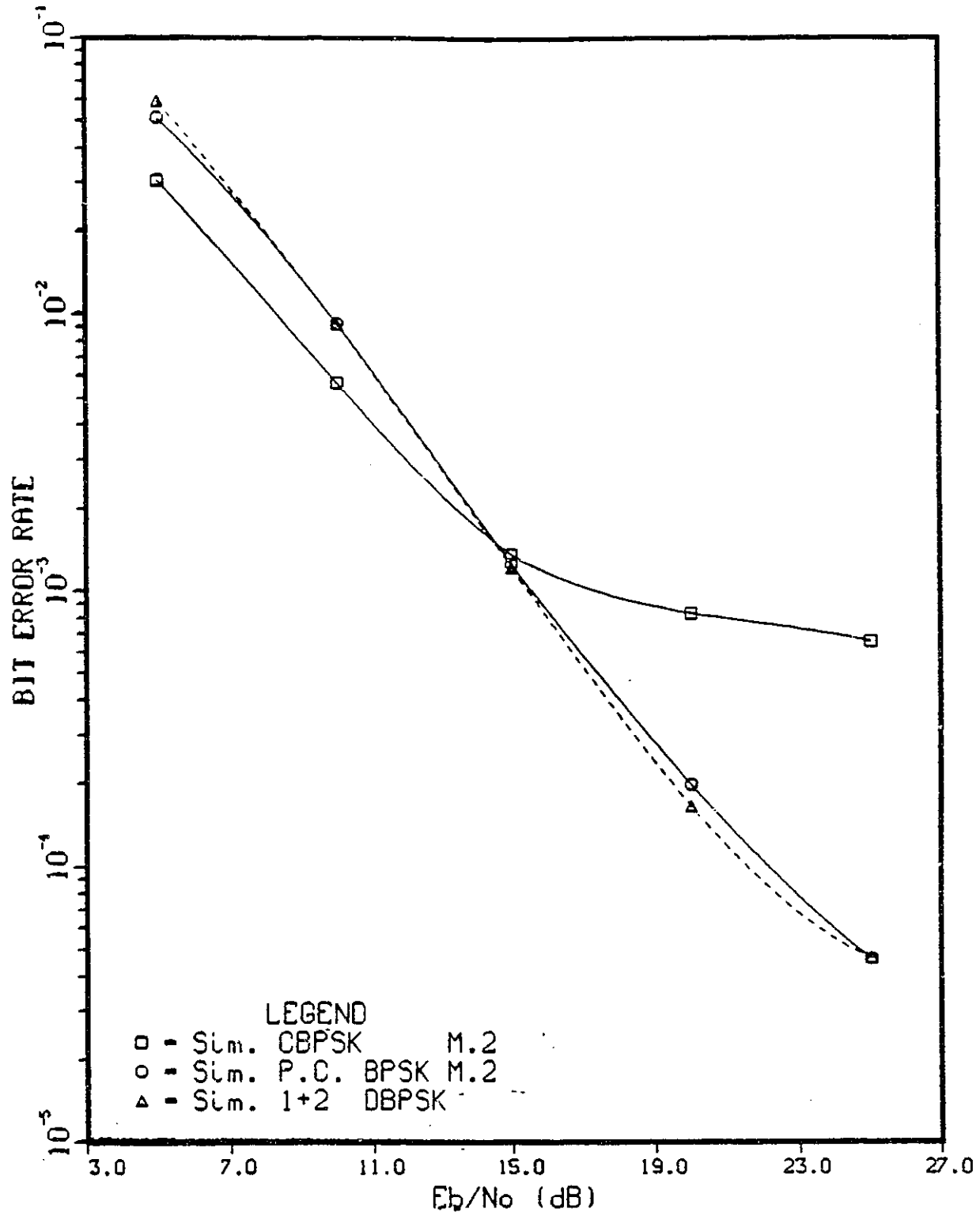

Figure 4.10: BER performance of partially coherent detection of BPSK in Rician channels using Model 2 (M.2) of Section 2.3, for $K = 6$dB, loop SNR $\xi = 15$dB and $BT = 0.01$.

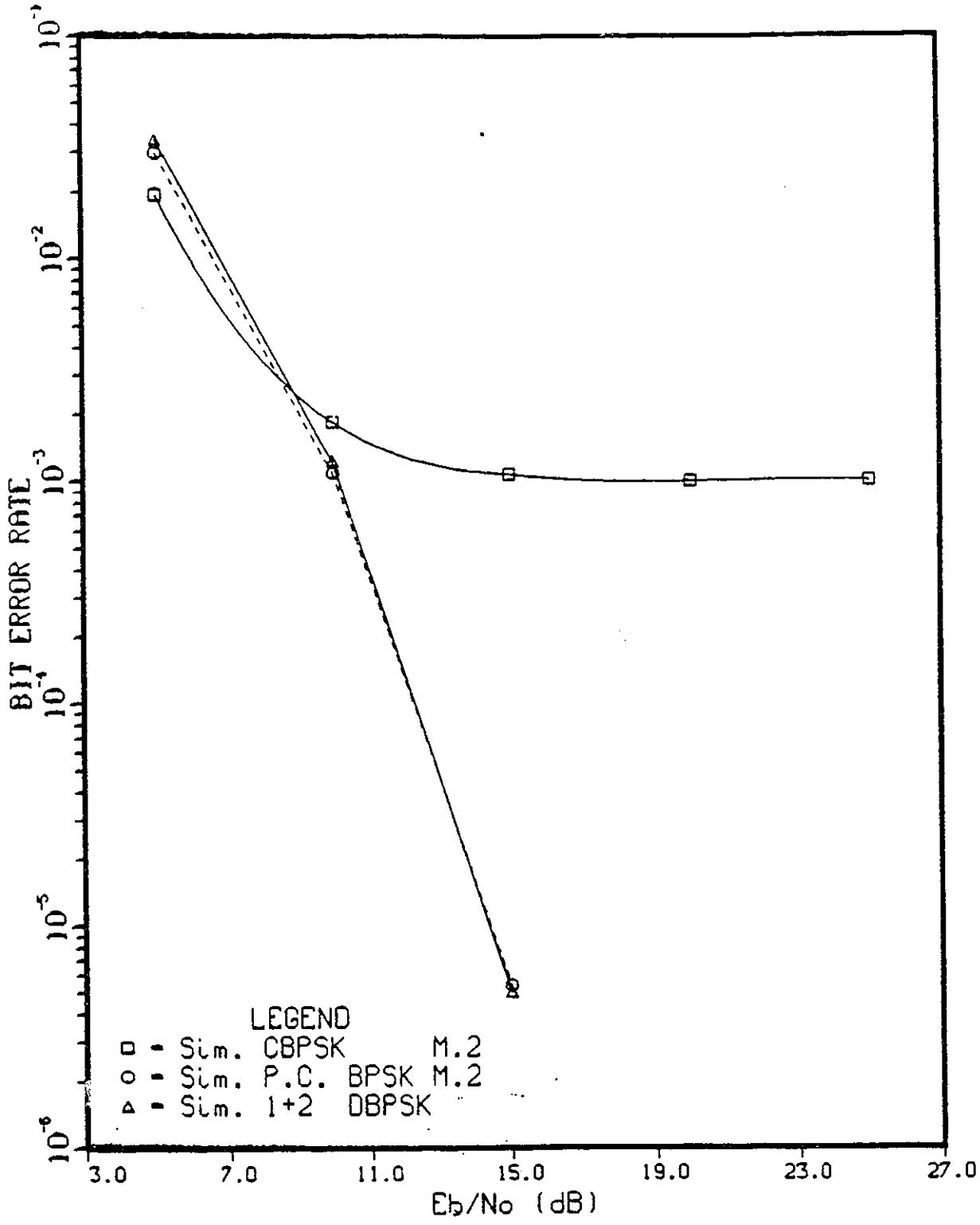

Figure 4.11: BER performance of partially coherent detection of BPSK in Rician channels using Model 2 (M.2) of Section 2.3, for $K = 10$dB, loop SNR $\xi = 10$dB and $BT = 0.01$.

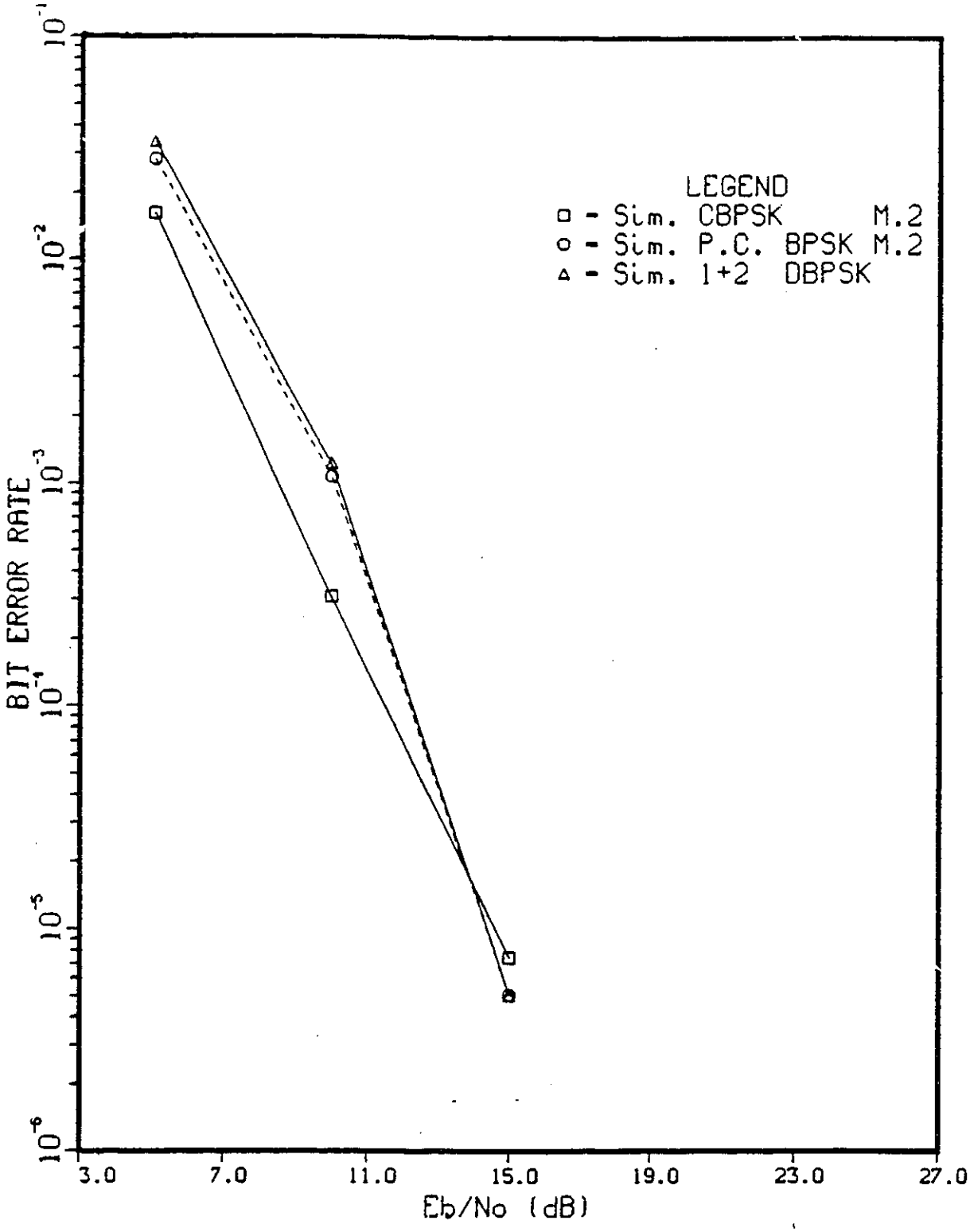

Figure 4.12: BER performance of partially coherent detection of BPSK in Rician channels using Model 2 (M.2) of Section 2.3, for $K = 10$dB, loop SNR $\xi = 15$dB and $BT = 0.01$.

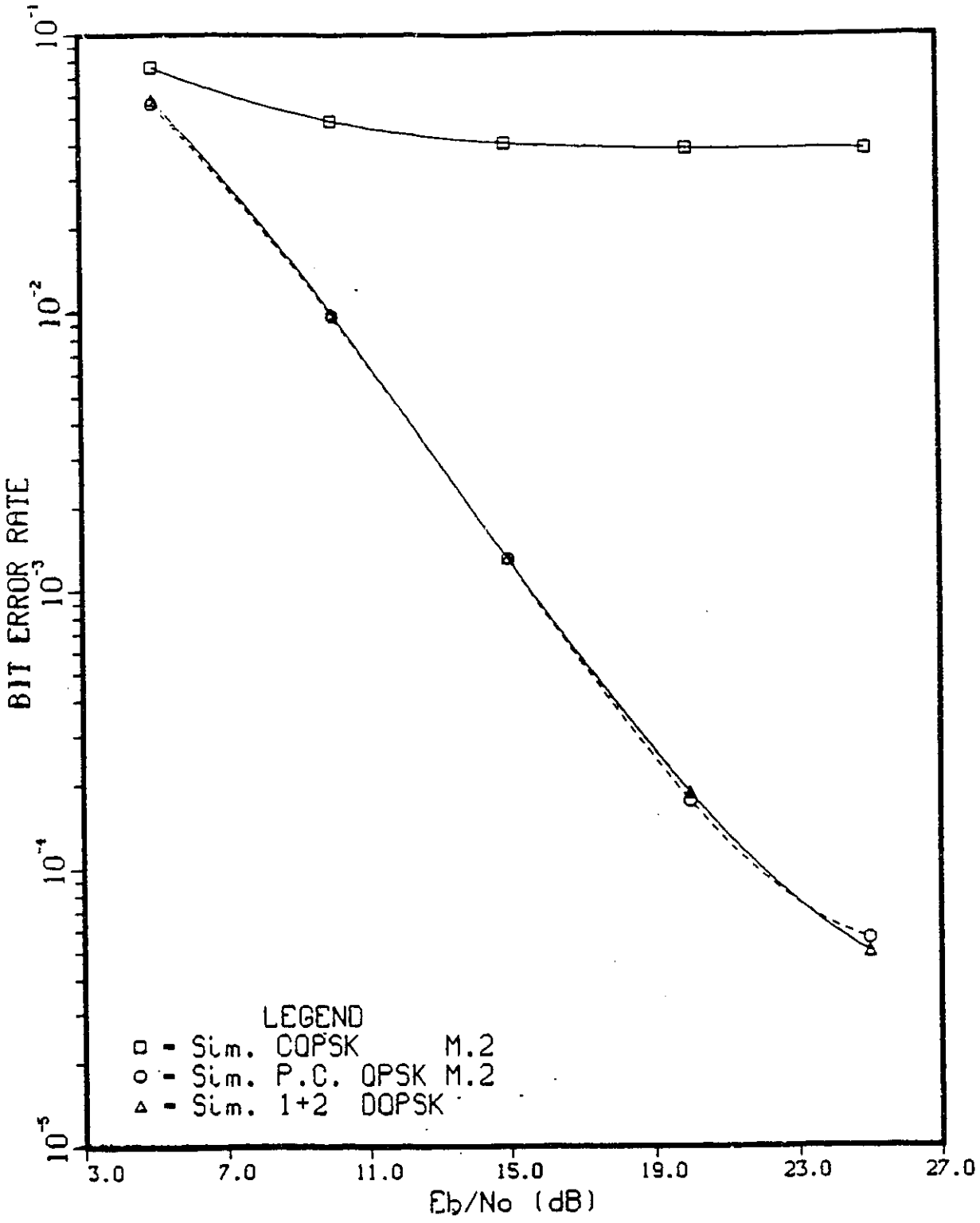

Figure 4.13: BER performance of partially coherent detection of QPSK in Rician channels using Model 2 (M.2) of Section 2.3, for $K = 6$dB, loop SNR $\xi = 10$dB and $BT = 0.01$.

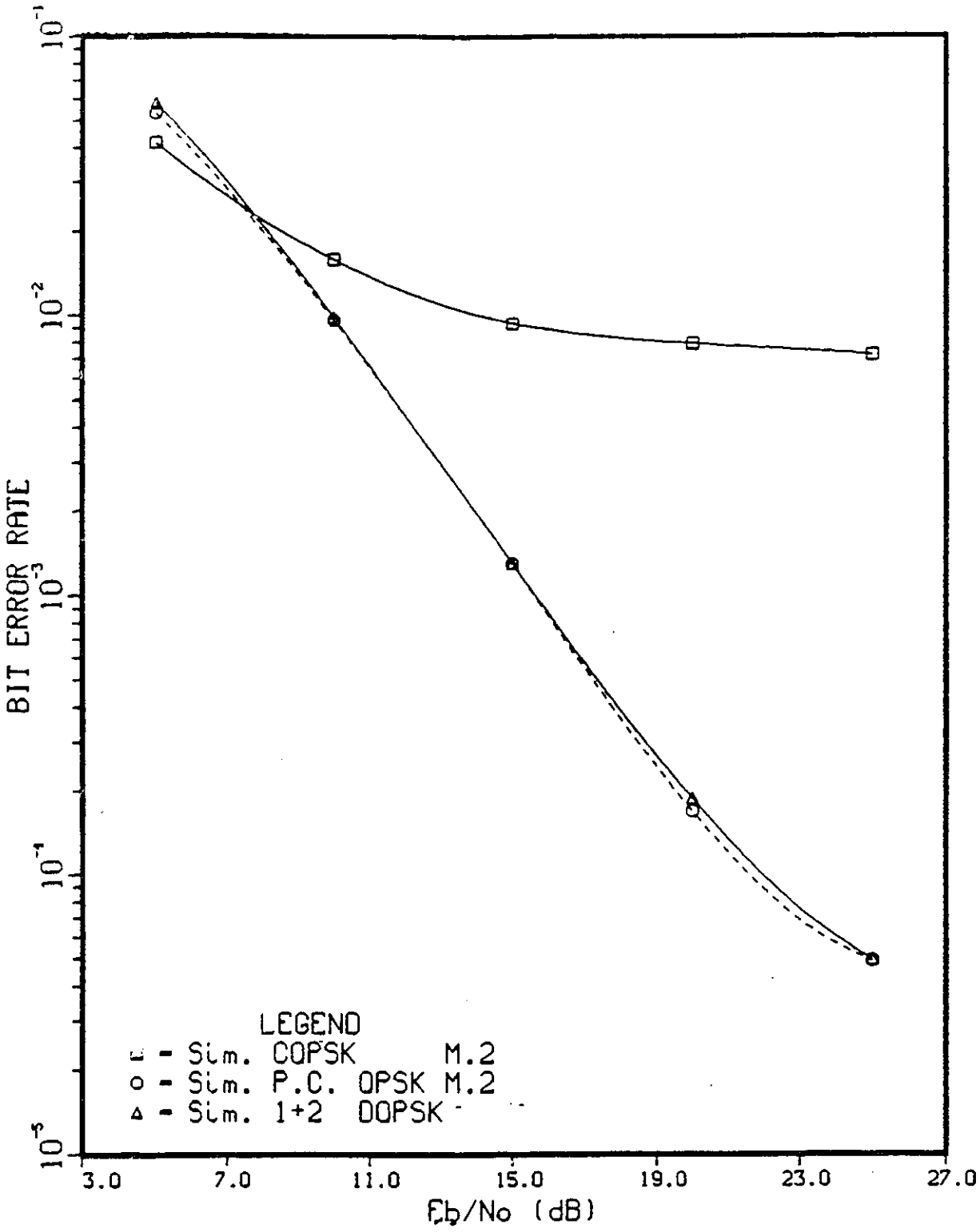

Figure 4.14: BER performance of partially coherent detection of QPSK in Rician channels using Model 2 (M.2) of Section 2.3, for $K = 6$dB, loop SNR $\xi = 15$dB and $BT = 0.01$.

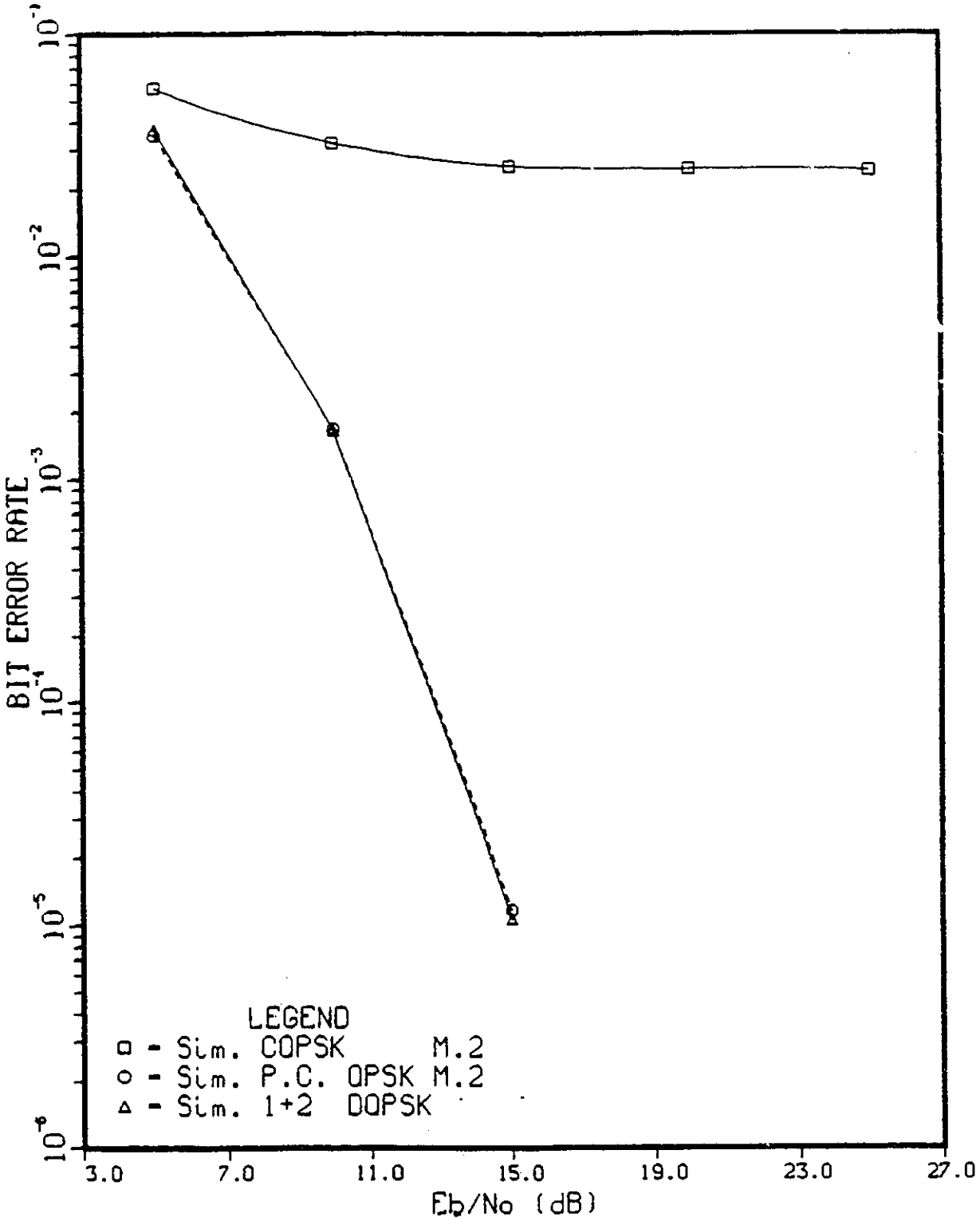

Figure 4.15: BER performance of partially coherent detection of QPSK in Rician channels using Model 2 (M.2) of Section 2.3, for $K = 10$dB, loop SNR $\xi = 10$dB and $BT = 0.01$.

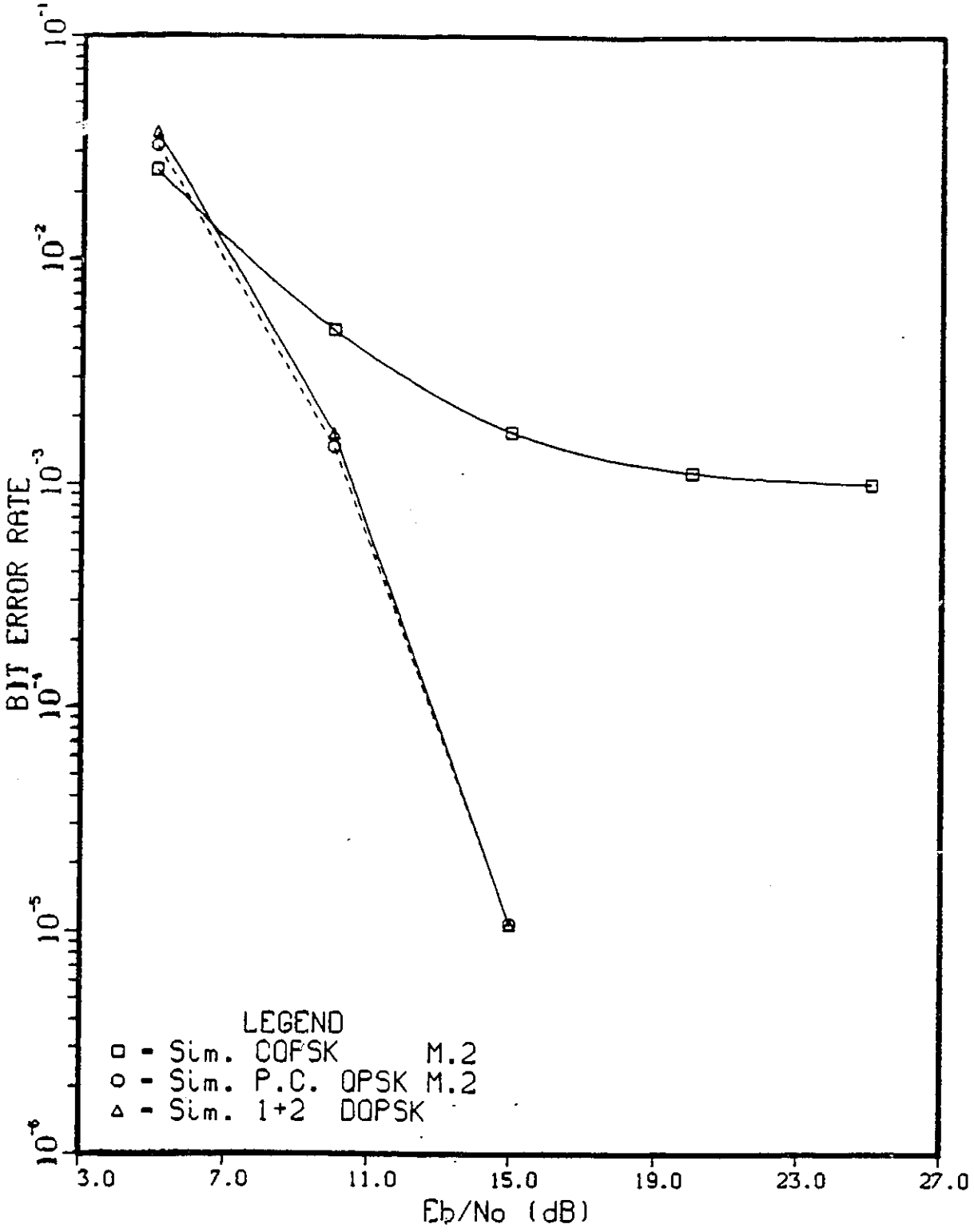

Figure 4.16: BER performance of partially coherent detection of QPSK in Rician channels using Model 2 (M.2) of Section 2.3, for $K = 10$dB, loop SNR $\xi = 15$dB and $BT = 0.01$.

4.4 Conclusion

In this chapter, metric expressions for partially coherent detection were derived and then applied to PSK signals. The metric expression for high $\frac{E_b}{N_0}$ case was interpreted and by truncation a modified metric expression was obtained. BER performance of uncoded BPSK and QPSK were obtained in slowly varying Rician channels by using Viterbi decoding for maximum likelihood detection for the modified metric expression. The performance curves showed that partially coherent detection has no significant improvement compared to multidifferential detection.

For BPSK, the results obtained were not very surprising. For QPSK case, since it is more affected from phase noise, it was expected that partially coherent detection would have some improvement over multidifferential detection. This can be explained by the strong correlation induced on the samples of the filtered Gaussian process used in the Rician models due to the narrow bandwidth of the filter and by the strength of the direct component relative to the diffuse component.

The results obtained suggest that in order for the partially coherent detection to have a better BER performance, there should be serious degradation in differential detection so that the coherent component will have an important contribution to the BER performance. Furthermore, the employment of additional differential detectors should also be contributing to the performance of the receiver. It is well known that [26] for coded systems, in AWGN channels differential detection has a more serious degradation compared to coherent detection due to the correlation introduced in between the symbols and this correlation introduced will more likely lead to error pairs or bursts. This fact suggests that partially coherent detection of coded systems can provide considerable improvements.

Chapter 5

CONCLUSIONS AND SUGGESTIONS FOR FURTHER RESEARCH

In this thesis, models to implement both the noisy phase reference due to the noise let in by the loop filter of the carrier recovery circuit and Rician fading channels were introduced. It has been shown that the pdf of the phase noise and the amplitude of the fading samples match well with the analytically derived ones in literature. Except for the BER performance of BPSK in AWGN channels with a noisy phase reference, it has also been shown that the simulation results match reasonably well with the analytical or simulation results available in literature.

Considering that coherent detection will perform poorly in the presence of phase noise and fading, we tried to apply partially coherent detection which is a more general case of noncoherent detection to improve the performance of noncoherent detection. After we derived a general metric expression and examined it under two different cases: low $\frac{E_b}{N_0}$ and high $\frac{E_b}{N_0}$, we applied these metric expressions to PSK signals. Considering that a communication system would generally operate at high $\frac{E_b}{N_0}$ values and that the metric expression is simpler, we used the one for high $\frac{E_b}{N_0}$. In order to simplify the receiver structure and the detection process, the metric expression was truncated, ending up with a receiver that consists of a coherent detector and a

two symbol differential detector. Partially coherent detection metric was a weighted combination of multidifferential detection and coherent detection having ξN_0 as the coefficient of the coherent term. As the signal to noise ratio of the loop increases, under the condition where coherent detection would perform better, the weight of the coherent term would increase and vice-versa.

Simulations were run using Viterbi decoding to obtain the BER performances of uncoded BPSK and QPSK in slowly varying Rician channels with (where coherent detection is involved) and without considering the noisy phase reference. The simulation results showed that there was no significant improvement in partially coherent detection of uncoded BPSK and QPSK, compared to differential detection. In QPSK case, unlike the BPSK, our expectation was to get some improvement when compared to differential detection.

As a further research, BER performance of partially coherent detected coded systems can be investigated. As have been stated in the conclusion section of Chapter 4, due to the serious degradation that the correlation introduced in between the symbols might have bring, we believe that the performance of partially coherent detection will improve considerably compared to multidifferential detection. Furthermore, as the metric expressions suggest, the decoding can be done in blocks starting with small block lengths. We believe that partially coherent detection will give significant improvements compared to differential detection for coded systems. The performance of partially coherent detection can be compared to other detection schemes under other channel conditions (e.g. Rayleigh fading channels, fading channels where there is also shadowing, fast fading channels).

Bibliography

[1] R. E. Ziemer, W. H. Tranter, *Principles of Communications - Systems, Modulation and Noise*, Houghton Mifflin Company, Boston, 1990.

[2] J. W. Modestino, S. Y. Mui, "Convolutional Code Performance in the Rician Fading Channel", *IEEE Transactions on Communications*, Vol. COM-24, No.6, pp. 592-605, June 1976.

[3] F. Davarian, "Digital Modulation for an Aeronautical Mobile Satellite System" in *GLOBECOM '87, IEEE Global Telecommun. Conf. Rec.*, pp. 42.1.1-8, 1987.

[4] D. Divsalar, M. K. Simon, "Trellis Coded Modulation for 4800-9600 bits/s Transmission Over a Fading Mobile Satellite Channel", *IEEE Journal on Selected Areas in Communications*, Vol. JSAC-5, No.2, pp. 162-175, Feb. 1987.

[5] J. C. Haartsen, R. C. Den Dulk, "Novel Circuit Design and Implementation of Adaptive Phase Comparators", *Electronic Letters*, Vol. 23, No.11, pp. 551-552, May 1987.

[6] J. Eijselendoorn, R. C. Den Dulk "Improved Phase-Locked Loop Performance with Adaptive Phase Comparators", *IEEE Trans. Aerospace and Elec. Sys.*, Vol. AES-18, pp. 323-333, May 1982.

[7] Y. Tunca, D. Makrakis, A. Yongaçoğlu, "Optimal Partially Coherent Detection of Block-Coded PSK and CPM Signals", in *Proc. of Canadian Conf. on Electr. and Comp. Engg.*, 12.3.1-12.3.4, Ottawa, Ont., Sept. 1990.

[8] P. A. Bello, "Aeronautical Channel Characterization in the Rician Fading Channel", *IEEE Transactions on Communications*, Vol. COM-21, No.5, pp. 548-563, May 1973.

[9] F. Davarian, "Fade Margin Calculation for Channels Impaired by Rician Fading", *IEEE Transactions on Vehicular Technology*, Vol. VT-34, No.1, pp. 41-44, Feb. 1985.

[10] L. J. Mason, "Error Probability Evaluation for Systems Employing Differential Detection in a Rician Fast Fading Environment and Gaussian Noise", *IEEE Transactions on Communications*, Vol. COM-35, No.1, pp. 39-46, Jan. 1987.

[11] Chun Loo, "A Statistical Model for a Land Mobile Satellite Link", *IEEE Transactions on Vehicular Technology*, Vol. VT-34, No.3, pp. 122-127, Aug. 1985.

[12] M. Lecours, J.-Y. Chouinard, G. Y. Delisle, J. Roy, "Statistical Modeling of the Received Signal Envelope in a Mobile Channel", *IEEE Transactions on Vehicular Technology*, Vol. VT-37, No.1, pp. 204-212, Nov. 1988.

[13] M. K. Simon, D. Divsalar, "The Performance of Trellis Coded Multilevel DPSK on a Fading Mobile Satellite Channel", *IEEE Transactions on Vehicular Technology*, Vol. VT-37, No.2, pp. 78-91, May 1988.

[14] S. G. Wilson, R. W. Sutton, E. H. Schroeder, "Differential Phase-Shift Keying Performance on L-Band Aeronautical Satellite Channels : Test Results and a Code Evaluation", *IEEE Transactions on Communications*, Vol. COM-24, No.3, pp. 374-380, March 1976.

[15] Y. Miyagaki, N. Morinaga, T. Namekawa, "Error Rate Performance of M-ary DPSK Systems in Satellite/Aircraft Communications" in *ICC '79, Proc. IEEE Int. Conf. Commun.*, pp. 34.6.1-6, 1979.

[16] J. H. Lodge, M. L. Moher, S. N. Crozier, "A Comparison of Data Modulation Techniques for Land Mobile Satellite Channels", Vol. COM-24, No.6, pp. 592-605, June 1974.

[17] Y. Miyagaki, N. Morinaga, T. Namekawa, "Double Symbol Error Rates of M-ary DPSK in a Satellite Aircraft Multipath Channel", *IEEE Transactions on Communications*, Vol. COM-31, No. 12, pp. 1285-1289, Dec. 1983.

[18] R. G. Mckay, P. McLane, E. Biglieri, "Analytical Performance Bounds on Average Bit Error Probability for Trellis Coded PSK Transmitted Over Fading Channels" in *ICC '89, Proc. IEEE Int. Conf. Commun.*, pp. 9.2.1-7, 1989.

[19] I. Korn, "M-ary FSK with Limiter Discriminator Detection and DPSK with Differential Phase Detection in a Rician Fading Channel", *International Journal of Satellite Communications*, Vol. 8, pp. 363-368, 1990.

[20] C. Loo, "Digital Transmission Through a Land Mobile Satellite Channel", *IEEE Transactions on Communications*, Vol. COM-38, No. 5, pp. 693-697, May 1990.

[21] A. J. Viterbi, "Phase-locked loop dynamics in the presence of noise by Fokker-Plank Techniques", *Proc. IEEE*, Vol. 51, pp. 1737-1753, Dec. 1963.

[22] J. F. Öberst, "Generalized Phase Comparators for Improved Phase-Locked Loop Acquisition", *IEEE Transactions on Communications*, Vol. COM-19, No. 6, pp. 1142-1148, Dec. 1971.

[23] S. Saito, S. Hiroshi, "Fast-Carrier Tracking Coherent Detection with Dual-Mode Carrier Recovery Circuit for Digital Land Mobile Transmission", *IEEE Journal on Selected Areas in Communications*, Vol. JSAC-7, No. 1, pp. 130-139, Jan. 1989.

[24] A. J. Viterbi, *Principles of Coherent Communication*, Mc Graw Hill Inc., New York, 1966.

[25] H. L. Van Trees, *Detection Estimation, and Modulation Theory*, Part I, John Wiley and Sons Inc., New York, 1968.

[26] J. J. Jr. Spilker, *Digital Communications by Satellite*, Prentice-Hall Inc., Englewood Cliffs, New Jersey, 1977.

[27] T. Aulin, C.-E. W. Sundberg, "Partially Coherent Detection of Digitall Full Response Continuous Phase Modulated Signals", *IEEE Transactions on Communications*, Vol. COM-30, No.5, pp. 1096-1117, May 1982.

[28] W. Harold, N. Kingsbury, "A Partially Coherent Detector for Continuous Phase Modulation", *IEEE Journal on Selected Areas in Communications*, Vol. JSAC-7, No. 9, pp. 1415-1426, Dec. 1989.

[29] H. Leib, S. Pasupathy, "The Phase of a Vector Perturbed by Gaussian Noise and Differentially Coherent Receivers", *IEEE Transactions on Information Theory*, Vol. IT-34, No. 6, pp. 1491-1501, Nov. 1988.

[30] W. C. Y. Lee, *Mobile Communication Engineering*, Mc Graw Hill Inc., New York, 1982.

[31] J. G. Proakis, *Digital Communications*, Mc Graw Hill, New York, 1989.

[32] E. Lutz, E. Plöchinger, "Generating Rice Processes with Given Spectral Properties", *IEEE Transactions on Vehicular Technology*, Vol. VT-34, No. 4, pp. 178-181, Nov. 1985.

[33] E. A. Lee, D. G. Messerschmitt, *Digital Communication*, Kluwer Academic Press, Boston, 1988.

[34] W. B. Lindsey, M. K. Simon, *Telecommunication Systems Engineering*, Prentice-Hall Inc., Englewood Cliffs, New Jersey, 1974.

[35] S. A. Rhodes, "Effect of Noisy Phase Reference on Coherent Detection of Offset-QPSK Signals", *IEEE Transactions on Communications*, Vol. COM-22, No. 8, Aug. 1974.

[36] S. Crozier, M. Murthy, M. El-Tanany, R. K. Tiedemann, *Study of the Applicability of the INMARSAT System to the Aeronautical Mobile Satellite Service*, Draft Final Report, Annex 3, Modulation and Coding, Miller Communications Systems, March 1984.

[37] D. Divsalar, M. K. Simon, "Multiple-Symbol Differential Detection of MPSK", *IEEE Transactions on Communications*, Vol. COM-38, No. 3, pp. 300-308, Mar. 1990.

[38] D. Makrakis, K. Feher, "Optimal Noncoherent Detection of PSK Signals", *Electronic Letters*, pp. 398-401, March 15, 1990.

[39] M. A. Herro, J. M. Nowack, "Simulated Viterbi Decoding Using Importance Sampling", *IEE Proceedings*, Vol. 135, Part F, No. 2, pp. 133-142, Apr. 1988.

[40] K. S. Shanmugam, P. Balaban, "A Modified Monte-Carlo Simulation Technique for the Evaluation of Error Rate in Digital Communication Systems", *IEEE Transactions on Communications*, Vol. COM-28, No. 11, pp. 1916-1924, Nov. 1980.

[41] P.E.K. Chow and D.H.S.Ho, "Improving DCPSK Transmission by Means of Error Control", *IEEE Trans. on Communication*, Vol. COM-19, Oct. 1971, pp. 715-719.

[42] T. Masamura et.al., "Differential Detection of MSK with Non-reduntant Error Correction", *IEEE Trans. on Communication*, Vol. COM-27, pp. 912-919, June 1979.

[43] S. Samejima et.al., "Differential PSK System with Non-reduntant Error Correction", *IEEE JSAC*, Vol. SAC-1, No. 1, pp. 74-81, Jan. 1983.

[44] D. Makrakis, et. al., "Novel Receiver Structures for Systems Using Differential Detection" in *Proceedings of ICDSC-7*, pp. 681-688, May 1986.

[45] A. Yongaçoğlu, D. Makrakis, H. Ohnishi, K. Feher, "A New Receiver for the Differential Detection of GMSK", in *GLOBECOM '86, IEEE Global Telecommun. Conf. Rec.*, pp. 29.5.1-6, 1986.

[46] D. Makrakis, et.al., "A new Soft Decision Sequential Decoder for the Differential Detection of TFM", in *GLOBECOM '87, IEEE Global Telecommun. Conf. Rec.*, pp. 8.81-4, Nov. 1987.

[47] D. Makrakis, et. al.,"An Improved Viterbi Decoder for the Differential Detection of Continuous Phase Modulation Schemes", in *Proceedings of IEEE WESCANEX '88*, pp. 18-21, May 1988.

[48] D. Makrakis, et. al., "A sequential decoder for the Differential Detection of Trellis Coded PSK Signals", in *Proc. of the International Conf. on Communications (ICC '88)*, pp. 1433-1438, June 1988.

[49] D. Makrakis and K. Feher, "Multiple Sequential Detection of Continuous Phase Modulation Signals", accepted for publication in *IEEE Transactions on Vehicular Technology.*

[50] A. Yongaçoğlu, D. Makrakis, and K. Feher, "Differential Detection of GMSK Using Decision Feedback", *IEEE Trans. on Communication*, Vol. COM-36, pp. 637-649, June 1988.

[51] D. Makrakis and P.T. Mathiopoulos, "Trellis Coded Non-Coherent QAM: A New Bandwidth and Power Efficient Scheme", Proc. of IEEE Veh. Tech. Conf.(VTC'89), pp. 95-100, April 1989.

[52] D. Makrakis and P.T. Mathiopoulos, "Non-Coherent Multilevel Trellis Coded Continuous Phase Modulation" in *ICC '89, Proc. IEEE Int. Conf. Commun.*, pp. 792-797, June 1989.

[53] D. Makrakis, K. Sreenath, and K. Feher, "Optimal and near Optimal Detection of Trellis Coded Signals", in *GLOBECOM '90, IEEE Global Telecommun. Conf. Rec.*, pp. 401.3.1-5, Dec. 1990.

[54] D. Makrakis, "Improved Non-Coherent Receivers", Part I: "Evaluation Under Non-ideal Conditions", Part II: "Optimal and Asymptotically Optimal Decoders", *Communication Research Centre Technical Report*, May 1991.

[55] D. Divsalar, M. K. Simon, "The Performance of Trellis Coded MDPSK with Multiple Symbol Detection", *IEEE Transactions on Communications*, Vol. COM-38, No. 9, pp. 1391-1403, Sep. 1990.

[56] D. Makrakis and K. Sreenath, "Generalized Non-Coherent Sequential Detection of PSK Sinals, Part I& II", accepted for publication in *IEE Proceedings, Part I.*